FINAL REPORT

# METEOROID IMPACT FLASH ANALYZER

R134/FR1



SUBMITTED TO

NATIONAL AERONAUTICS AND SPACE ADMINISTRATION
MANNED SPACECRAFT CENTER
HOUSTON, TEXAS

CONTRACT NO. NAS9-8788

10 DECEMBER 1969

**Computing Devices of Canada Limited**
a subsidiary of
CONTROL DATA CORPORATION

NASA CR 102057

FINAL REPORT

# METEOROID IMPACT FLASH ANALYZER

R134/FR1

SUBMITTED TO

NATIONAL AERONAUTICS AND SPACE ADMINISTRATION
MANNED SPACECRAFT CENTER
HOUSTON, TEXAS

CONTRACT NO. NAS9-8788

10 DECEMBER 1969

PREPARED BY

B. JEAN
H. HENSHAW

Computing Devices of Canada Limited
a subsidiary of
CONTROL DATA CORPORATION

TABLE OF CONTENTS

## LIST OF ILLUSTRATIONS

LIST OF ILLUSTRATIONS (Continued)

LIST OF ILLUSTRATIONS (Continued)

SUMMARY

This report presents the conclusions of a research program aimed at the determination of micrometeoroid mass, velocity and composition from its impact flash signature. A previous phase had demonstrated that flash intensity and rate of change of intensity for a metallic projectile impact generated flash is a very rapid varying function of the projectile diameter and velocity. In the present phase the same study has been applied to actual meteorite materials, Canyon Diablo iron and Bruderheim stone.

The radiation emitted in the impact flash has been spectroscopically analyzed by a cluster of four photomultipliers monitoring the impact flash through four narrow band interference filters. With the Meteoroid Impact Flash Analyzer the intensity and rate of change of intensity has been studied for projectiles of two different meteoritic materials, at different velocities, diameters and shapes.

The sum of the data collected for Canyon Diablo iron and Bruderheim stone projectiles does not yet lead to a firm determination of the exponent of the power laws which relate intensity and rate of change of intensity with the projectile velocity. The same conclusion can be given for the projectile diameter influence. This is due to the spread of experiments over several varied parameters. More data points will be needed to positively define the relationship. However, a power law trend has been experienced.

Experiments have been conducted to develop the capability of the identification of specific elements present in the projectile, from the experimental observation of their spectral emission at specific wavelengths. The results obtained from a cluster of five photomultipliers monitoring five narrow spectral bands, have demonstrated that a measurement of the amplitude of the signal cannot be used for element identification. However, the possibility of obtaining the sought information from an integrated signal is excellent.

The inability to use signal amplitude for material identification seems to suggest the presence of radiation due to ionized species or continuum at the observed wavelengths. Preliminary consideration suggests that this will not be detrimental, and may in fact be beneficial, to the extension of the power law relationship to higher velocities. These newly observed phenomena warrant further study.

# 1. INTRODUCTION

An experimental study of the radiation emitted when a hypervelocity metallic projectile impacts a cadmium target has been reported in Reference 1. It has been demonstrated that for a given composition of the impacting projectile, the intensity and rate of change of intensity of the radiation generated at impact are functions of the projectile velocity and diameter. As a corollary this study has indicated that a measurement of the flash intensity and rate of change of intensity can reveal the velocity and mass of the impacting projectile provided its composition is known. Since part of the emitted radiation contains line emission corresponding to the elements present at impact, spectroscopic analysis of the flash can also lead to knowledge of the projectile's composition.

This principle has been considered as a means of measuring the characteristics of micrometeoroids in space from a measurement of the characteristics of the flash produced when they impact on a target of known composition.

The goal of the present program was to verify the above concept in the laboratory by the study of the flash produced by the impact of a projectile made from meteoritic material. The diagnosis of the radiation emitted was to be carried out by a detector system similar to a unit that is to be used in a space experiment. This sensor package, consisting of nine narrow band filters corresponding to nine selected line emissions of the flash, has been constructed and calibrated. The choice of the proper filters was made by both theoretical and experimental work. For this purpose firings have been conducted to study the profile of some cadmium emission lines in the impact flash. The filters have been chosen to monitor target emission lines, background emission and lines which could lead to identification of the composition of the projectile.

It is also speculated that certain meteorites may contain carbon. Its detection in space by the impact flash is of interest, so

special attention has been given to find out if carbon can be excited by the hypervelocity impact mechanism and its radiation spectroscopically detected.

## 2. THE IMPACT FLASH ANALYZER

The optical system for light collection must satisfy the following conditions:

(1) The radiation collected by the system must not be strongly dependent on the position of the micrometeoroid impact point on the target. A variation by a factor of about 2 is acceptable.

(2) The optical dispersion system must have sufficient resolution to isolate single lines of cadmium without including excess background radiation. This limits the entrance slit width of spectrograph or the size of the acceptance cone of an interference filter. At present, a half maximum bandwidth of about 80Å is envisioned.

(3) The system must be sufficiently sensitive to detect the smallest and slowest micrometeoroids of interest.

It is difficult to satisfy all three conditions with a spectrograph. Conditions 1 and 3 require a spectrograph with a very large aperture, and condition 2 requires an instrument with a small aperture. Condition 3 requires a wide entrance slit, and condition 2 requires a narrow entrance slit. By using narrow band pass interference filters instead of a spectrograph, it is possible to satisfy all three conditions in a simple manner. An additional advantage of the filter system over the spectrograph is that the filter system is relatively insensitive to small changes in detector position, while the spectrograph system is critically sensitive to both the spectrograph exit slit position and the grating position.

The impact flash analyzer consists of a set of filters and monitoring photomultipliers. These elements are described in turn below.

### 2.1 The Filters

The optical filters selected for the analyzer consist of the following: those to provide information on size and velocity, those to provide information on meteoroid type, and those used to detect carbon.

Procedures in the selection of each of the three types of filter will be discussed below.

With the use of interference filters the angle of incidence of the radiation must be restricted within limits dictated by the accepted decrease of transmissivity of the filters at the wavelength of interest at the maximum incidence angle. This can be achieved in two different manners. In a first approach a ground quartz light diffuser is used to collect the radiation emitted by an impact flash point source located at any angle on a plane target normal to the diffuser. In order to restrict the angle of incidence of the radiation on the filters, a limiter consisting of tubes with a diameter to length ratio equal to the tangent of the acceptable angle, is placed between the diffuser and the filters. The diffuser will have to be lambertian to avoid preferential direction of transmittance. In such a case the transmission and diffusion losses can be very important. In a second approach no diffuser and no angle of incidence limiter is used. In this case the angle of incidence of the radiation on the interference filters is fixed by limiting the physical dimensions of the target such that no radiation sources can be located outside the permissible angle. This has the disadvantage of reducing the size of the collecting area but by allowing no light losses, lower meteoroid impact flash can be collected, thus a larger number of events can be recorded. This approach can be accomplished by properly selecting the filter bandwidth and wavelength at maximum transmission. This is the method which has been selected and which is described in the following paragraphs.

Two factors influence the selection of the filter bandwidth and wavelength of maximum transmission: spectral distribution of the emitted radiation (i.e, line profile) and maximum angle of incidence of the radiation on the filter. If, for example, the emitted radiation is a sharp line emission and all the radiation falls on the filter at $0^{o}$ (measured from the filter normal), then a very narrow bandwidth filter centered exactly at the emission wavelength would be satisfactory. If the emission is broadened line emission and the angle of incidence is $0^{o}$, a

filter with more bandwidth will be advantageous, but the maximum transmission should still be centered at the wavelength of maximum emission. When we consider angles of incidence other than $0^{o}$, however, the situation changes. Three things happen to the passband of a filter when the radiation is incident at angles other than $0^{o}$: the bandwidth increases, the maximum transmission decreases, and the wavelength of maximum transmission shifts to shorter wavelengths (see Reference 1). The possible serious consequences of these effects is shown in the diagram below, where it is assumed that the emission line is sharp and the filter centered at the emission wavelength at an angle of incidence $\theta$. The filter bandpass has shifted such that very little of the incident line emission is transmitted.

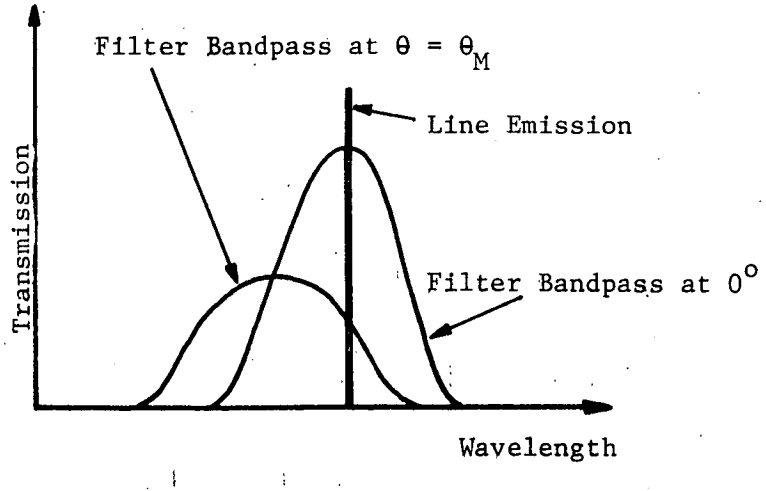


Sketch A.

Consider the case where the filter is not centered at the emission wavelength, but rather at some higher wavelength. This situation is shown in Sketch B. In this case, the filter passes the same amount of line radiation at $\theta_M$ as it does at $0^{o}$. The optimum choice of filter passband is seen to depend on the angle of the incident radiation. If the angle of incidence varies from $0^{o}$ to $\theta_M$, then the optimum filter will not be centered at the emission wavelength, but at some larger wavelength.

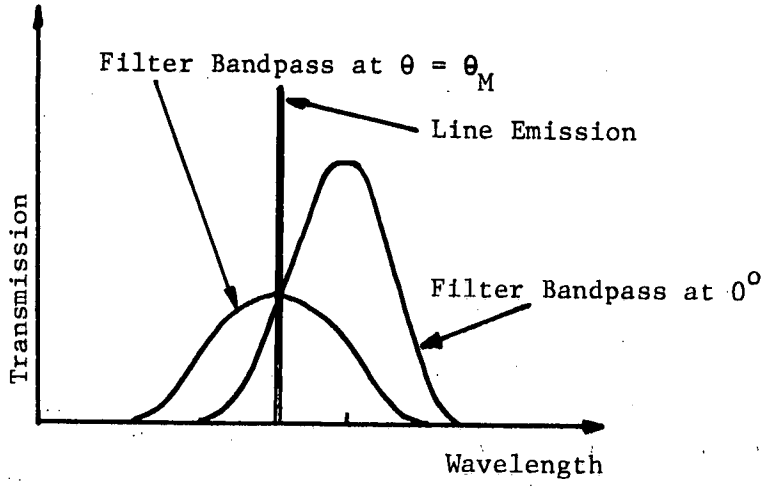


Sketch B.

In order to evaluate the peak wavelength shift and the filter transmissivity at angle of incidence θ (Reference 2), the following equations can be used.

$$\frac{\lambda_D - \lambda_\theta}{\lambda_D} \equiv K\theta^2 \qquad (1)$$

$$\frac{T(\theta)}{T_o} \equiv \exp. \left[-\left(\lambda_\theta - \lambda_D\right)^2 2 \left(\frac{\Delta\lambda}{2.35}\right)^2\right] \qquad (2)$$

$\lambda_D$ is the filter's design wavelength, $\lambda_\theta$ is the wavelength of maximum transmission at angle of incidence θ, this is the emission wavelength investigated, K is a constant depending on the particular filter used, $T(\theta)$ is the peak filter transmission at angle of incidence θ, $T_o$ is the peak filter transmission at angle of incidence $0^o$, $\Delta\lambda$ is the filter bandwidth at half maximum. For any given maximum angle of incidence, the above equations can be used to define $\lambda_D$, $\Delta\lambda$, and K such that $\frac{T(\theta)}{T_o} \equiv f$ for any

given angle $\theta$ such that $-\theta_M \leq \theta \leq \theta_M$ where f is some specified fraction. For example, when f = 1/2 and $\theta_M = 15^o$, then $\lambda_D, \Delta\lambda$, and K can be chosen such that the radiation transmitted by the filter from a constant intensity source will not decrease more than a factor 2 as $\theta$ is varied from $0^o$ to $\pm 15^o$. The actual choice of $\theta_M$ will depend either on the physical constraints of the actual satellite experiment or on the upper bound that has been calculated for the filters used. In the example chosen, the intensity of the studied emission will be constant at $0^o$ and $\pm 15^o$.

If the radiation source emitted continuum radiation as well as line emission, the situation would be a little more complicated. In the extreme case where the radiation was all continuum and the intensity was independent of wavelength for the small range of wavelengths considered, then the shift of the filter's peak wavelength with angle of incidence would not be important, but the reduction of peak transmission with angle of incidence would be important.

It is evident from the above discussion that the choice of optimum filter parameters depends on both the line profile and the angle of incidence of the radiation. The angle of incidence of the radiation for the laboratory program is $0^o$. Therefore, the filter's transmission band has been chosen such that it peaks at the cadmium line of interest, i.e., 3261Å, 3610Å, or 5085Å. In the present case where $\theta_M = 0^o$, only the filter's bandwidth remains to be specified. Experiments conducted to deduce the filter's optimum bandwidth from emission line measurements are described below.

We fired three shots with the width of the exit slit of the polychromator set successively at 500 $\mu$, 2000 $\mu$, and 8000 $\mu$, corresponding to filter bandwidths of 5Å, 20Å, and 80Å respectively. The projectile in each case was a .318 cm copper sphere. Results of the shots are shown in the table below. All intensities are normalized to a velocity arbitrarily chosen at 5.2 km/sec by multiplying the observed intensity by $(5.2/V)^8$. The choice of this normalizing factor is discussed in Section 4.

| Shot No. | Effective Bandwidth Å | Velocity (km/sec) | Pressure Torr | Normalized Intensity, uw/cm$^2$ @ 1M | | | |
|---|---|---|---|---|---|---|---|
| | | | | 3261Å | 3610Å | 4900Å | 5085Å |
| 171 | 5 | 5.88 | $3.8 \times 10^{-5}$ | 25. | 160. | 15.6 | 151. |
| 166 | 20 | 5.24 | $4.0 \times 10^{-5}$ | 105. | 430. | -- | 454. |
| 173 | 80 | 5.98 | $4.0 \times 10^{-5}$ | 450. | 1100. | 284. | 1240. |

For the two regions, 3261Å and 4900Å, the intensity increases approximately linearly with the spectral bandwidths. At 4900Å, which corresponds to a background wavelength region where no line emission exists, linearity was expected as the results show. The behaviour of the 3261Å can be explained on the grounds that at a bandwidth of 20Å, the sensor detects the presence of cadmium emission at 3252Å and at a bandwidth of 80Å the emission of copper at 3247Å and 3273Å, and cadmium at 3248Å. The line profile at 3610Å and 5085Å is not flat since the intensity increases less than linearly with spectral bandwidth. Based on the results obtained, an approximate line profile can be drawn for these two lines. Figures 1 and 2 show the results obtained. It was also observed that the shape of the initial pulse of light does not change as the effective bandwidth is increased from 5Å to 80Å. Correspondingly the filter bandwidth has been selected to be 80 to 100Å. Four wavelengths have been chosen for the filters used to provide information about the size and velocity of the impacting particle: 3261Å, 3610Å, 5085Å, and 4900Å. The first three wavelengths correspond to cadmium emission lines and the last wavelength corresponds to a region free of cadmium emission lines, i.e, to a region of background radiation.

The transmissivity of each filter has been measured. The filters were successively mounted in the focal plane of the spectrograph behind a 500 micrometer wide slit covering a bandwidth of 5Å. The spectral distribution of the continuum radiation of a quartz incandescent lamp, as seen through the filter, was monitored by a photomultiplier. The results,

expressed in terms of percentage of the maximum transmissivity as a function of wavelengths, are given in Figure 3 for the four filters used.

To provide information on meteoroid types, five appropriate filters have been selected. The selection has been based on the following arguments. A comparison is made of the concentration of the different elements present in the different types of meteorites as expressed in the following table obtained from Reference 3.

| | Iron | Stoney-Iron | Stony |
|---|---|---|---|
| Fe | 91 | 55 | 16 |
| Mg | .03 | 12 | 14 |
| Si | .01 | 8 | 21 |
| Ca | .02 | -- | 1.8 |
| Al | - | -- | 1.6 |

Table of The Concentration of the Most Important Elements in the Different Meteorite Types

One can see that apart from the iron, elements can be coupled in pairs to give a unique determination of types of stony or stony-iron by their presence or absence. This can be achieved by grouping Mg-Si and Ca-Al. It also happens that the Ca-Al pair has a group of lines concentrated in the same spectral region, namely the $Ca^+$ 3934Å, 3968Å and Al 3944Å, 3961Å lines. Similarly Mg-Si pair have lines 30Å apart at 2852Å and 2881Å respectively.

A filter peaking at 3942Å with a half width of 80Å was selected to identify the Ca-Al. A second filter peaking at 2866Å with a bandwidth of 80Å was also selected to identify the pair of lines pertaining to the emission lines across the whole visible and ultra violet regions of the spectrum, with its most important transitions in the 3737Å region. A corresponding filter was then selected at 3735Å. The detection of carbon

is achieved by the selection of a filter at the 2478Å emission line of carbon. Finally a filter bandwidth of 80Å was selected in a spectral region essentially free of iron transitions, this filter peaks at 2707Å. Figure 4 gives the transmissivity curves of these last filters.

This choice of filters can be visualized by means of Figure 5, where the integrated spectra of the radiation emitted by the impact of projectiles made from CanDi, Bruderheim and carbon materials are displayed with the bands of the filters selected. For the laboratory experiment where the radiation incidence is maintained close to $0^{\circ}$, the filters have been selected with their peak transmission at the selected wavelengths.

## 2.2 Photomultipliers

EMI Type 9601B photomultipliers have been chosen as the light detectors. They are head-on type with a diameter of 0.9 inch. They have an S-11C response with a cutoff at 2100Å in the ultra violet and 6000Å in the yellow. The output signal of the photomultiplier is fed to a 500 ohm load resistor then to an emitter follower. Electroscopes are then used to record the signal. A circuit diagram of the voltage divider and emitter follower is given in Figure 6. The photomultipliers are mounted in two clusters of four and five units respectively. This was done to mount the clusters at two different windows on the impact area in order avoid having a large radiation incidence on the filters. The mechanical construction of one unit is such that the voltage divider and the emitter follower are contained in a cylinder of the same dimension as the photomultiplier itself. These elements, photomultiplier, divider and emitter follower, are contained in a single tubular holder. In front of each photomultiplier is mounted an aperture holder, a neutral density filter holder and the interference filter. Figure 7 shows four assembled units which form a cluster. A detailed drawing of the construction is given in Figure 8.

## 2.3 Calibration of the Photomultipliers

Each photomultiplier was calibrated in order to correlate its voltage to the absolute radiation intensity. A mercury ultra violet standard lamp mounted 1 meter in front of controlled apertures of the photomultipliers was used as a standard source. The apertures consisted of calibrated pin-holes. The lamp itself is calibrated such that the intensity of the 3650Å mercury group of lines falling on a surface of 1 $cm^2$ located 1 meter from the source is 60 microwatts when operated at the specified current and voltage. Using a narrow band filter of known transmissivity at 3650Å and a set of controlled apertures, the voltage response of the photomultiplier versus the intensity falling on the photo cathode has been measured. Typical results are given in Figure 9 for four photomultipliers. It can be observed in the response curves that the voltage is not a linear function of the intensity but varies as the intensity to some power, where the exponent is different for each photomultiplier. This situation is associated with the construction of the dynode-electrode of the EMI tubes selected. This non-linearity requires a good control over the high voltage at which the tubes operate, and that each photomultiplier be individually treated. This shortcoming is, however, compensated by the extended operating range of the photomultiplier since the exponent is smaller than unity, nearly equal to 0.70 in each case.

Prior to each firing, the response of the photomultipliers is checked for consistency against a constant intensity cadmium light source.

## 2.4 Installation of the Analyzer

The flash analyzer has been mounted behind a quartz window to view the flash in the plane of the target along a line nearly perpendicular to the line of flight (see Figure 10). The incidence of the radiation, in the worst case, is $5^\circ$ and would correspond, for the interference filter, to a peak wavelength shift of approximately 0.1% (Reference 2).

## 3. MICROMETEOROID DETECTION SYSTEM

The flash detection system comprises a target area, photomultiplier sensor array equipped with interference filters cut to accept radiation in carefully chosen regions of the spectrum, signal processing package, storage, and telemetry interface. The physical arrangement is shown in Figure 11. The target area would preferably be located on the back of a solar panel, since these are usually oriented at right angles to the sun, and such locations are therefore protected from direct solar radiation. The various parts and sub-assemblies are discussed in the following paragraphs.

### 3.1 Sensors

The minimum detectable flash depends on flash intensity, sensor sensitivity, noise, non-flash light levels, and physical layout. The most sensitive practicable photo sensitive devices for use as detector are photomultiplier tubes and continuous strip type photomultiplier, such as the Bendix Channeltron.

The channeltron appears attractive at first glance due to lower dark currents and lower apparent power requirements. Further examination reveals the requirement for light collection optics of appreciable dimensions, if the system light sensitivity is to match that available with PM tubes without optics. The noise signals due to dark current of the PM tubes are not severe and are rejected by the three-channel coincidence circuitry incorporated in the system.

Since the flash duration phenomenon is of the order of 0.2 to 5 microsecond duration, the system requires wide band circuitry. The PMs would operate in the linear pulse mode, and a minimum emission of four electrons per 200 nanosecond period (during the flash) has been adopted as a lower limit for acceptance as a true signal. This emission rate results from an equivalent light level at the photo cathode of approximately $1.4 \times 10^{-4}$ microwatts. (ASCOP 541A-05M or EMI 9601B).

The figure just quoted sets the minimum effective flash intensity at the PM cathode of $3 \times 10^{-5}$ microwatts per square cm. The minimum flash actually detectable depends on target geometry and distance from target to PM photo cathode.

## 3.2 Target

The original concept suggested the use of a cadmium layer on an aluminum plate. It has since been pointed out by the NASA Technical Monitor that cadmium sublimates rather rapidly in vacuum. A target of different material may eventually have to be selected. The system described herein is for a cadmium target since extensive data has been collected with cadmium in the course of the impact flash study.

The configuration proposed is that of a sector of an annulus subtending a maximum angle limited by interference filter transmission band shift. See Figure 11. Two areas are considered, one square meter and ten square meters. Two identical impacts on any two points on the target surface should not differ in intensity at the detectors by more than a factor of about 2. Then for a one radian subtended angle the ten square meter target requires maximum and minimum radii of 6.3 and 4.4 meters and the one square meter requires 2.0 and 1.4 meter dimensions.

The target area selection affects both the minimum detectable impact flash intensity and the frequency of recorded events. From the NASA data on sporadic meteoritic flux (Reference 3) one square meter will experience 0.1 impacts per hour average rate for particles of $10^{-12}$ grams or larger: a ten square meter area will therefore show ten times this rate.

Due to the inverse square law applying along the radii of the two targets, identical impact flashes occurring at corresponding locations on the two targets will have an intensity ratio of 10 to 1 at the PM photo cathodes. Consequently the minimum energy flash detectable on the ten square meter target will be higher by an order of magnitude relative

to the one square meter figure. This factor reduces the number of detectable events for the ten square meter target to 5 times that of the one square meter area. This point is discussed further in a following paragraph.

The minimum particle size whose impact flash would be detected anywhere on the target plate may be determined by use of Figures 12 and 13. Figure 12 shows predicted flash intensities for various particle masses and velocities; Figure 13 is taken from Reference 4, and shows flux rates for the spectrum of particle sizes.

From the PM tube data and geometry, the minimum detectable flash energy corresponds to particles of $1.8 \times 10^{-9}$ grams impacting at 12 km/sec and $10^{-11}$ grams at 30 km/sec, on one square meter target. Corresponding minimum sizes for the ten square meter target are $1.2 \times 10^{-8}$ and $7 \times 10^{-11}$ grams respectively.

The event rates for these sizes are .013 and 0.07 events per hour respectively for impacts at 12 and 30 km/sec on one square meter targets, and 0.007 and 0.04 events per hour per square meter on the ten square meter target. The net event rate ratio is better than five to one for the ten square meter target area. If problems of storage and deployment are not too severe a ten meter area is the obvious choice.

The thickness of the target material has been suggested as equal to the radius of the largest particle which might reasonably be expected to impact within a one year period. For example, with aluminum as target material, a particle of $10^{-3}$ grams having density of 3 indicates a thickness of 0.2 mm. A thickness of 0.4 mm of aluminum would weigh about 10 kilograms - support structures and other components extra.

## 3.3 Sensor Package

There are nine PM tubes in the package. Four carry filters which accept cadmium lines: these tubes provide flash intensity (I) and flash rise time (dI/dt) data. Three tubes carry specific filters to accept

iron, magnesium-silicon, and calcium lines: these provide the data for classification of the type of meteoroid. The two remaining tubes provide signals from carbon lines and background radiation level.

The physical disposition of the tubes is outlined in Figure 11. The target plate would necessarily be given an optical polish to provide a highly specular surface to minimize the level of stray light reaching the tube cathodes.

Since the average current supplied by the PM tube anodes would be very low, the necessary dynode bleeder currents could be reduced to a few microamperes. The charge storage for heavy pulse currents would be provided by adequate dynode bypass capacitors: since the frequency of events is very low, the capacitor charge depletion due to one event would be restored before the next flash would be likely to occur.

## 3.4 Signal Treatment

Since the impact flash is of such short duration, any attempt to store and transmit the flash signal pulses directly would require circuit bandwidths of the order of 30 to 40 megacycles per channel and impose excessive demands in terms of storage and telemetry. The alternative is to convert dI/dt and I data into quasi-static voltages, quantize, and store in digital form. The stored data may then be read out by any standard telemetry technique. A proposed flash intensity channel block diagram is given in Figure 14.

The intensity signals channels would each comprise a charge amplifier, charge pump, rate meter circuit, quantizer and two coincidence circuits. The rise time circuits for each of the four channels would comprise a differentiating circuit driven by the rate meter. Since very low intensity flashes would provide only a few charge pulses during the 200 to 400 nanosecond period, the rise time data in such cases would reflect rise times of individual pulses: such data would be rejected. A minimum of twenty pulses would be required to provide an intensity signal

whose derivative would be accepted. Suitable filtering would be incorporated to limit the maximum rise time to 15 to 20 nanoseconds: a two or three pole low pass filter should suffice.

The identification channels would employ only the intensity signal circuits, and could be operated in peak reading or integrated signal mode. In the latter mode an integration period of ten microseconds would provide accumulation of charges due to both spike and tail of the flash: the scientific reasons for selection of this mode are discussed in another section of this report. A block diagram of one identification channel is given in Figure 15.

## 3.5 Quantizing

The target geometry is such that for a given flash intensity located at the near and far edges (radially) of the target plate, an intensity ratio of 2 to 1 would be experienced. Consequently the quantizing levels have been set to provide signals corresponding to the following table.

QUANTIZED SIGNAL LEVEL RATIOS

| Level | Range Limits | |
|---|---|---|
| Q1 | 1 | 3 |
| Q2 | 3 | 10 |
| Q3 | 10 | 30 |
| Q4 | 30 | 100 |
| Q5 | 100 | 300 |
| Q6 | 300 | 1000 |
| Q7 | 1000 | Open |

The range of seven levels may be expressed in binary form by 3 bit coding.

Since flash intensities may range over a $10^8$ to 1 ratio, and

only about $10^3$ ratio can be accommodated by linear operation of the PM tubes, operation of the sensor array at stepped levels of PM gain would be required. To cover the lower energy higher flux events the system may be operated for perhaps a one month period at maximum gain, and the remainder of the year at reduced gain to acquire the higher energy lower flux rate data.

In the case of channeltrons, a given tube would carry up to six multiplier strips operating at different gains and thereby cover the full signal range simultaneously. The penalty paid for this advantage is the need for collection optics and more circuitry to accommodate the added number of signal sources. This approach will be examined further.

### 3.6 Storage

Since the use of PM tubes limits the number of Q levels to 7, a 3 bit code per channel would be sufficient to uniquely code a given level. In the case of multi-strip channeltrons 15 Q levels would be required to cover 8 decades: a 4 bit code would then be required.

The four intensity and four rate channels thus require storage for 40 bits per event (including parity): the five identification channels require 25 bits for intensity data and parity, plus 3 classification bits. Total storage, allowing for other data storage, should therefore total 80 bits per event.

Assuming a ten square meter target and minimum detectable particle size of $10^{-10}$ grams, the average impact rate per 6 hour period for sporadic flux is given as 0.25. According to Reference 3, stream flux during showers may be an order of magnitude higher, or 2.5 events per 6 hours period. Storage capacity for 12 to 16 events would therefore appear to be adequate, assuming data would be readout every six to ten hours during stream periods and every 24 hours for the strictly sporadic environment.

## 3.7 Coincidence Logic Functions

Since all multiplier devices experience noise pulses of random distribution, some measures must be taken to reject charge contributions accruing from such pulses. The PM tube types suitable for this system are specified to have $10^{-9}$ amps or less dark current. This corresponds to an electron low rate of 6300 electrons per second at the photo cathode for a PM gain of $10^{6}$. PM electron ballistics and circuitry bandwidth would provide a pulse width of the order of 15 nanoseconds for a single electron pulse into the first dynode. Since the intensity data channel gate is only open for one microsecond, the probability of a false pulse occurring during the gate period is about 0.7%.

To reduce the probability of false signals being accepted, four three-input AND gates would be incorporated to require simultaneous signals in at least three of the four channels before the signal would be transferred as valid data storage. The probability of a false event under these conditions is improved to about $2\times10^{-4}$% in a one second interval or about 4% in a 6 hour interval.

The first Q level would be set to trigger only for pulse counts of four or more electrons in each channel. This requirement improves the false signal probability to better than $10^{-2}$% for interval PM noise sources over a six hour period.

In addition, in each channel a separate coincidence arrangement is proposed in which any single pulse will fire a 50 to 100 nanosecond gate. If pulses follow sufficiently rapidly to hold the gate open for two hundred nanoseconds, the three-input AND gates are armed and will accept data provided the three channel coincidence requirement is fulfilled.

High stray light levels may also result in false readings. An extra PM sensing the background light level, and having a 50 to 100 kc circuit bandwidth would perform two functions. At low light levels due to stray illumination a signal would be generated to reject data going

out of Q1 levels or Q2 levels, depending on ambient light intensity. A separate coding would be entered in storage any time an event occured, the coding indicating the ambient light intensity.

In the event ambient light reached a level dangerous to the PM tubes in the array, the background sensor would generate a control signal to reduce or shut off the high voltage power supply while the excessive level persisted.

## 3.8 Readout of Stored Data

Since the data would be stored in binary form the telemetry bandwidth requirements are quite ordinary, and would be fulfilled by standard digital links.

The data format can be arranged to suit NASA PCM Telemetry Standards (Reference 5); the flash intensity and rate codes can be contained in one 32 bit word, and other data (shut down counts, program status, operating mode) in a third 32 bit word. Three 32 bit words per event would therefore be required, with a total of 15 events to be cleared in any one readout cycle.

The split phase type of binary coding would appear to offer advantages for serial readout, in that simpler gating and storage readout circuitries are possible.

Figure 16 shows a block diagram of the overall electronic system that it is proposed for retrieval of the photometric data for space application.

# 4. PARAMETRIC EXPERIMENTAL STUDIES

## 4.1 Launch Techniques

The launch techniques are in most respects similar to those used in the previous phase of this research program and were fully described in Reference 1. A few mechanical modifications have been made. With the use of friable meteoritic material for projectiles, the Mylar diaphragm mounted between the dump tank and the travelling section had to be removed. Special precautions were taken to keep the gun gases from reaching the target prior to the projectile. Baffle plates were installed along the path taken by the projectiles. The evacuation of the whole firing range, including dump tank, to a pressure of $5 \times 10^{-5}$ Torr was achieved by a more efficient installation of the 6" diameter diffusion pump and by the addition of two liquid nitrogen cold traps. Except for the study of ambient pressure effects on flash intensity, all the firings reported herein were conducted in an evacuated range of $5 \times 10^{-5}$ Torr or better. To insure the value of the pressure readings at the impact area, cold cathode vacuum gauges were occasionally calibrated relative to a standard gauge. The data points which have been collected in the course of this program are listed in Table 1.

## 4.2 Meteorite Materials

A large portion of the firings were conducted with projectiles made from meteoritic material. The materials used for this program were representative of meteorites collected on earth. The iron type is a piece of Canyon Diablo meteorite. Its composition and structure have been studied by the Center of Meteorite Studies in Arizona (Reference 6). The stony-iron type is a fragment of the Bruderheim meteorite whose composition and structure were studied and reported in Reference 7. The Bruderheim meteorite is a hyperstene chondrite, and proved most difficult to launch. The specimen used consists primarily of a very friable aggregate of ground mass made of remnants of shock fractured chondrules. The cohesive forces of this material are very weak. For this reason, this

material has been very difficult to launch, the impact success rate has been very low and only a few data have been collected using it as a projectile in spite of the very special precautions taken in the selection of the samples. The meteoritic projectile diameters ranged from 0.3 mm to 4.8 mm.

## 4.3 Pressure Effects on Flash Intensity

We had shown in the previous phase of this research program (Reference 1) that the spike intensity is a function of range pressure. Our results at that time indicated that the effect was quite small, and could be ignored compared to other sources of error. Larger variations of spike intensity experienced due to the range modification led us to wonder if the pressure effect could really be ignored. As a result, we conducted a series of experiments to determine the magnitude of the effects of range pressure on impact flash intensity after proper baffles have been installed. We launched 3.2 mm mild steel spheres at 5.2 km/sec at range pressures ranging from $4 \times 10^{-5}$ Torr to one atmosphere. Results of the firings are shown in Figures 17 through 19. Figure 17 shows the variation of tail intensity with range pressure, where the tail is defined as the broad, slowly rising pulse of radiation following the initial spike. The shape of the curve can be explained as follows. Below about $10^{-1}$ Torr, the radiation in the tail was produced by interaction of the jet of material produced by the impact (shaped-charge theory) and the surrounding atmosphere. There was little interaction with the target face since highly polished targets were used. As the range pressure decreased the interaction between the jet and the surrounding atmosphere decreased, and thus the intensity of the tail decreased. From the figure, the approximate relationship is $I(\text{tail}) \propto P^{\frac{1}{2}}$. Above about $10^{-1}$ Torr, effects such as ablation of the projectile and shock waves ahead of the projectile could possibly affect the impact to give the results shown in the figure. Above $10^{-1}$ Torr, the approximate relationship is $I(\text{tail}) \propto P^{-.135}$.

As a result of these studies, we re-affirm our belief stated previously (Reference 1), that the tail intensity will not be a useful

parameter for a satellite experiment for velocity and size determination in the high vacuum of interplanetary space (since its peak will depend in a random way on the local target surface finish), except as a possible means of material identification.

Results for the variation of spike intensity with range pressure are shown in Figures 18 and 19. In both figures, the intensity is normalized to a velocity of 5.2 km/sec by multiplying by $(5.2/V)^8$. The variation of the spike intensity at a wavelength of 3261Å (cadmium line) is shown in Figure 18. The variation with pressure is not large, and unlike the tail intensity, the spike intensity increases with decreasing pressure, the relationship being approximately $I(\text{spike}) \propto p^{-1/6}$. This means that a 100% error in pressure measurement (factor of 2) will result in an error in the intensity measurement of 16%.

The broadband spike intensity shown in Figure 19 exhibits a similar dependence on range pressure. We conclude that the spike intensity will continue to be a good parameter in the high vacuum of space.

## 4.4 Parametric Studies of Meteoritic Projectiles

Data have been collected on the impact flash characteristics influenced by the velocity, size and shape of projectiles made from meteoritic material when impacting a cadmium target. The impact flash spike intensity and rate of change of intensity at different wavelength bands centered at emission lines of cadmium and at 4900Å in the background have been measured. The diagnosis was conducted with the impact flash analyzer described in Section 2.

### 4.4.1 Velocity Dependence

The variation of the peak spike flash intensity with projectile velocity for projectiles of various sizes made from Canyon Diablo iron, and copper, is presented in Figures 20 through 23 showing the pertinent data which have been collected during the course of the present program.

Because of the structure of the Bruderheim stony material Canyon Diablo iron has been used most as projectile material. By the end of the program the effort has been concentrated mainly on 1.2 millimeter diameter spherical projectiles in order to establish the relationship between flash characteristics and projectile velocity. No more than 7 data points have been collected for a diameter of 1.2 millimeters at the four selected wavelength bands. Projectiles of any other diameter each have less data accumulated. In Figures 20 to 23 a power law trend can readily be observed. The scatter of the data allows a visual choice of slopes in the log-log plots between 7.5 and 9 for the different wavelengths. This is at variance with the conclusion of Reference 1, but whether this variation is real or due to a poor statistical sample in data collection will have to be demonstrated in further experiments. In the figure, a slope of 8 has been drawn across the points as a reference.

Some spherical Bruderheim projectiles have been successfully launched. It has been possible to fire projectiles, up to 1.6 mm in diameter, to a velocity of 6.0 km/sec. The peak spike intensity behaviour for the points obtained follows the trend observed for the Canyon Diablo iron projectile. For projectiles of equivalent size, the Bruderheim flash is slightly more intense than the Canyon Diablo. The data obtained are given in Figures 24 to 27. A power law trend similar to the one observed for copper or Canyon Diablo can be observed, but the scarcity of data does not allow a confirmation of the exponent. A reference line with a slope of 8 has been drawn across the data points.

The variation of rate of change of intensity with velocity is presented in Figures 28 to 31, for the Canyon Diablo and copper material and in Figures 32 to 35 for the Bruderheim stone material. In previous work involving the impact of copper spheres on cadmium (Reference 1) it was found that dI/dt varies as the 6th power of the velocity. In the present case a power law trend has been observed but the value of the exponent is surely larger than the previously obtained value. A reference line with a slope of 7.6 has been drawn across the collected data points. This slope has been obtained by averaging the four best visual fit slopes

which could be drawn at the four wavelengths measured.

### 4.4.2 Diameter Dependence

Intensities, and rates of change of intensities, have been normalized to an arbitrarily chosen velocity of 5.2 km/sec by multiplying the results by $(5.2/V)^{8}$ and $(5.2/V)^{7.6}$ respectively in accordance with the power trend law described above.

A strong dependence on diameter can be concluded from the best visual fit line drawn across the data points as seen in Figures 36 to 43. There is an average tendency for the intensity to vary as the fourth power of the diameter and for the rate of change of intensity as about the third power. One notices however, an important data spreading at a single diameter and in some cases a tendency for the point to lie on a curve of decreasing slope rather than a straight line. This tendency could be the result of scatter, which in turn depends stronly on the normalizing velocity power; or it could be physical. The limited Bruderheim data obtained are shown in Figures 44 to 51. The small number of data collected do not allow any conclusions to be drawn. A best visual fit of the data obtained may be indicative of a trend which in some cases resembles the data observed for the Canyon Diablo. The general behaviour observed will thus have to be clarified by the collection of more data when the projectile diameter is the only parameter permitted to vary.

### 4.4.3 Shape Effects

The influence of the shape of the projectiles on the intensity has been evaluated in the firing of polyhedron, oblate spheroid and prolate spheroid shaped Canyon Diablo iron projectiles with a mass of an equivalent 1.2 mm diameter sphere. The results are presented in Figure 52. These results have been normalized to the same velocity and their relative variation of intensity and rate of change of intensity are shown at the four monitored wavelength bands. Both prolate and oblate show very

large variations in flash intensity at all wavelengths. This behaviour actually confirms the correctness of the theoretical model used to describe the origin of the impact flash. In this model the radius of the impacting surface is the governing factor in the flash and jet generation. Thus the oblate spheroid, which presents a large radius of curvature at the impact point, will produce a flash whose intensity corresponds to that radius. The situation is reversed for the prolate spheroid. The observed intensities correspond to those anticipated for the radius of curvature of the impacting surfaces in each case.

In the case of the polyhedron shaped projectiles, if the number of facets is large the projectile will behave more like the corresponding sphere. The number of facets that can be filed on a projectile will increase with the projectile diameter, consequently smaller variations will be expected for polyhedron shaped projectiles of larger size. This effect is observed with 3.2 mm copper projectiles as reported in Reference 1, and presented in Figure 53. This experiment is aimed to evaluate the amount of intensity fluctuation which may arise from actual micrometeorite impacts. It is to be expected that a spherical projectile is the most probable if the micrometeorite has been produced in the melted form, or will be made of facets if it is broken fragments of a larger parent; oblate or prolate spheroid are statistically the least likely shapes.

## 4.5 Material Identification

In the course of our research on impact flash, the time integrated radiation energy has been spectroscopically examined from the near infrared to the ultraviolet region of the electro-magnetic spectrum. Time and space integrated spectrograms have revealed that the radiation is characterized by line emission of the elements involved in the collision, or their ions. If the spectrum is space resolved, continuum is also observed at the impact point peaking at spectral regions where persistent line emissions are recorded. Consequently, from the experimental observation of the spectrograms, it appeared possible to uniquely

identify the presence or absence of certain emission lines which could lead to an identification of the composition of the projectile, and this could be achieved electronically monitoring those wavelength bands where the presence or absence of the selected emission could be observed. Spectrograms of the radiation emitted at impact for copper, Canyon Diablo meteorite iron, Bruderheim stone and carbon are presented in Figure 5. A schematic representation of the filter bandwidth location in the spectrum is also given.

Thus a second cluster of flash sensors has been installed at the experimental area, to test the feasibility of meteorite type identification by monitoring the radiation at specified wavelength bands. The filters have been selected following the description given in Section 2. The bands have been chosen such that no or very little contribution from foreign elements should be observed at the selected band as seen on the spectrogram of Figure 5.

In order to test the concept, a copper projectile was launched against cadmium. The spectrogram shown in Figure 54 shows that, as expected, no radiation is recorded at the 3735Å, 2866Å, and 2480Å bands. A weak presence of aluminum and calcium can be detected at the 3966A band and the CD II 2748Å transition in the 2707Å band. According to this picture of the phenomenon, no or very little signal should be received from the photomultipliers monitoring these bands. The experiment, however, has clearly demonstrated the contrary, as seen in photomultiplier records shown in Figure 55. Similar results have been obtained for Bruderheim and Canyon Diablo impacts. The results are tabulated in Table 2. A comparison between all the material used, Figure 56 shows that the intensity of all wavelength bands follows a pattern which is independent of the material involved.

Since the short duration pulse is unexpectedly seen at all wavelength bands, regardless of material, this suggests that the pulse is caused by phenomena other than line emission or line broadening. Two possibilities are that the radiation in the pulses arises either from

ionized species which happen to radiate briefly in these bands, or from a high temperature plasma radiating as a black body. The reason why the spectrograms do not show signs of emission other than the line and line braodening of certain transitions, is associated with the fact that the spectrogram responds to radiation, whereas the photomultiplier observes the intensity amplitude of the very short duration initial pulse. In the case of the spectrogram the short duration pulse may be completely missed by the emulsion, in spite of its large amplitude.

The above interpretation would not be at odds with our theoretical model of the flash, which suggested that the short duration pulse of radiation originates in high temperature material, radiating only as the angle between the projectile and target surfaces passes through the "critical angle". The presence of ionization has indeed been spectroscopically observed for a projectile of magnesium-lithium impacting a cadmium target at 9.9 km/sec in an in-house experimental program, Figure 57. Due to the impact energy involved at these velocities, the ionization is very well observed. The distribution of intensities in Figure 57 also tends to suggest the presence of continuum radiation. If continuum radiation is the major contributor to the observed spike intensity at higher impact velocities, then this will lend weight to the expectation that a power law relationship between intensity and velocity will exist even at velocities much higher than those achieved in our experiments. The peak intensity will in this case depend on black body temperature which will increase with impact velocity. Line emission, on the other hand, which depends on the concentration of the atomic species will decrease with the appearance of ions at higher impact velocities. The atomic emission will re-appear with decreasing temperature as the impact proceeds. The possibility of material identification still remains since spectrograms of the flash have repeatedly been recorded which uniquely defined the elements involved in the collision. The information recorded on the spectrogram will have to be retrieved electronically. This can possibly be achieved by replacement of the time integrating emulsion by a time integrating photomultiplier circuit. This could be adapted to the existing sensor package.

## 4.6 Carbon Identification

Firings have been conducted to determine experimentally if an impact of a carbon projectile on a cadmium target at velocities of 6 to 7 km/sec will be sufficient to excite some of the carbon transitions. The most persistent line of carbon is a transition at 2478Å, which corresponds to 5.0 e.v. According to energy and momentum conservation, as described by Clark (Reference 8), a minimum velocity of 9.4 km/sec is required to excite a 5.0 e.v. transition in a carbon-cadmium impact. However, in early impact flash experiments it was proved that transitions of 5.2 e.v. in aluminum-aluminum impacts could be observed at velocities of 6.5 km/sec. From the conservation laws, such a transition should theoretically require an impact velocity of 8.6 km/sec minimum. The observation of ionization at the impact point at 5 km/sec is a good indication that the hard sphere conservation rule does not hold. A similar agreement has been given to evaluate the chance of exciting the 2478Å transition in carbon by the hypervelocity impact process.

Sintered carbon projectiles were launched. This material turned out to be too friable to resist the launching accelerations. Cut diamond specimens were used and again launch difficulties were experienced. A diamond projectile with its culet set in the sabot stuck to one of the launching sabot fragments and flew off line. Reversing the projectile such that the specimen rested with its table on the sabot face, the projectile impacted on its culet. No flash was observed for reasons which can be explained by the shaped-charge theory.

A blunt nosed full calibre Zelux polycarbonate projectile was also fired at 6 km/sec. The spectrum obtained shows the 2478Å carbon emission line among all other lines associated with the impurities and elements used in the formation of Zelux.

Still better results have been obtained with a 3.2 mm sphere of "electro graphitic" carbon launched against cadmium at 7 km/sec. The spectrum obtained is reproduced in Figure 58. It shows among impurities the presence of highly excited cadmium and the presence of carbon emission

at 2478Å, singly ionized at 2846Å and a faint line at 2296Å corresponding to a doubly ionized carbon transition.

## 5. CONCLUSION

In the course of the present program a meteoroid impact flash analyzer was constructed. It consists of a package containing nine photomultipliers monitoring, through specially selected narrow band interference filters, nine different wavelength bands of the electromagnetic spectrum in order to provide information on the characteristics of the meteoroid size, velocity and composition.

The laboratory verification of the concept has been conducted by monitoring the radiation emitted by the impact of a projectile on a target. The first phase of the experimental research has proved the validity of the concept for copper impacting cadmium. In the present program the verification of the concept was extended to actual samples of meteorite material impacting a cadmium target.

Prior to the meteorite analysis experiments, firings were conducted to evaluate the influence exerted by the ambient range pressure on the flash characteristics. This influence, which predominates in the recorded tail of the flash, can be neglected for the spike if the pressure is maintained below $10^{-4}$ Torr.

Profiles of the cadmium emission lines to be monitored by the photo-sensor have been studied in a series of firings in order to properly select the bandwidth of the filters. The profile thus obtained led to a choice of a filter bandwidth of 80Å to 100Å.

The determination of the meteorite projectile velocity and size from a measure of its impact flash characteristics is a feasible task. A strong influence of the projectile parameters on the flash intensity and rate of change of intensity has indeed been observed and measured. However, the data which have been collected in the course of the present program for meteorite materials do not yet fully confirm the empirical relationships which related the impact flash characteristics to the projectile parameters for copper (Reference 1). The variation of I and dI/dt as respectively the 8th and 7.6 power of the velocity is still

subject to uncertainty due to the too large a spread over several parameters (diameter, velocity, material and shape). This could be clarified by data collected in fixed diameter Canyon Diablo iron spheres launched at various velocities, in order to have a better distribution of data.

The dependence of the flash intensity and rate of change of intensity with projectile diameter for Canyon Diablo is still open to discussion for the same reason. In a log-log presentation of the empirical law the linearity of the variation of the logarithm of the intensity and rate of change of entensity with the logarithm of the projectile diameter may be subject to question. A deviation from linearity seems to be present at large diameters in some cases but whether this effect is real or simply due to the spread of the data remains to be determined. This could be clarified by the firing of Canyon Diablo iron projectiles at constant velocity.

In the case of Bruderheim material, the results generally follow those previously obtained for copper, and Canyon Diablo. However, as yet only few data are available.

Results have been obtained from the unit of the analyzer built to provide information on the meteorite type from the impact signature. It has been observed that the spike peak intensity at different wavelength bands has the same relative amplitude irrespective of the elements present at impact. This unexpected observation reopens the question of the exact nature of the radiation emitted in the spike and calls for a series of controlled experiments to define it. The existence, however, of a unique spectral distribution recorded photographically for each type of projectile material suggests that a time-integrated photomultiplier signal may be used to identify the emission of specific elements in a given wavelength band.

## 6. REFERENCES


1. Rollins, T.L. Jean, B. — Impact Flash for Micrometeoroid Detection. ComDev Report 9899/FR1, NASA Contract NAS9-6790, May 1968.

2. Linder, S.L. — Applied Optics 6, 1201, (1967).

3. Krinov, E.L. — Principles of Meteoritics. Pergamon Press.

4. — NASA Design Standard Bulletin No. DS-21.

5. — Pulse Code Modulation Telemetry Standard. NASA Goddard Space Flight Center, January 27, 1966.

6. Duke, M., Maynes, D., Brown, H. — Journal of Geophysical Research 66, 3557, (1961).

7. Moore, C.G., Birrel, P.J., Lewis, C.F. — Geochim. Cosmochim. ACTA 31, 1885, (1961).

8. Clark, J.S., Kadesch, R.R., Grow, R.W. — Spectral Analysis of the Impact of Ultra Velocity Copper Spheres into Copper Targets. AFOSR TN 60-13, September 1959.

| Shot No. | 151 | 154 | 155 | 160 | 161 | 162 | 163 | 164 | 166 | 171 | 173 |
|---|---|---|---|---|---|---|---|---|---|---|---|
| Velocity, km/sec | 5.29 | 5.16 | 3.78 | 5.22 | 5.00 | 5.08 | 5.11 | 5.19 | 5.24 | 5.88 | 5.98 |
| Pressure, Torr | $10^{-1}$ | 9.0 | 760 | $4x10^{-5}$ | $3.5x10^{-5}$ | $1.5x10^{-2}$ | $2.5x10^{-4}$ | $2x10^{-3}$ | $4x10^{-5}$ | $3.8x10^{-5}$ | $4x10^{-5}$ |
| Projectile Material | Fe | Fe | Fe | Brud. | Fe | Fe | Fe | Fe | Cu | Cu | Cu |
| Projectile Dia. (mm) | 3.18 | 3.18 | 3.18 | 1.0 | 3.18 | 3.18 | 3.18 | 3.18 | 3.18 | 3.18 | 3.18 |
| Exit Slit (microns) | 2000 | 2000 | 2000 | 2000 | 2000 | 2000 | 2000 | 2000 | 2000 | 500 | 8000 |
| Broadband Intensity | 20,000 | 11,400 | 6,450 | | 500 | | 1000 | 3000 | | | |
| 3261Å I, $\mu w/cm^2$ @ 1M | | | | | 119. | 6.4 | 93. | 83. | 110. | 67. | 1370. |
| dI/dt, $\mu w/cm^2$/sec @ 1M | | | | | 1850. | 178. | 1320. | 1270. | 245. | 172. | 1340. |
| 3610Å I, $\mu w/cm^2$ @ 1M | | | | 29.8 | | | | | 445. | 433. | 3390. |
| dI/dt, $\mu w/cm^2$/sec @ 1M | | | | | | | | | | | |
| 4900Å I, $\mu w/cm^2$ @ 1M | | | | | | | | | | 42.2 | 86.5 |
| dI/dt, $\mu w/cm^2$/sec @ 1M | | | | | | | | | | | |
| 5085Å I, $\mu w/cm^2$ @ 1M | | | | 13.7 | | | | | 470. | 409. | 3790. |
| dI/dt, $\mu w/cm^2$/sec @ 1M | | | | | | | | | | | |

Table 1A

Table 1A. Record of Firings

| Shot No. | 189 | 190 | 193 | 196 |
|---|---|---|---|---|
| Projectile Material | Brud. | Brud. | Brud. | Brud. |
| Projectile Velocity km/sec | 6.01 | 6.21 | 7.20 | 6.85 |
| Projectile Diameter (mm) | 1.0 | 1.0 | 1.0 | 1.5 |
| Projectile Mass (mgr.) | 1.5 | 1.4 | 1.7 | 6.1 |
| Range Pressure Torr ($10^5$) | 2.1 | 2.6 | 4.0 | 3.8 |
| Broadband Spike Relative Intensity | 45 | 77 | 100 | 200 |
| Broadband Rate of Change of Intensity | $1.2 \times 10^3$ | $1.1 \times 10^3$ | $2.6 \times 10^3$ | $4.4 \times 10^3$ |

Table 1B. Record of Firings

| Shot No. | 202 | 203 | 204 | 206 | 208 | 209 | 211 | 212 | 228 | 254 | 255 |
|---|---|---|---|---|---|---|---|---|---|---|---|
| Projectile Material | Cu | Diamond | Cu | Cu | Cu | Cu | Cu | Cu | Cu | Cu | Cu |
| Projectile Dia. (mm) | 1.2 | 1.8/2.0 | 1.2 | .6 | .6 | .6 | .3 | .3 | 1.2 | .6 | .6 |
| Projectile Mass (mgr) | 6.4 | 5.9 | 8.4 | 1.1 | 1.3 | .7 | .25 | .3 | 8.13 | 1.2 | 1.2 |
| Velocity (km/sec) | 6.7 | 6.31 | 6.36 | 6.33 | 6.99 | 7.2 | 5.95 | 7.04 | 5.93 | 5.31 | 5.17 |
| 5085Å I, $\mu w/cm^2$ @ 1M | | | 34.6 | 15.84 | 48.44 | 31.4 | .204 | 16.28 | 84.7 | No Spike | No Spike |
| dI/dt, $\mu w/cm^2/sec$ @ 1M | | | 945.7 | 177 | 1097 | 717.6 | 5.56 | 281.4 | 1377.1 | " | " |
| $I\ (5.2/V)^8$ | | | 6.9 | 3.3 | 4.5 | 2.3 | .069 | 1.4 | 29.6 | | |
| $dI/dt\ (5.2/y)^{7.6}$ | | | 204.7 | 39.7 | 115.8 | 60.5 | 1.9 | 28.1 | 507.0 | | |
| 3610Å I, $\mu w/cm^2$ @ 1M | | | 6.58 | 13.45 | 1.795 | 24.95 | .26 | 7.83 | 125.5 | | |
| dI/dt, $\mu w/cm^2/sec$ @ 1M | | | 111.6 | 404 | 19.16 | 357.7 | 6.53 | 92.95 | 2148.5 | | |
| $I\ (5.2/V)^8$ | | | 1.31 | 2.82 | .172 | 1.84 | .088 | .693 | 43.9 | | |
| $dI/dt\ (5.2/V)^{7.6}$ | | | 24.2 | 90.6 | 2.02 | 30.2 | 2.34 | 9.30 | 791.6 | | |
| 4900Å I, $\mu w/cm^2$ @ 1M | 21.09 | | 77.2 | | 21.15 | 16.38 | | 10.66 | 115.9 | | |
| dI/dt, $\mu w/cm^2/sec$ @ 1M | 280.5 | | 995.0 | | 407.6 | 285.0 | | 220. | 1692.6 | | |
| $I\ (5.2/V)^8$ | 2.77 | | 15.4 | | 2.00 | 1.21 | | .944 | 40.5 | | |
| $dI/dt\ (5.2/y)^{7.6}$ | 40.8 | | 215.4 | | 43.0 | 24.0 | | 22.0 | 623.6 | | |
| 3261Å I, $\mu w/cm^2$ @ 1M | | | | | | | | | 150 | | |
| dI/dt, $\mu w/cm^2/sec$ @ 1M | | | | | | | | | 6500 | | |
| $I,(5.2/y)^8$ | | | | | | | | | 52.4 | | |
| $dI/dt\ (5.2/y)^{7.6}$ | | | | | | | | | 2395. | | |

SPECTRUM

Table 1C

| Shot No. | 257 | 258 | 268 | 270 | 289 | 285 | 296 |
|---|---|---|---|---|---|---|---|
| Projectile Material | Brud. | Brud. | Brud. | Brud. | Brud. | Cu | Cu |
| Projectile Dia. (mm) | 1.2 | 1.2 | .6 | 1.6 | .3 | 1.2 | 1.2 |
| Projectile Mass (mgr) | 3.18 | 3.22 | .41 | 6.9 | | 5.8 | 7.3 |
| Velocity (km/sec) | 5.5 | 4.14 | 5.98 | 5.44 | 6.03 | 5.97 | 5.66 |
| 5085Å I, $\mu w/cm^2$ @ 1M | 183.6 | 16.08 | 7.31 | 227.01 | 1,065 | 32.5 | 157.4 |
| dI/dt, $\mu w/cm^2/sec$ @ 1M | 2595.4 | 266.9 | 179.3 | 1005.3 | 28.25 | 631.8 | 947.5 |
| I $(5.2/V)^8$ | 117,2 | 99.61 | 2.38 | 158,2 | .325 | 10.76 | 79.89 |
| dI/dt $(5.2/V)^{7.6}$ | 1694.6 | 1509.2 | 61.98 | 713.4 | 9.167 | 221.2 | 497.5 |
| 3610Å I, $\mu w/cm^2$ @ 1M | 161,5 | 24.7 | 13.32 | 224.8 | .997 | | 134.1 |
| dI/dt, $\mu w/cm^2/sec$ @ 1M | 855.9 | 618.4 | 227.2 | 6161.5 | 25.3 | | 979.4 |
| I $(5,2/V)^8$ | 103.1 | 153.0 | 4,35 | 156.6 | .304 | | 68.10 |
| dI/dt $(5.2/V)^{7,6}$ | 558.8 | 3496.9 | 78.54 | 4379.9 | 8.20 | | 514.2 |
| 4900Å I, $\mu w/cm^2$ @ 1M | 65,5 | 7.95 | 4,09 | | .68 | 37.6 | 1261.7 |
| dI/dt, $\mu w/cm^2/sec$ @ 1M | 1251,6 | 126.6 | 930.0 | | 13.0 | 865.9 | 1.265 |
| I $(5.2/V)^8$ | 41.81 | 49.24 | 1.33 | | .207 | 12.45 | 640.4 |
| dI/dt $(5.2/V)^{7.6}$ | 817.2 | 715,9 | 321,4 | | 4,21 | 303,1 | .664 |
| 3261Å I, $\mu w/cm^2$ @ 1M | 135,9 | 12,9 | 5,45 | 220,6 | .385 | 34 | 139.5 |
| dI/dt, $\mu w/cm^2/sec$ @ 1M | 4520,8 | 302,9 | 168,4 | 22307.3 | 6.81 | 319,8 | 2961.9 |
| I $(5.2/V)^8$ | 86,76 | 79,91 | 1,781 | 153.7 | .117 | 11,26 | 70.8 |
| dI/dt $(5.2/V)^{7.6}$ | 2951,7 | 1712.8 | 58.21 | 15831,4 | 2,209 | 111.9 | 1555 |

Table 1C





Table 1C. Record of Firings (continued)

| Shot No. | 306 | 320 | 322 | 325 | 312 | 318 | 323 | 328 | 332 | 333 |
|---|---|---|---|---|---|---|---|---|---|---|
| Projectile Material | Brud. | Brud. | Brud. | Brud. | CanDi | CanDi | CanDi | CanDi | CanDi | CanDi |
| Projectile Dia. (mm) | .6 | .6 | 1.2 | 1.2 | 3.2 | 1.2 | 4.8 | .3 | 2.4 | .6 |
| Projectile Mass (mgr) | .81 | .73 | 3.7 | 3.25 | 152.9 | 7,35 | 505.1 | | 61.9 | 1.14 |
| Velocity (kn/sec) | 4.16 | 7.33 | 7.51 | 4.97 | 4.98 | 7.29 | 5.35 | 5.32 | 6.12 | 6.15 |
| 5085Å I, $\mu w/cm^2$ @ 1M | .459 | 5.77 | | | 468.9 | 440.9 | | 1.45 | 326.6 | 2.44 |
| dI/dt, $\mu w/cm^2/sec$ @ 1M | 3.7 | 255.7 | | | 4054.4 | 3644.5 | | 23.05 | 6640.5 | 47.03 |
| $I\ (5.2/y)^8$ | 2,735 | .370 | | | 662.6 | 29.54 | | 1.2 | 88.72 | .637 |
| $dI/dt\ (5.2/y)^{7.6}$ | 20.17 | 18.81 | | | 5631,3 | 279.5 | | .002 | 1928.2 | 13.13 |
| 3610Å I $\mu w/cm^2$ @ 1M | .435 | 26.05 | 224.9 | 18.71 | 1649 | 504.4 | 963.5 | 1.61 | 695.9 | 3.13 |
| dI/dt, $\mu w/cm^2/sec$ @ 1M | 3.93 | 964.7 | 12152.4 | 443.1 | 19838.5 | 11762. | 11389.9 | 47.9 | 11310.1 | 109.9 |
| $I\ (5.2/y)^8$ | 2.6 | 1.67 | 11.88 | 26.86 | 2330 | 33.8 | 767.4 | 1.34 | 189.04 | .817 |
| $dI/dt\ (5.2/y)^{7.6}$ | 21,4 | 10.99 | 279.3 | 624.91 | 27554.4 | 902.3 | 9176.0 | .041 | 3279.29 | 30.702 |
| 4900Å I, $\mu w/cm^2$ @ 1M | ,531 | | 71.88 | 10.89 | 158,4 | 368.8 | 339.0 | .881 | 421.5 | 1.32 |
| dI/dt, $\mu w/cm^2/sec$ @ 1M | 4.95 | | 1784.8 | 226.1 | 1541.7 | 4489.9 | 5726.9 | 11.68 | 6837.4 | 37.59 |
| $I\ (5.2/y)^8$ | 3,16 | | 3.79 | 15.63 | 224.7 | 24.7 | 270.02 | .701 | 114.5 | .344 |
| $dI/dt\ (5.2/y)^{7.6}$ | 26,984 | | 109.23 | 318.87 | 27554.4 | 344.45 | 4613.7 | 9.409 | 1982.46 | 10.50 |
| 3261Å I $\mu w/cm^2$ @ 1M | .246 | 11,34 | 81.05 | 12.85 | | 394.2 | 303.3 | .583 | | .568 |
| dI/dt, $\mu w/cm^2/sec$ @ 1M | 4.57 | 180,5 | 1623.8 | 338.9 | | 6975.4 | 8562.1 | 19.32 | | 9.138 |
| $I\ (5.2/y)^8$ | 1.466 | .727 | 4.28 | 18.45 | | 26.426 | 239 | .464 | | .148 |
| $dI/dt\ (5.2/y)^{7.6}$ | 24,913 | 13.283 | 99.37 | 477.9 | | 535.13 | 7100 | 15.56 | | 2.552 |

Table 1C



Table 1C. Record of Firings (continued)

| Shot No. | 216 | 217 |
|---|---|---|
| Projectile Material | CanDi | CanDi |
| Projectile Dia. (mm) | 1.2 | .6 |
| Projectile Mass (mgr) | 7.0 | 1.0 |
| Velocity (km/sec) | 6.3 | 6.16 |
| 5085Å I, $\mu w/cm^2$ @ 1M | 194 | 5.27 |
| dI/dt, $\mu w/cm^2/sec$ @ 1M | 2641 | 83.47 |
| $I\ (5.2/V)^8$ | 41.79 | 1.35 |
| $dI/dt\ (5.2/V)^{7.6}$ | 614.5 | 23.0 |
| 3610Å I, $\mu w/cm^2$ @ 1M | 308.5 | 1.22 |
| dI/dt, $\mu w/cm^2/sec$ @ 1M | 3643. | 27.2 |
| $I\ (5.2/V)^8$ | 66.4 | .314 |
| $dI/dt\ (5.2/V)^{7.6}$ | 847.5 | 7.50 |
| 4900Å I, $\mu w/cm^2$ @ 1M | 121 | 3.22 |
| dI/dt, $\mu w/cm^2/sec$ @ 1M | 2334 | 52.66 |
| $I\ (5.2/V)^8$ | 26.06 | .830 |
| $dI/dt\ (5.2/V)^{7.6}$ | 543.0 | 14.53 |
| 3261Å I, $\mu w/cm^2$ @ 1M | 165.3 | .859 |
| dI/dt, $\mu w/cm^2/sec$ @ 1M | 1099. | 13.3 |
| $I\ (5.2/V)^8$ | 35.6 | .221 |
| $dI/dt\ (5.2/V)^{7.6}$ | 255.7 | 3.67 |

Table 1C

| 220 | 223 | 230 | 237 | 247 | 225 |
|---|---|---|---|---|---|
| CanDi | CanDi | CanDi | CanDi | CanDi | Z elux |
| 2.4 | 2.4 | 1.2 | 1.2 | 2.4 | 12.7 |
| 61.2 | 53.2 | 6.77 | 6.2 | 56.7 | 1750 |
| 6.04 | 4.09 | 3.59 | 7.04 | 5.2 | 5.85 |
| 337 | 17.1 | .945 | 212 | 298 | |
| 9200 | 323.3 | 29.3 | 3376. | 3180.2 | |
| 101.7 | 116.7 | 18.31 | 18.78 | 298 | |
| 2948.0 | 2005.0 | 489.5 | 337.6 | 3180.2 | |
| 748 | 14.11 | .566 | 259.9 | 389.1 | |
| 14934 | 331.1 | 22.7 | 7463.7 | 5306.2 | |
| 225.7 | 96.3 | 10.9 | 23.0 | 389.1 | |
| 4785.4 | 2053.4 | 379.2 | 746.4 | 5306.2 | |
| 497 | 19.3 | 1.04 | 127.2 | 225.2 | |
| 9176 | 439.4 | 14.72 | 2295.5 | 3200.9 | |
| 150 | 131.9 | 20.15 | 11.2 | 225.2 | |
| 2940.3 | 2725.9 | 245.9 | 229.5 | 3200.9 | |
| 394.2 | 8.72 | .48 | 66.9 | 212 | |
| 2791 | 84.3 | 15.37 | 2768.4 | 3782.7 | |
| 118.9 | 59.5 | 9.3 | 5.93 | 212 | |
| 894.3 | 522.8 | 256.7 | 276.8 | 3782.7 | |

CARBON SPECTRUM

Table 1C. Record of Firings (continued)

| Shot No. | 260 | 278 | 279 | 280 | 282 | 283 | 284 | 295 | 263 | 293 |
|---|---|---|---|---|---|---|---|---|---|---|
| Projectile Material | CanDi | CanDi | CanDi | CanDi | CanDi | CanDi | CanDi | CanDi | Carbon | Carbon |
| Projectile Dia. (mm) | .6 | 1.2 Polyhedron | 1.2 Prolate | 1.2 Oblate | 1.2 Polyhedron | 1.2 | 1.2 | 1.2 | 3.15 | 3.2 |
| Projectile Mass (mgr) | .7 | 9.73 | 6.42 | 7.92 | 6.01 | | 6.72 | 6.7 | 28.1 | 32.8 |
| Velocity (km/sec) | 7.27 | 4.72 | 4.66 | 5.14 | 4.71 | 4.58 | 5.94 | 5.66 | 7.57 | 7.13 |
| 5085Å I, $\mu w/cm^2$ @ 1M | 32.2 | | .555 | 74.6 | 17.05 | 8.11 | 32.6 | 22.1 | | |
| dI/dt, $\mu w/cm^2/sec$ @ 1M | 896.5 | | 13.7 | 1016. | 261 | 197.0 | 538.4 | 190.3 | | |
| $I\ (5.2/V)^8$ | 2.20 | | 1.33 | 81.8 | 37.0 | 22.6 | 11.2 | 11.2 | | |
| $dI/dt\ (5.2/V)^{7.6}$ | 70.2 | | 31.6 | 1499. | 550 | 223.9 | 195.8 | 99.9 | | |
| 3610Å I, $\mu w/cm^2$ @ 1M | 45.8 | 33.5 | .870 | 117 | 15 | 5.8 | | 19.55 | | |
| dI/dt, $\mu w/cm^2/sec$ @ 1M | 1528.9 | 755.5 | 13.0 | 1812. | 142 | 249. | | 240.0 | | |
| $I\ (5.2/V)^8$ | 3.13 | 72.7 | 2.09 | 128.3 | 33.1 | 16.1 | | 9.92 | | |
| $dI/dt\ (5.2/V)^{7.6}$ | 119.7 | 1577. | 29.9 | 1979. | 301 | 653.0 | | 126. | | |
| 4900Å I, $\mu w/cm^2$ @ 1M | 6.58 | 24 | .423 | 51.4 | 16.65 | 7.26 | 37.7 | 16.6 | SPECTRUM | SPECTRUM |
| dI/dt, $\mu w/cm^2/sec$ @ 1M | 128.3 | 291.3 | 16.7 | 818.3 | 206 | .149 | 1171. | 102.4 | | |
| $I\ (5.2/V)^8$ | .45 | 52.1 | 1.01 | 56.4 | 36.7 | 20.0 | 13.0 | 8.42 | | |
| $dI/dt\ (5.2/V)^{7.6}$ | 10.1 | 608.1 | 38.4 | 893.7 | 437. | 391. | 426.2 | 53.76 | | |
| 3261Å I, $\mu w/cm^2$ @ 1M | 30 | 9.34 | .47 | 48.0 | 4.74 | 1.26 | 37.3 | 10 | | |
| dI/dt, $\mu w/cm^2/sec$ @ 1M | 1175. | 205.9 | 14.6 | 851.6 | 62.5 | 43.9 | 823.8 | 137.8 | | |
| $I\ (5.2/V)^8$ | 2.05 | 20.3 | 1.13 | 52.7 | 10.4 | 3.49 | 12.86 | 5.07 | | |
| $dI/dt\ (5.2/V)^{7.6}$ | 92.1 | 429.9 | 33.7 | 930.1 | 132.6 | 115. | 299.6 | 72.3 | | |

Table 1C





Table 1C. Record of Firings (continued)

| WAVELENGTH (Å) | 5085 | 3610 | 4900 | 3261 | 2707 | 2866 | 3735 | 3942 | 2478 |
|---|---|---|---|---|---|---|---|---|---|
| Shot No. 289 - Bruderheim (.3 mm dia. - 6.03 km/sec) | | | | | | | | | |
| I, $\mu w/cm^2$ @ 1M | 1.065 | 1.07 | .68 | .385 | 6.86 | 2,12 | 1.325 | .494 | 3.31 |
| $I(5.2/V)^8 (1.2/d)^4$ | 83 | 83.4 | 53 | 30 | 535 | 165,3 | 103.3 | 38.5 | 258 |
| Shot No. 284 - CanDi (1,2 mm dia. - 5.94 km/sec) | | | | | | | | | |
| I, $\mu w/cm^2$ @ 1M | 32,6 | | 37,7 | 38,1 | 193,5 | 143.4 | 39 | 20.1 | 414 |
| $I(5.2/V)^8 (1,2/d)^4$ | 11,2 | | 12.96 | 13.2 | 66.5 | 49.3 | 13.4 | 6,91 | 142,2 |
| Shot No. 285 - Copper (1,2 mm dia. - 5.97 km/sec) | | | | | | | | | |
| I, $\mu w/cm^2$ @ 1M | 32.7 | | 37.6 | 34 | 194 | 143.5 | 39.1 | 18.4 | 451 |
| $I(5.2/V)^8 (1,2/d)^4$ | 10.73 | | 12,33 | 11.15 | 63.6 | 47.4 | 12.82 | 6.04 | 148 |

Table 2



Table 2. Intensities at Different Wavelengths for Different Materials

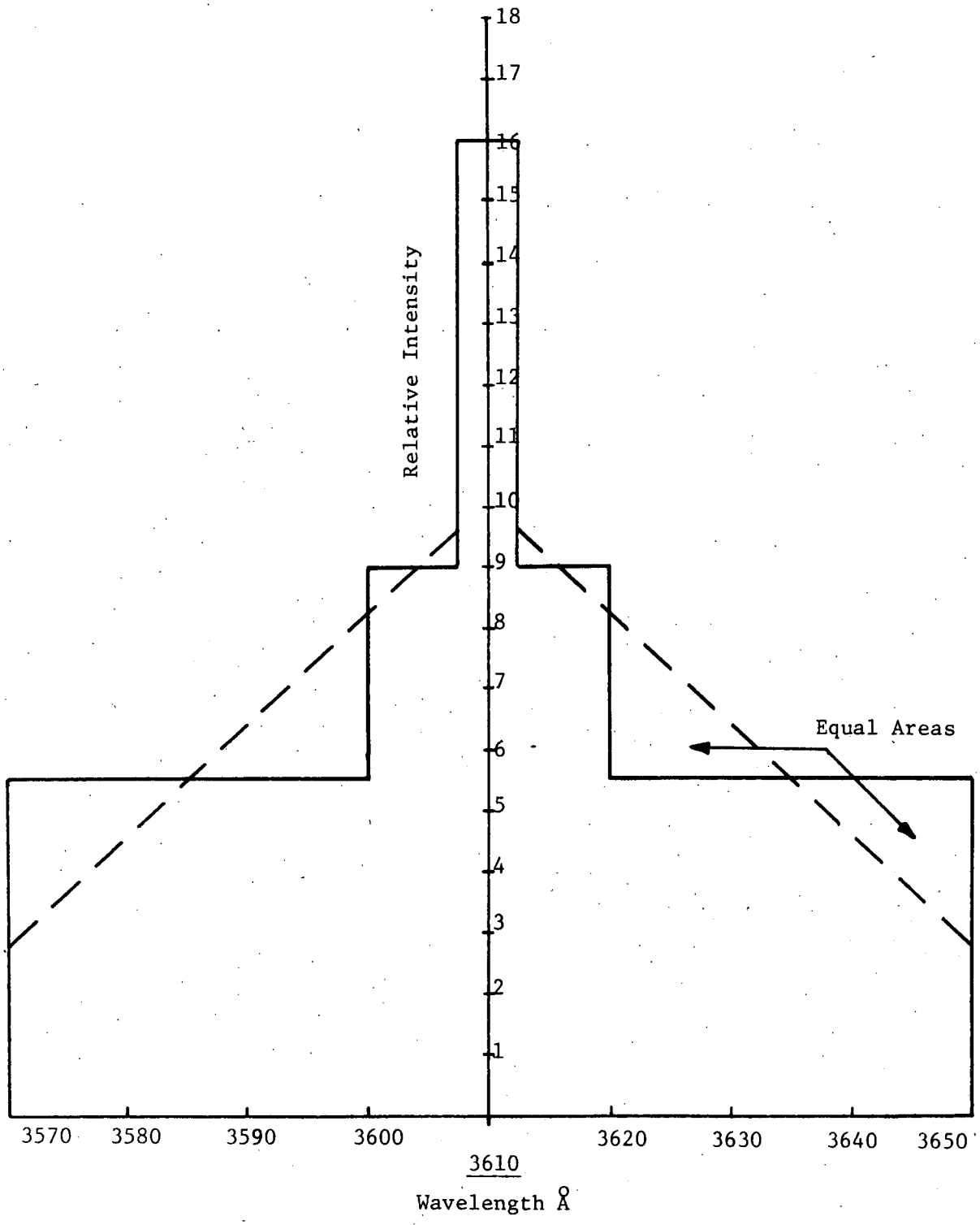


Figure 1. Spectral Distribution Around 3610Å Line

R134/FR1

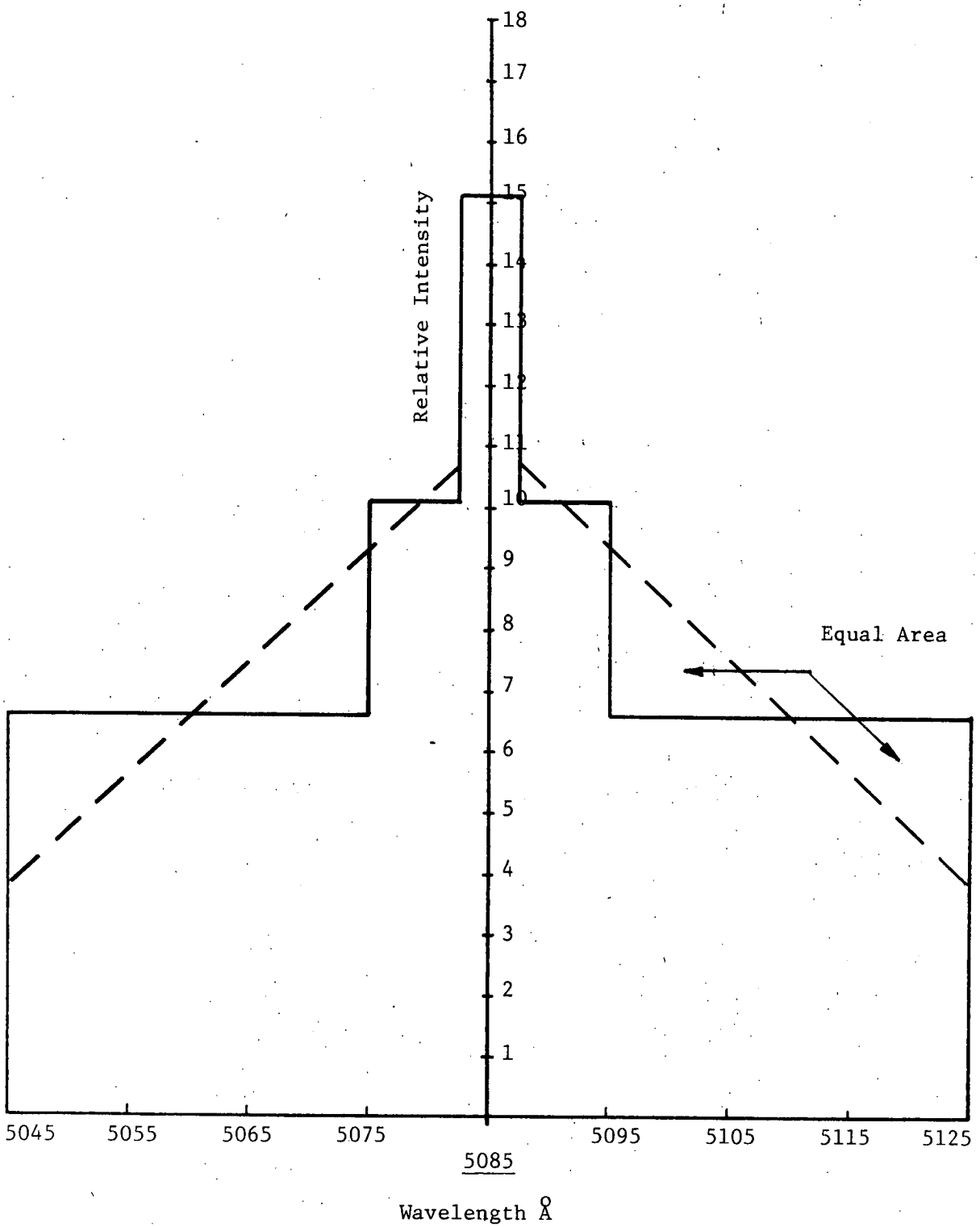


Figure 2. Spectral Distribution Around 5085Å Line

R134/FR1

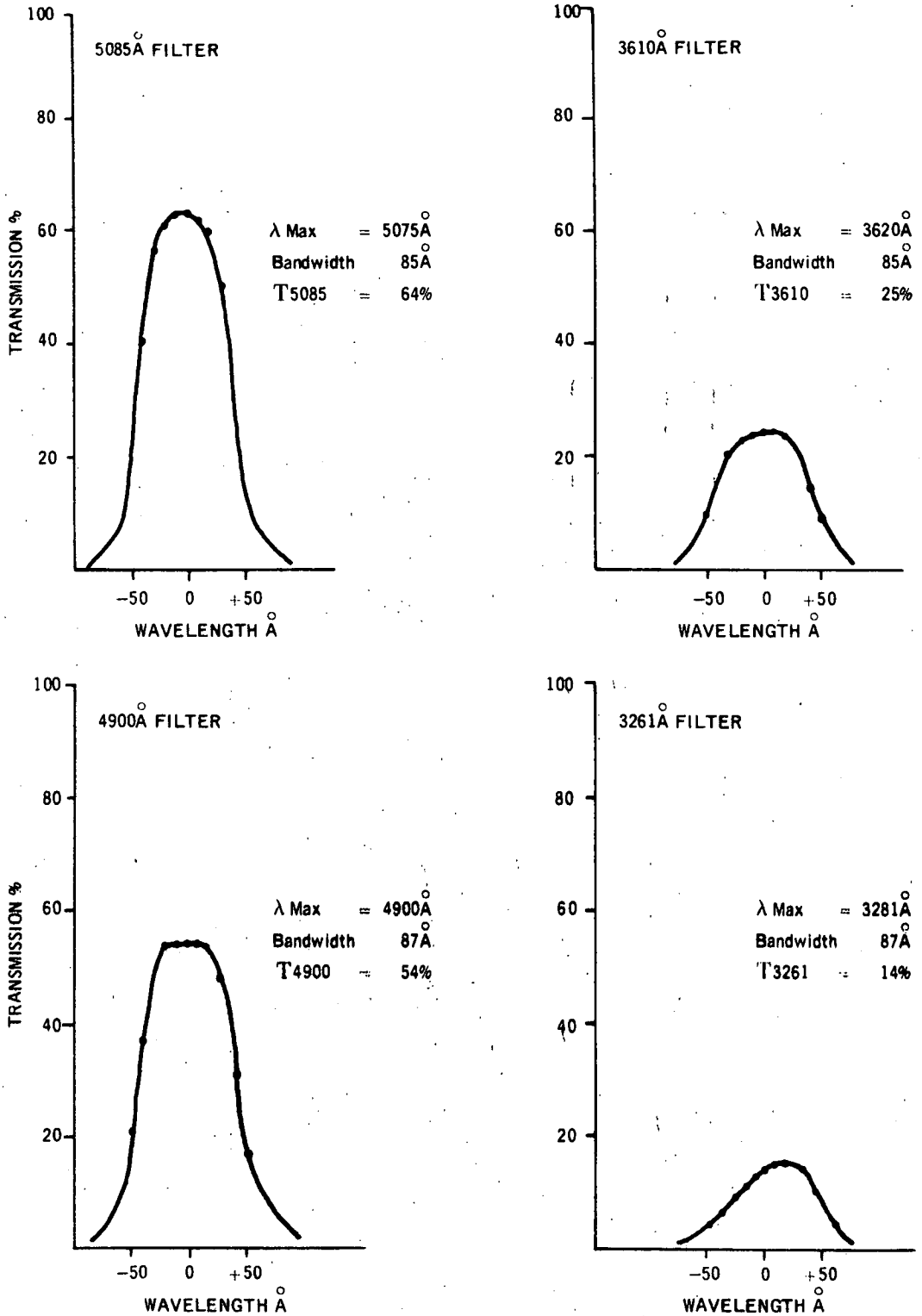


Figure 3. Transmissivity Curves of the Interference Filters Used to Monitor the Cadmium Emission

R134/FR1

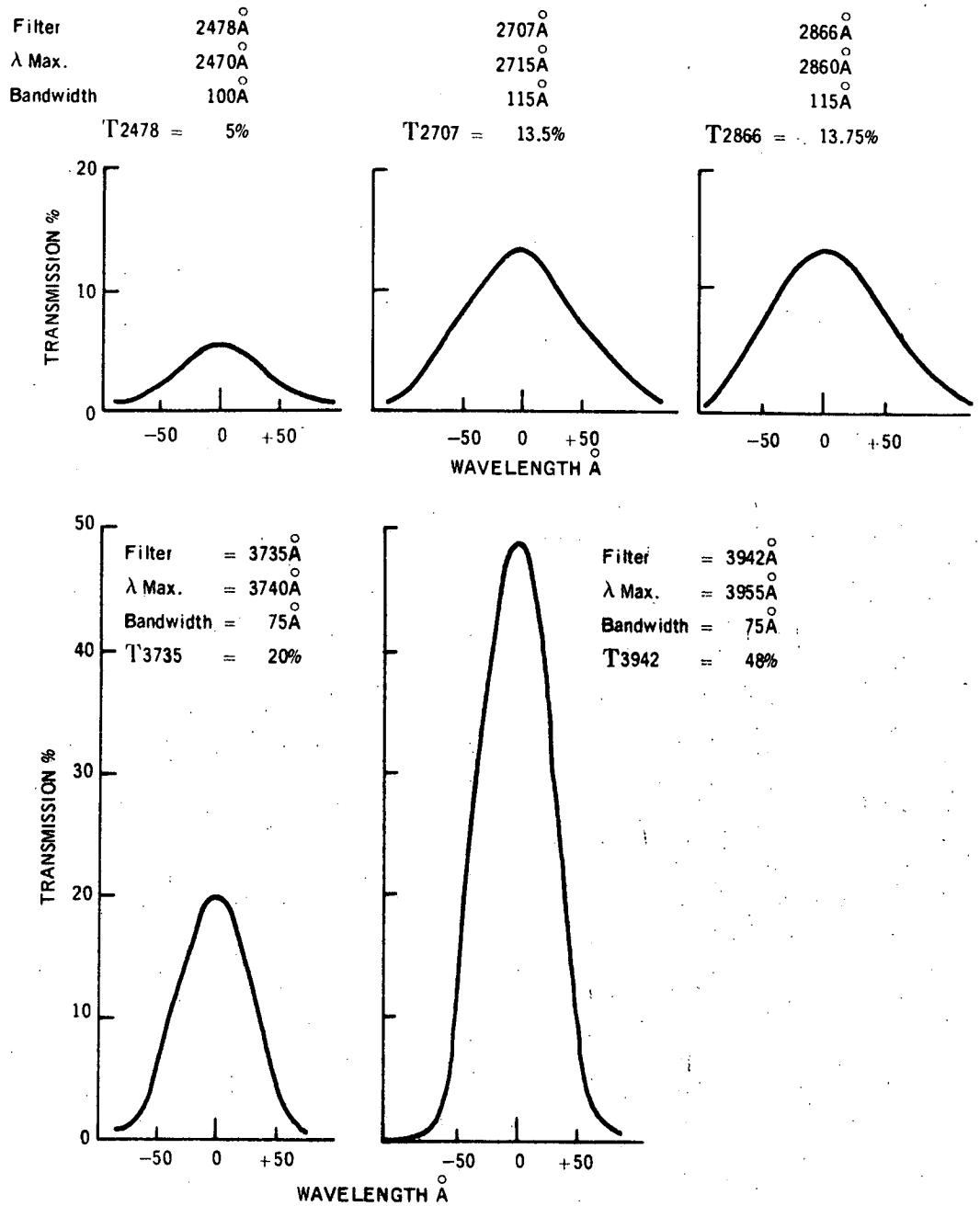


Figure 4. Transmissivity Curves of the Interference Filters Used for Meteorite Identification

R134/FR1

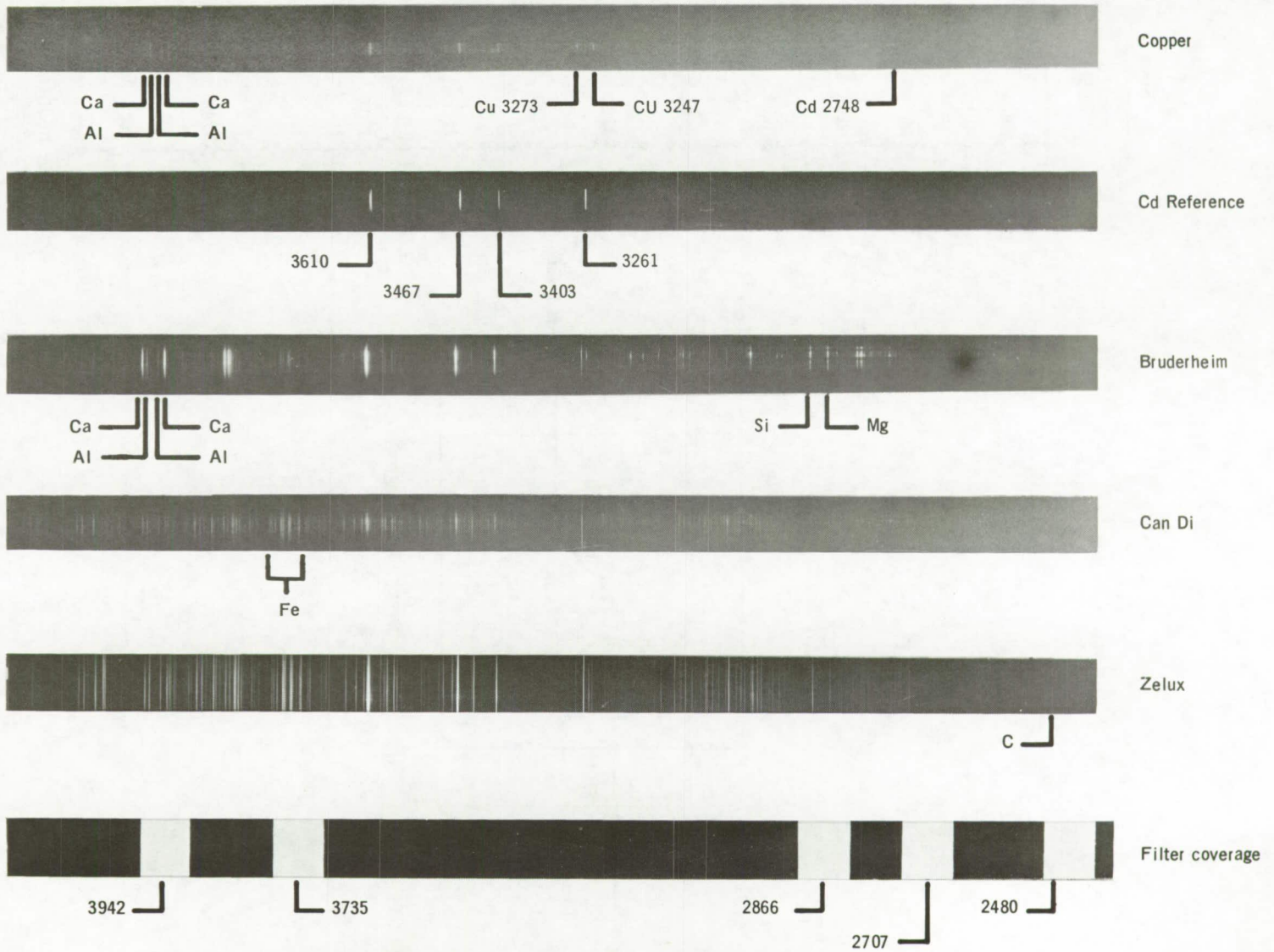


Figure 5. Comparative Presentation of Spectral Distributions for Bruderheim, CanDi, and Carbon Emission with Selected Filters

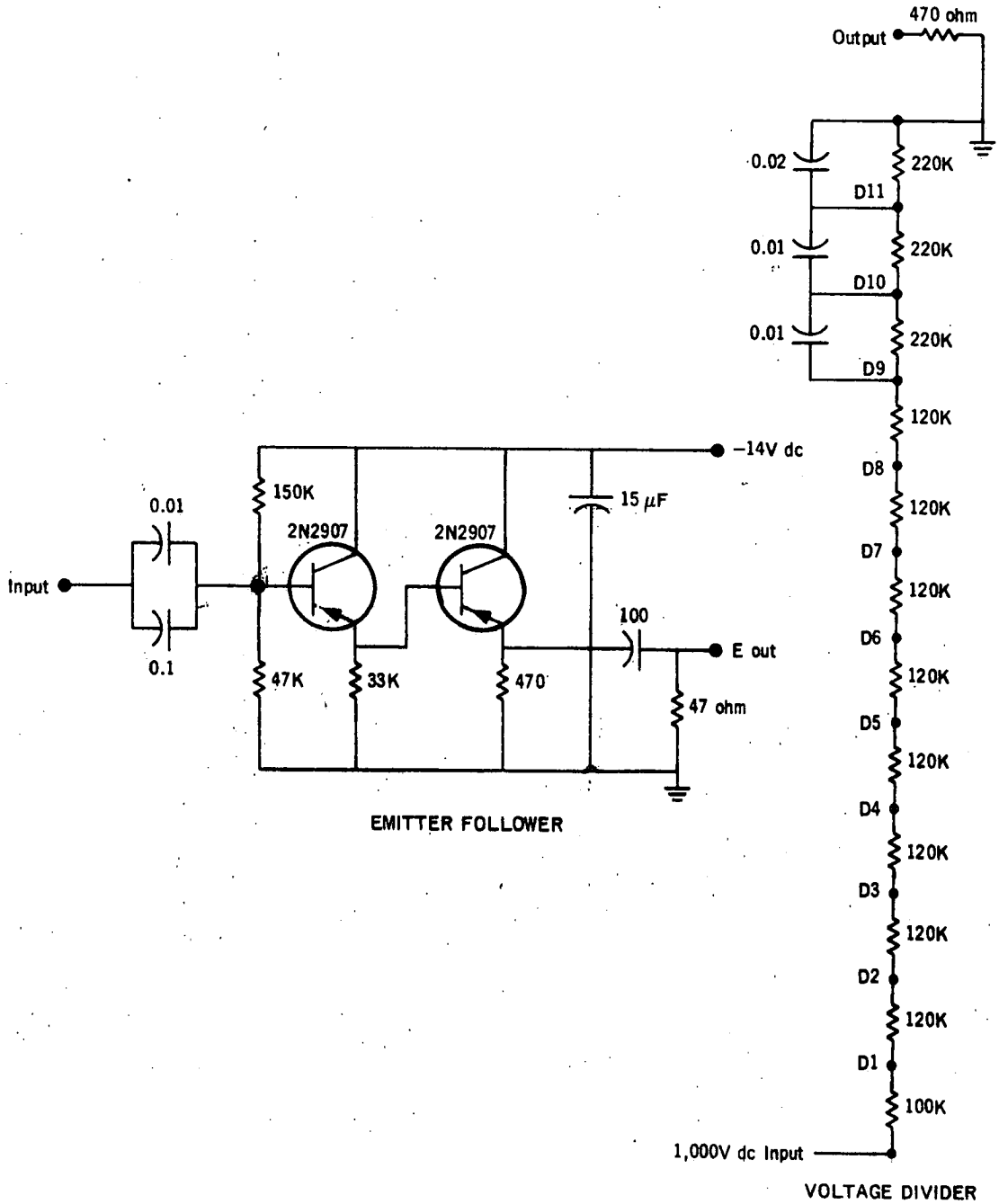


Figure 6. Circuit Diagram of the Photomultiplier Base Voltage Divider and Emitter Follower

R134/FR1

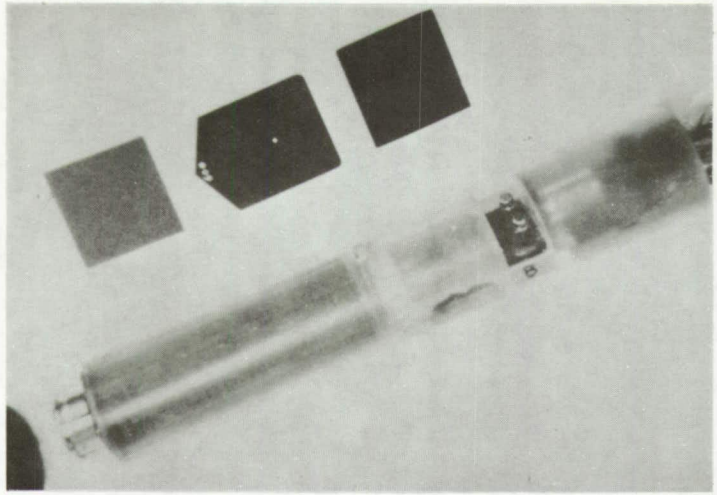

ASSEMBLED P.M. HOLDER WITH FILTERS AND APERTURE

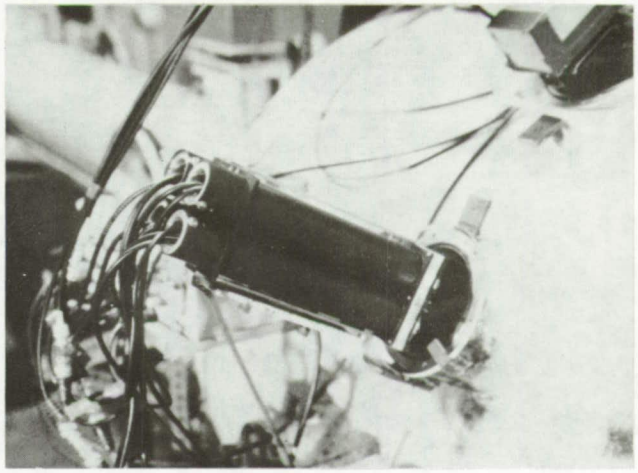

PACKAGE INSTALLED ON RANGE

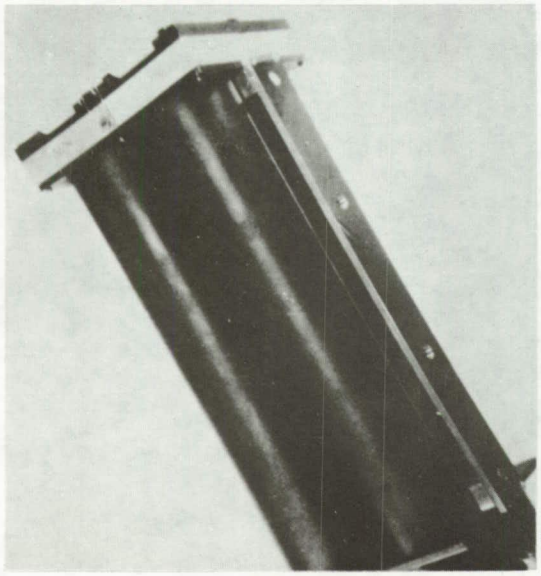

FOUR
PHOTOMULTIPLIER
PACKAGE SENSOR

Cd 3261Å
Cd 3610Å
Cd 5085Å
Bg 4900Å

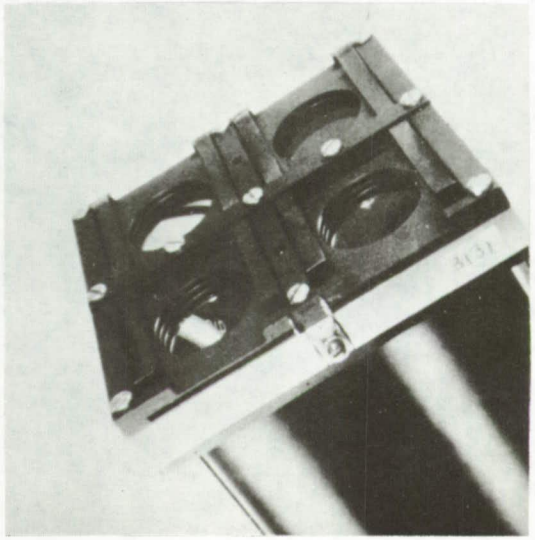

Figure 7. Sensor Package Assembly and Installation

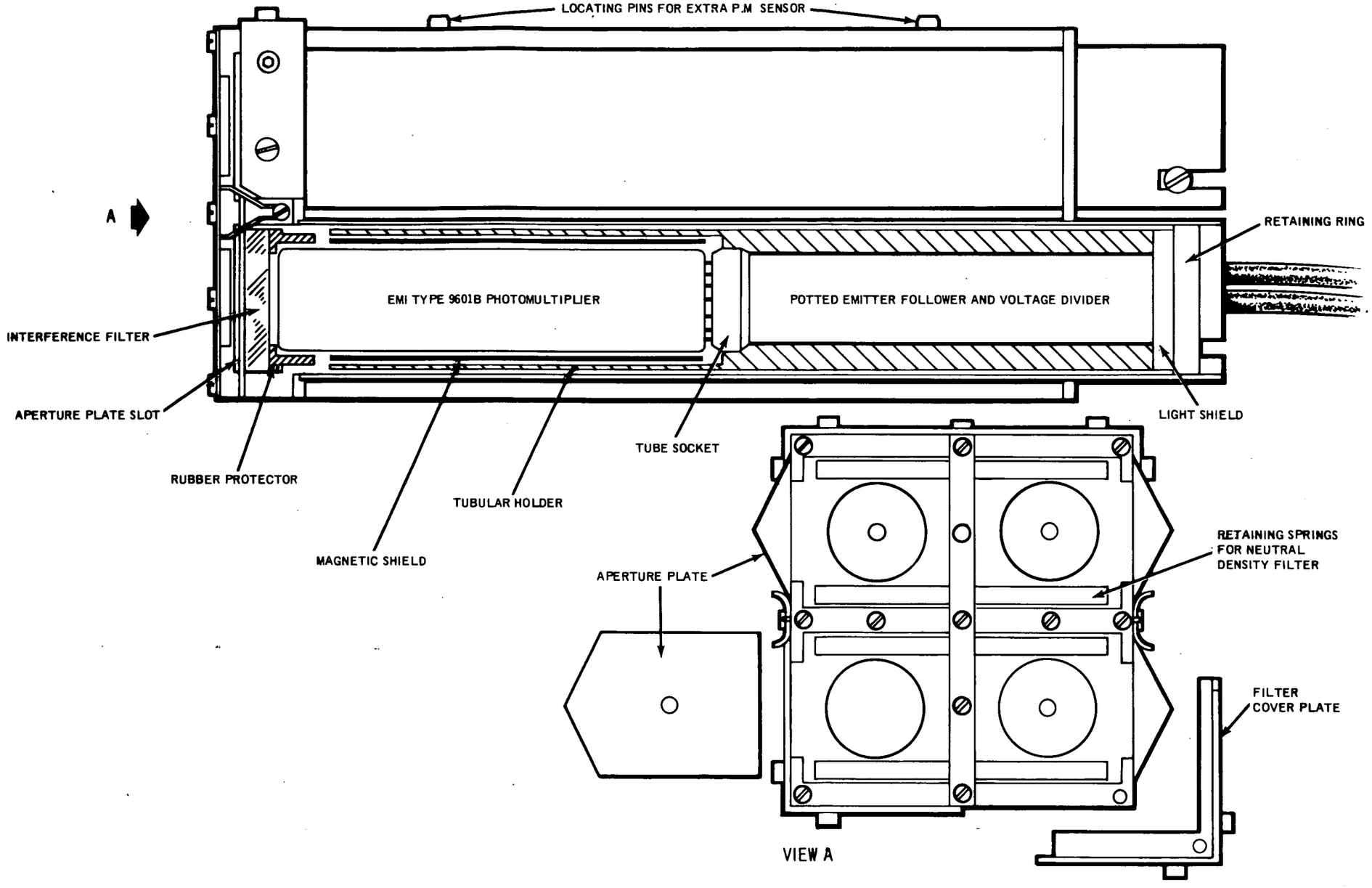


Figure 8.



Figure 8. Detailed Construction of a Photomultiplier Sensor Package

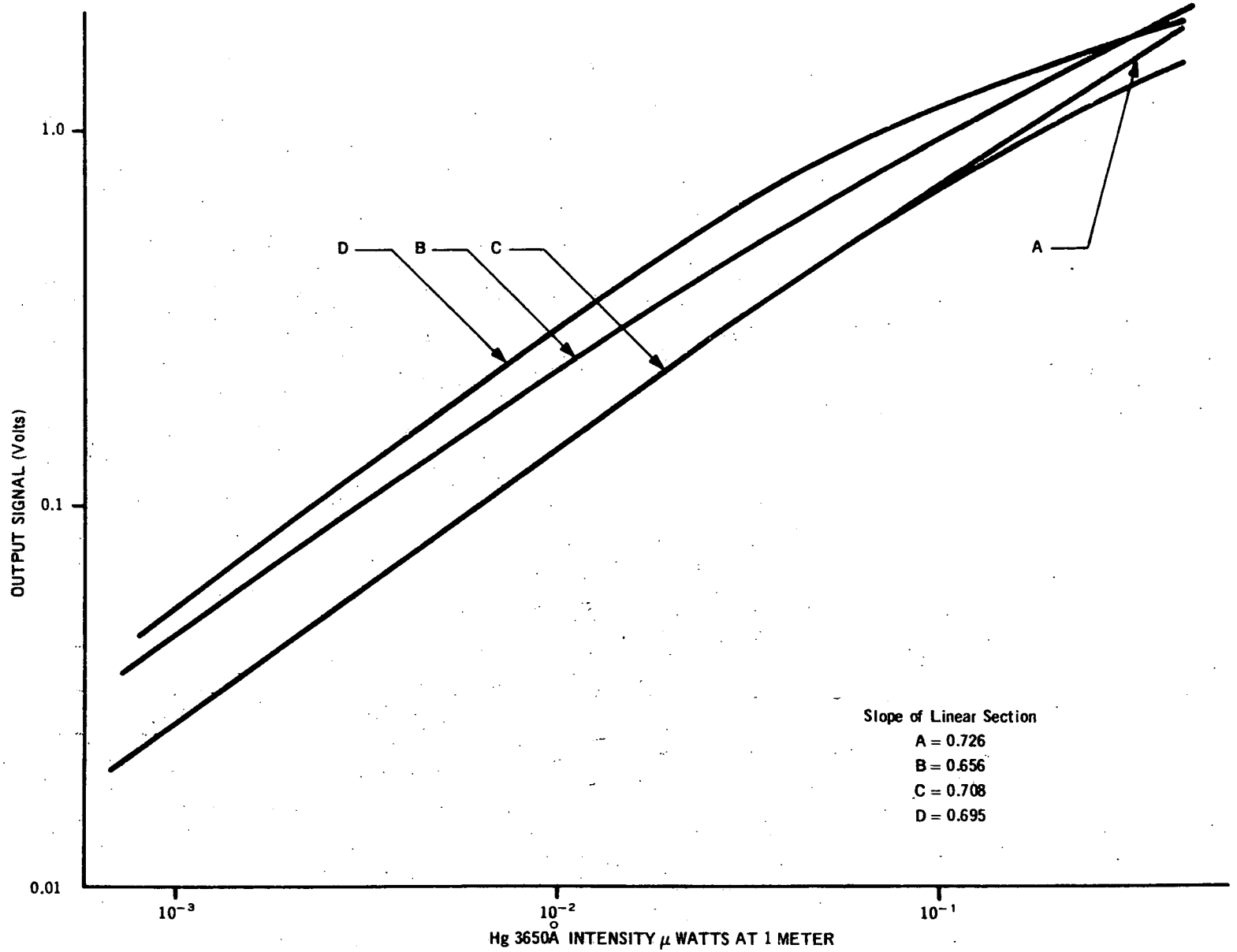


Figure 9. Photomultipliers Calibration Curves

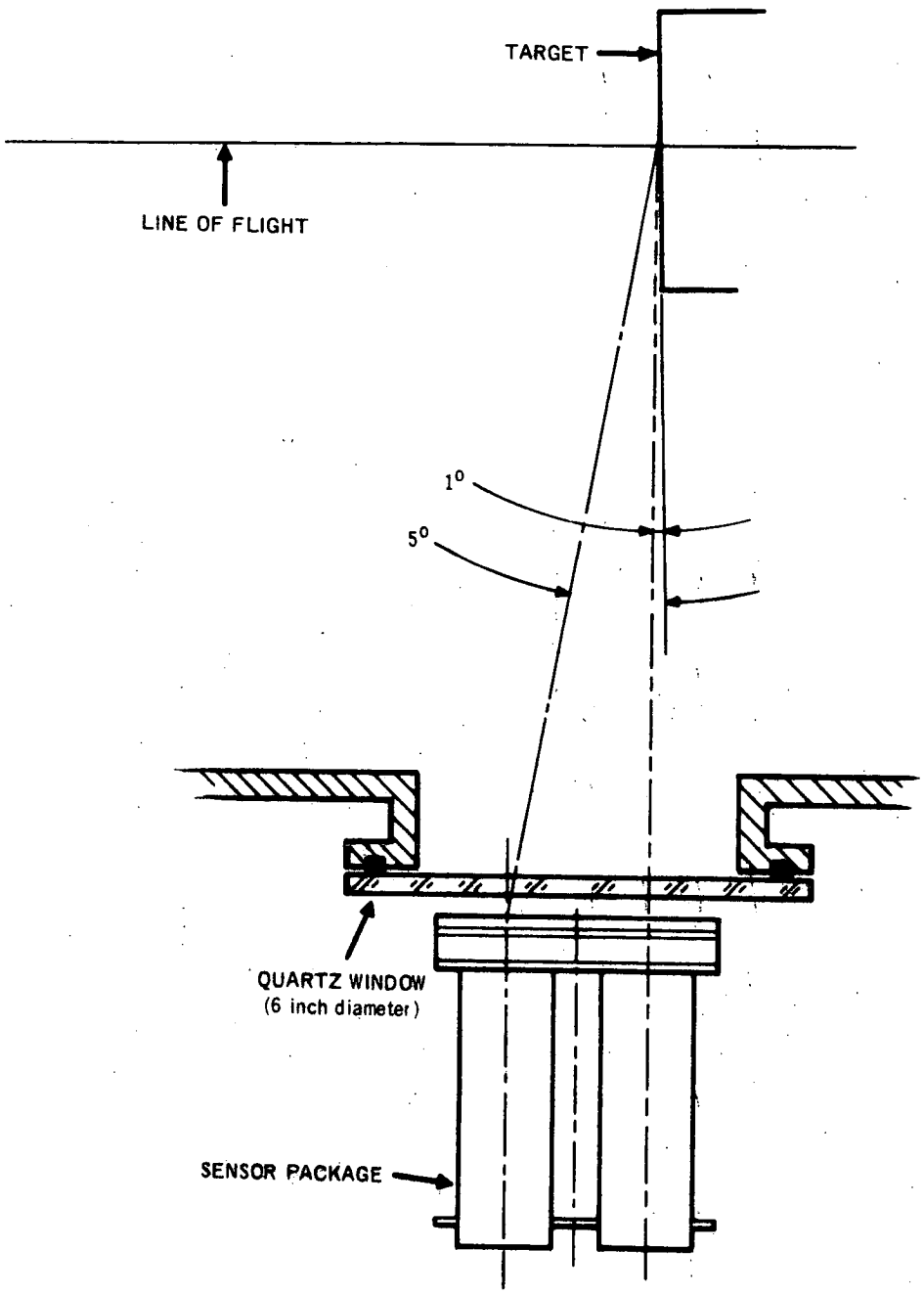


Figure 10. Schematic of the Impact Flash Sensor Package Mount

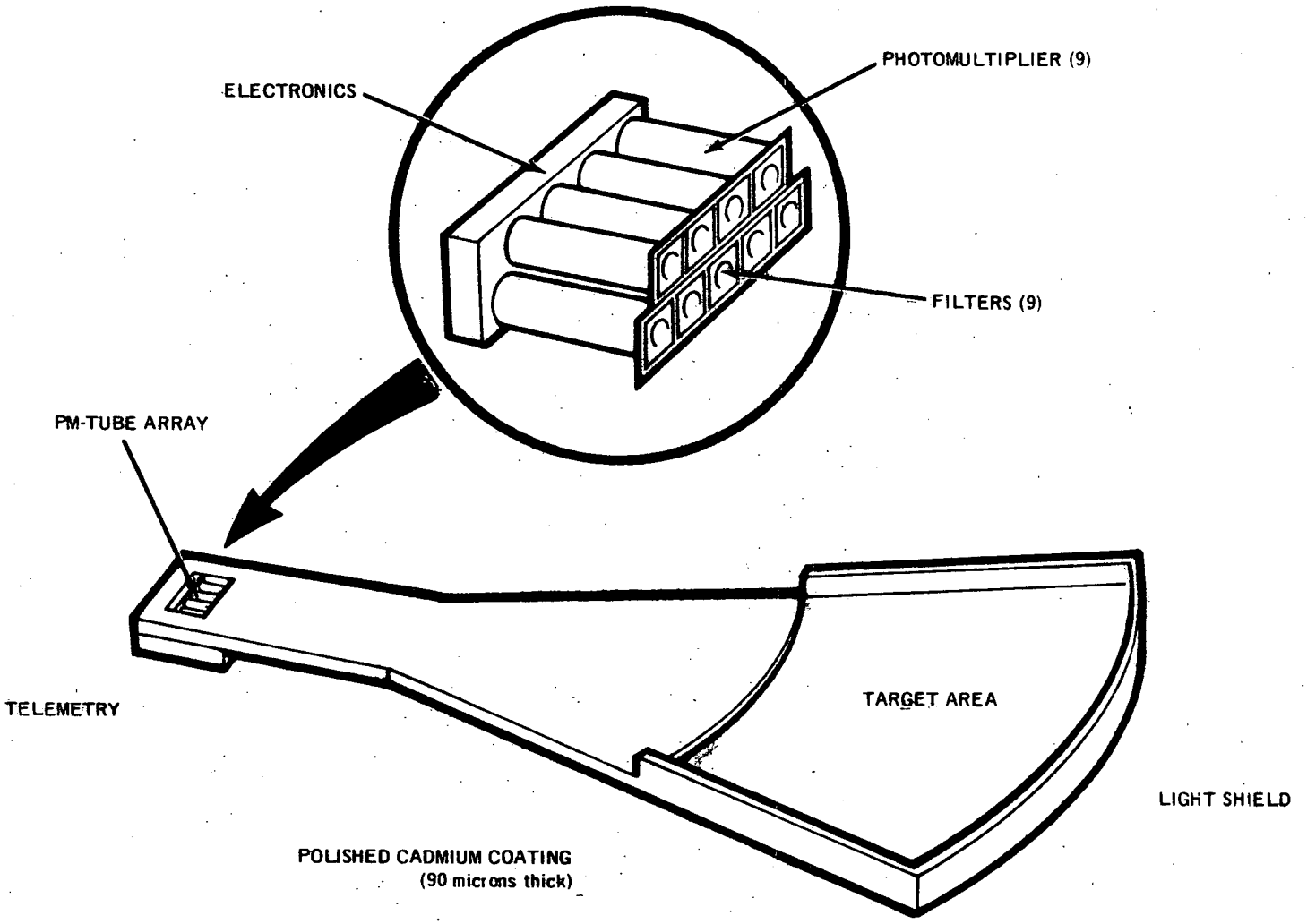


Figure 11. Target Panel - Sensor Configuration

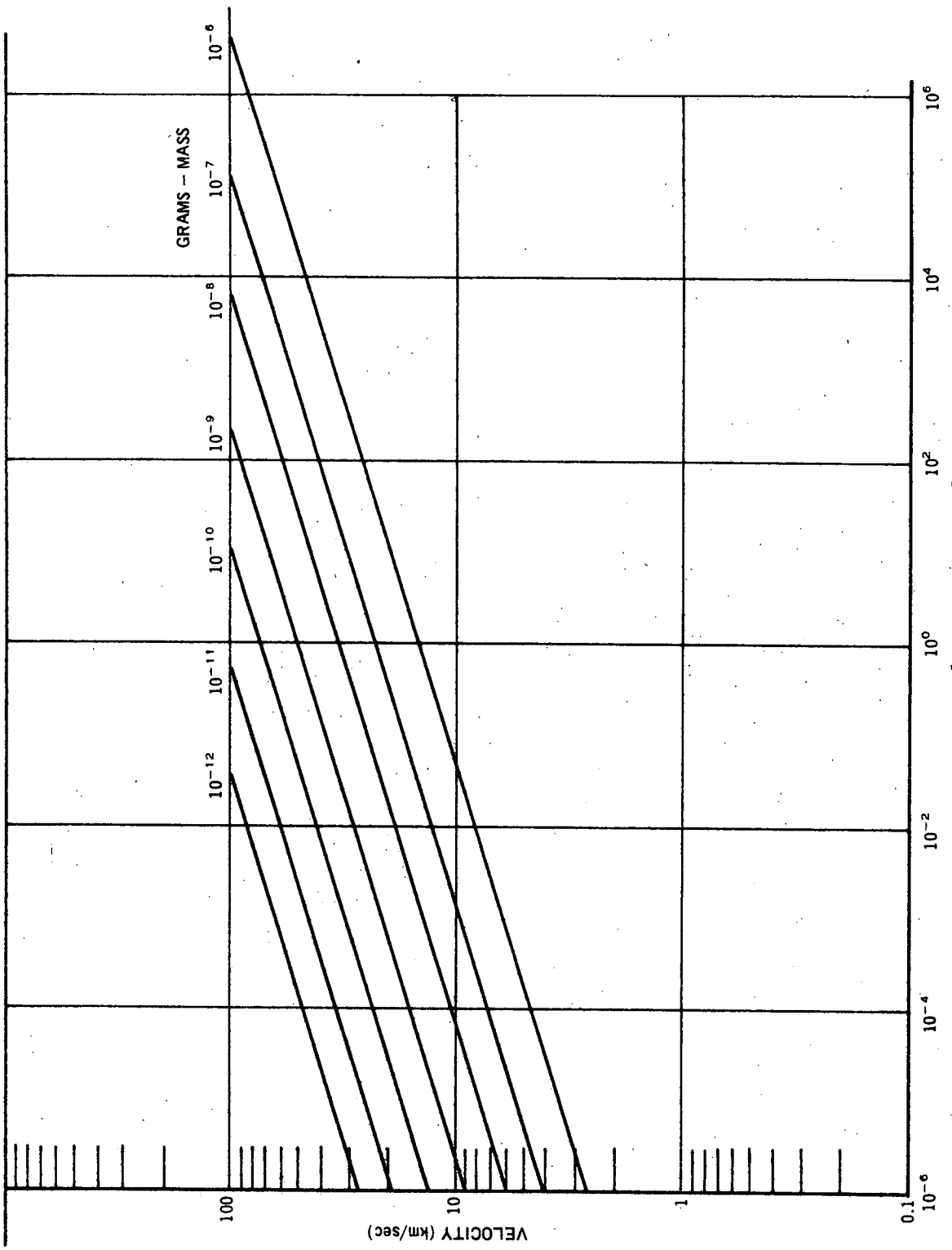


Figure 12. Velocity Vs. Flash Intensity - Cadmium Target, Cadmium Line Observed

Figure 12.

R134/FR1

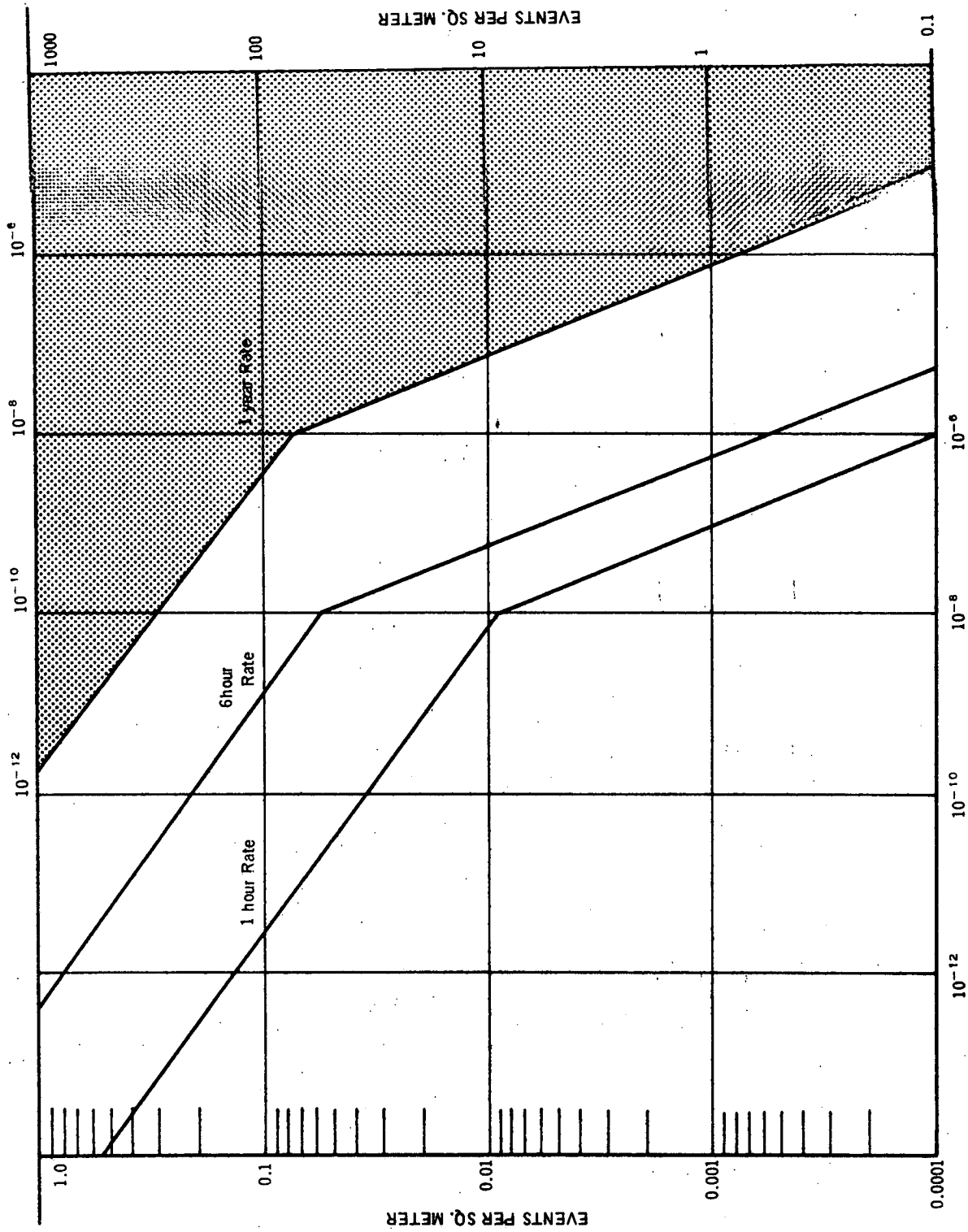


Figure 13. Meteor Flux

Figure 13.

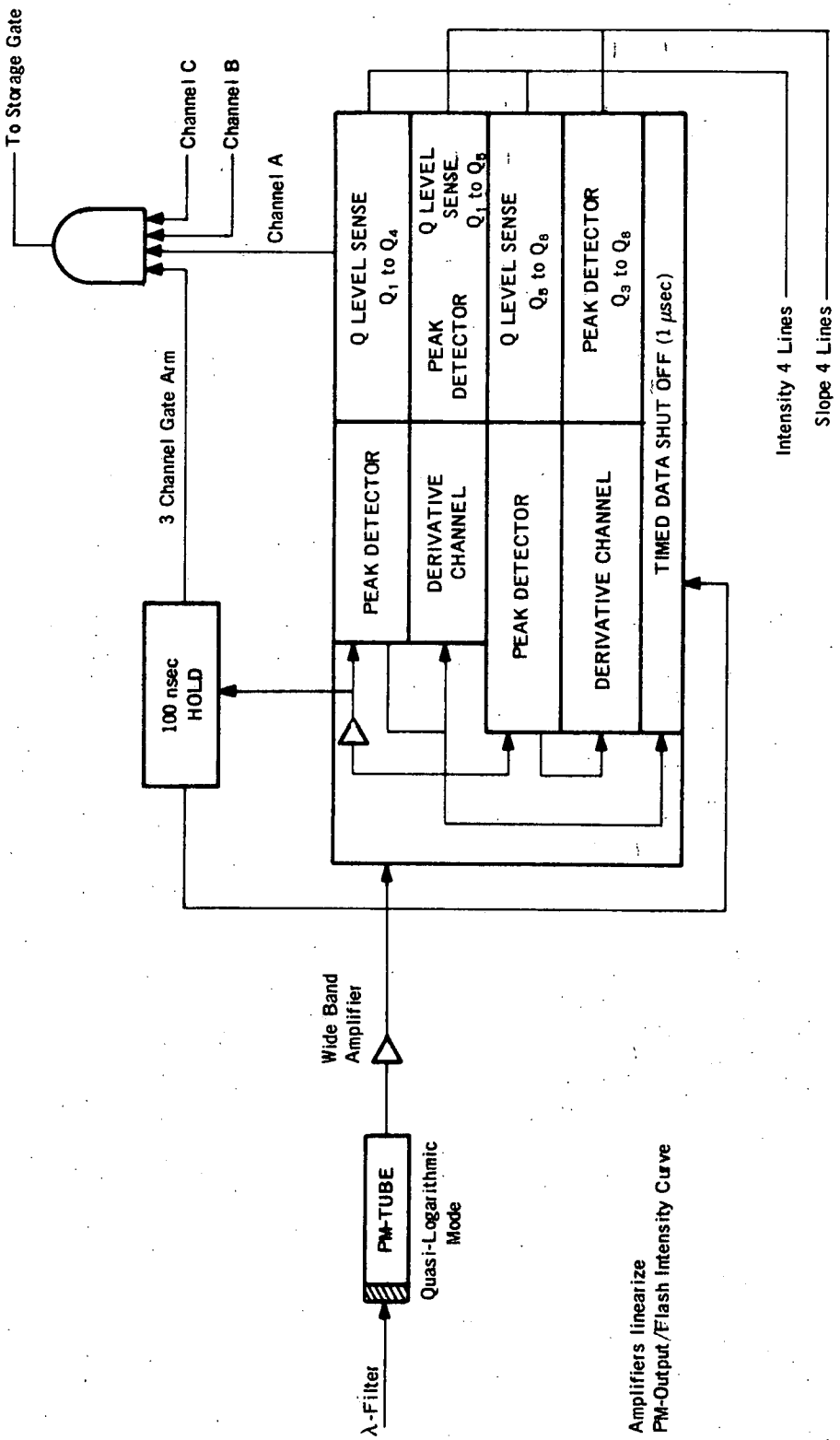


Figure 14. Flash Intensity Channel/Block Diagram

Figure 14.

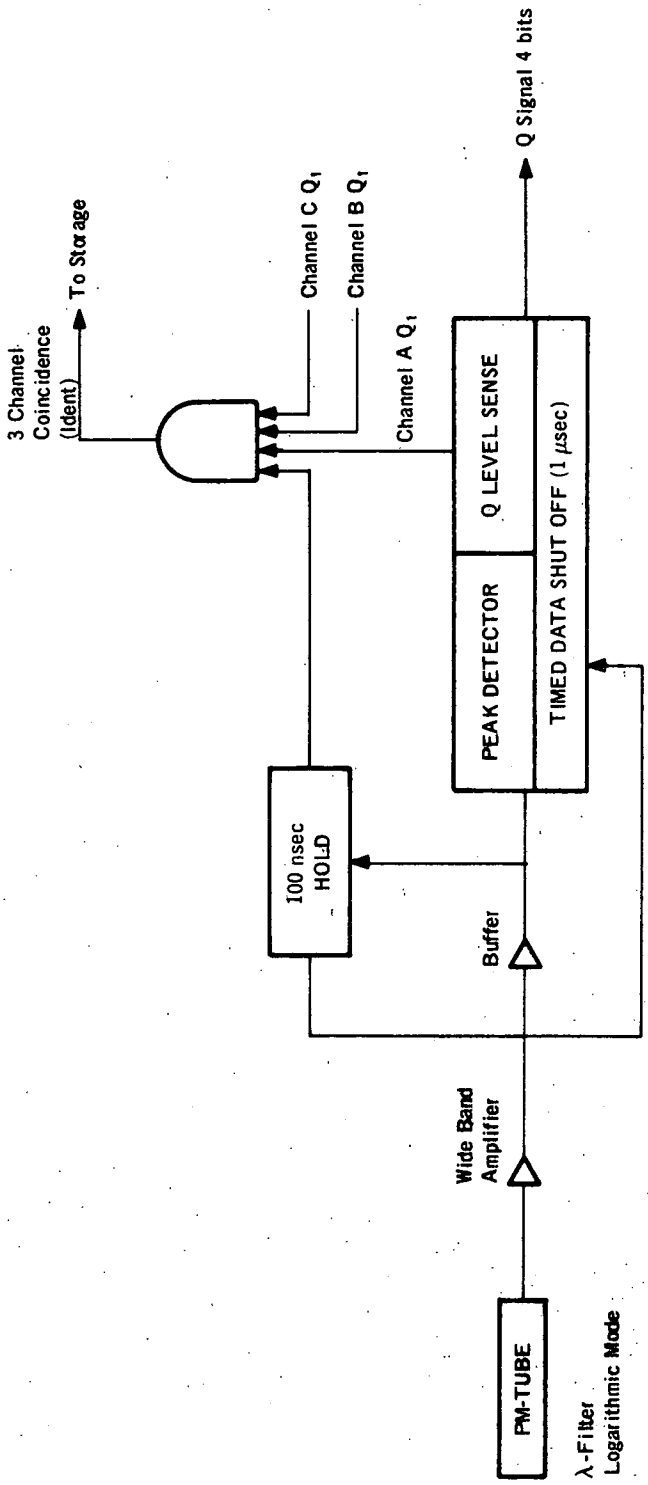


Figure 15. Identification Channel

Figure 15.

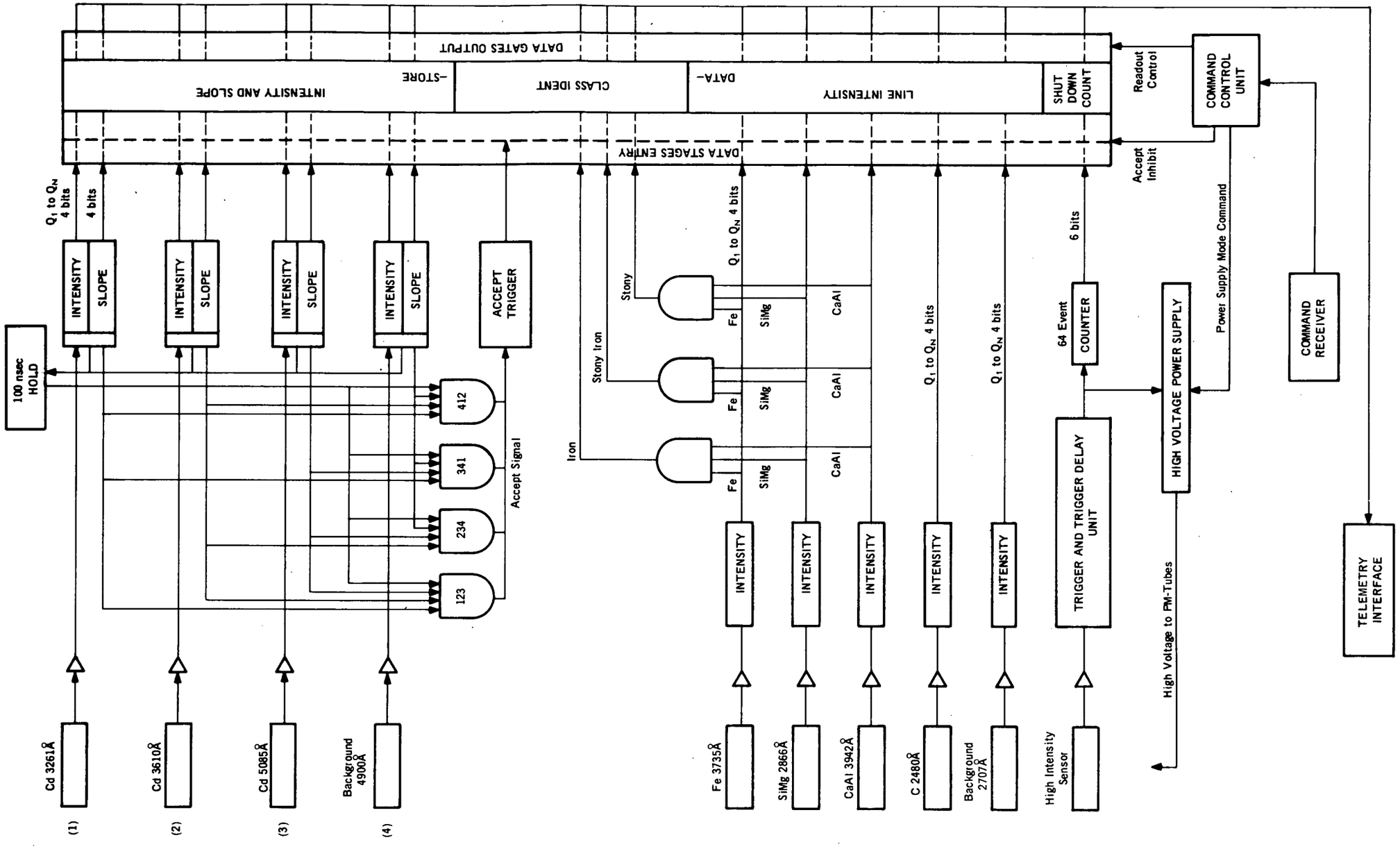


Figure 16.

Figure 16. Sensor Data System/Block Diagram

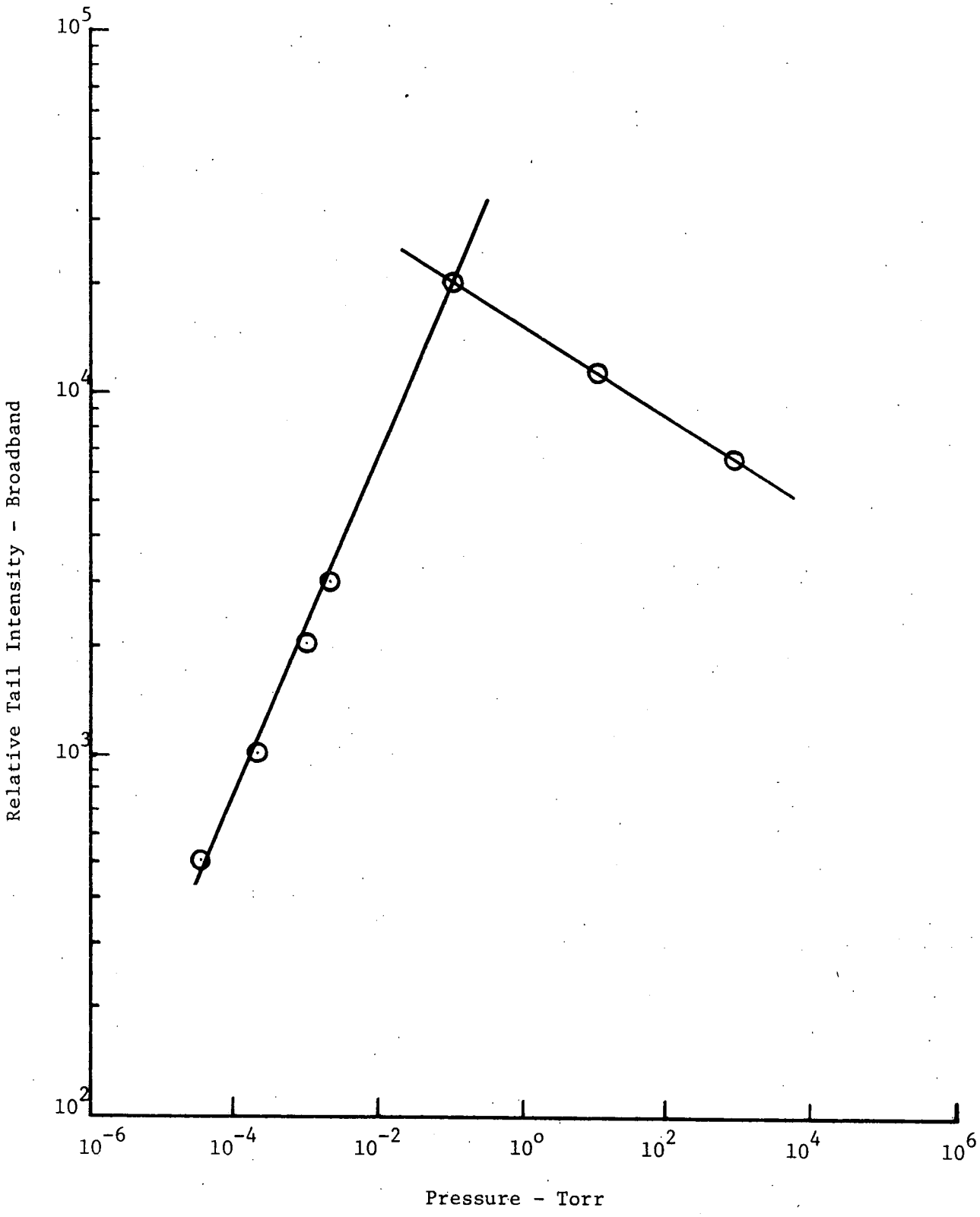


Figure 17. Pressure Dependence of Tail Intensity - Broadband

R134/FR1

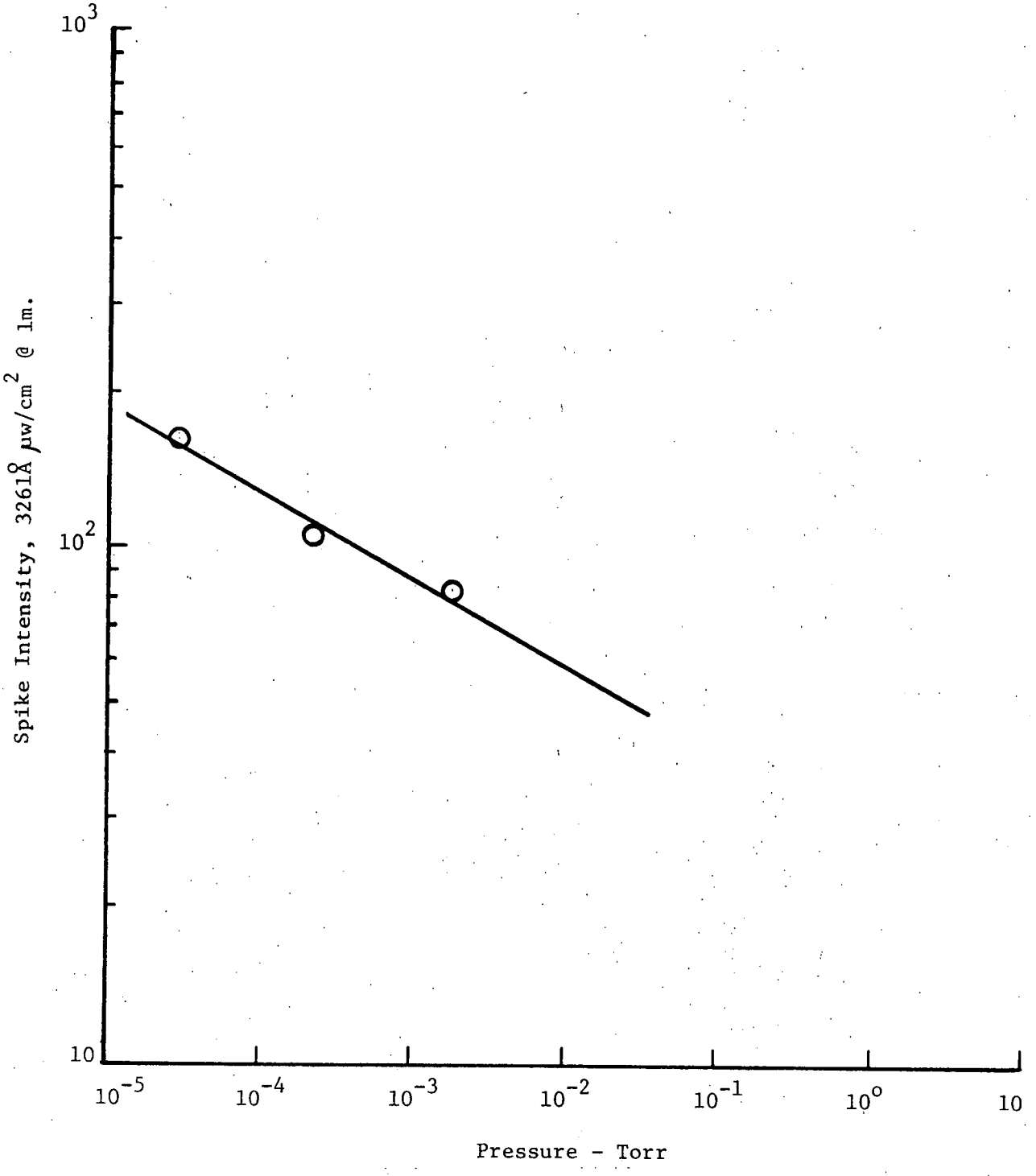


Figure 18. Pressure Dependence of Spike Intensity, 3261Å

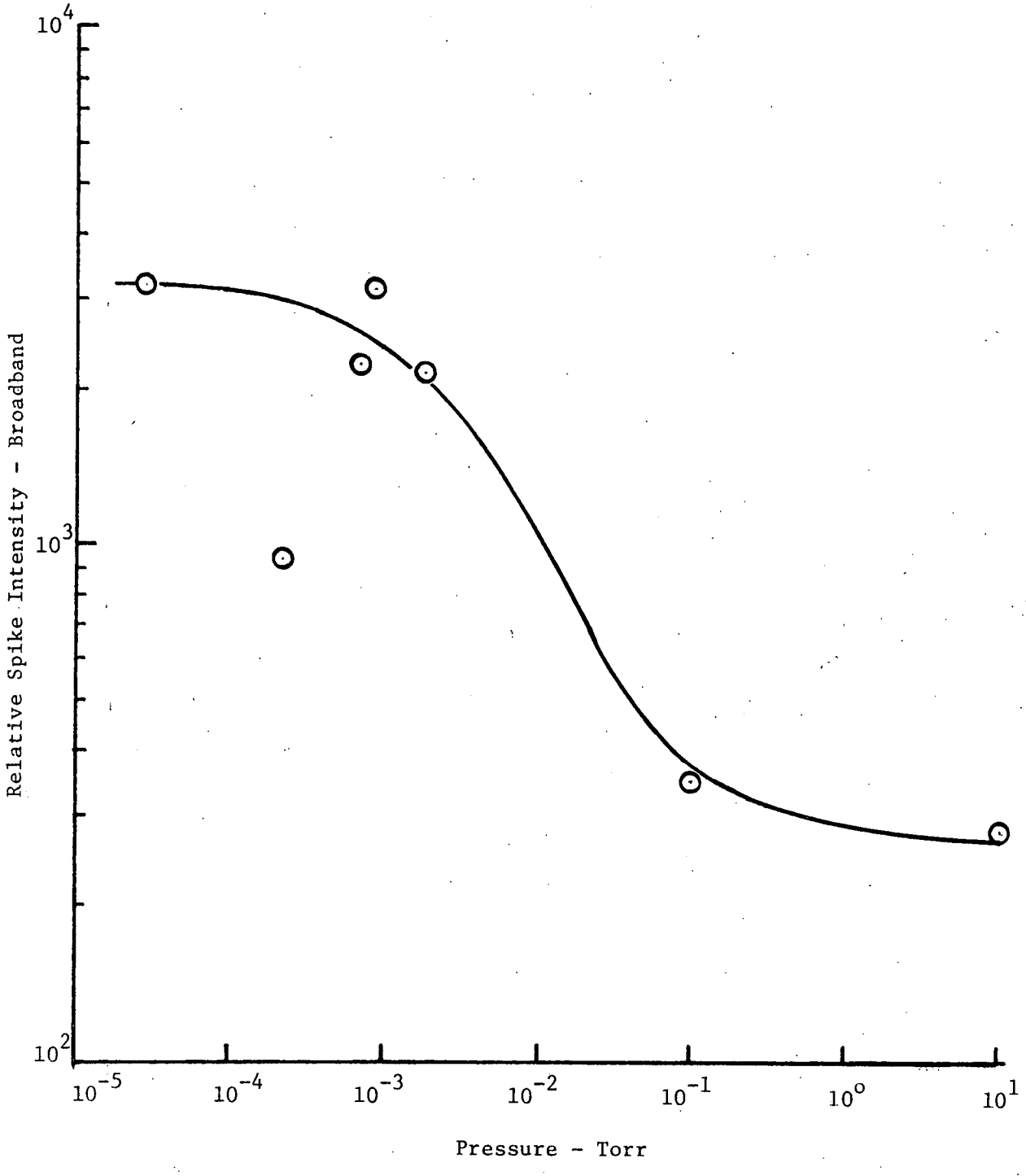


Figure 19. Pressure Dependence of Spike Intensity - Broadband

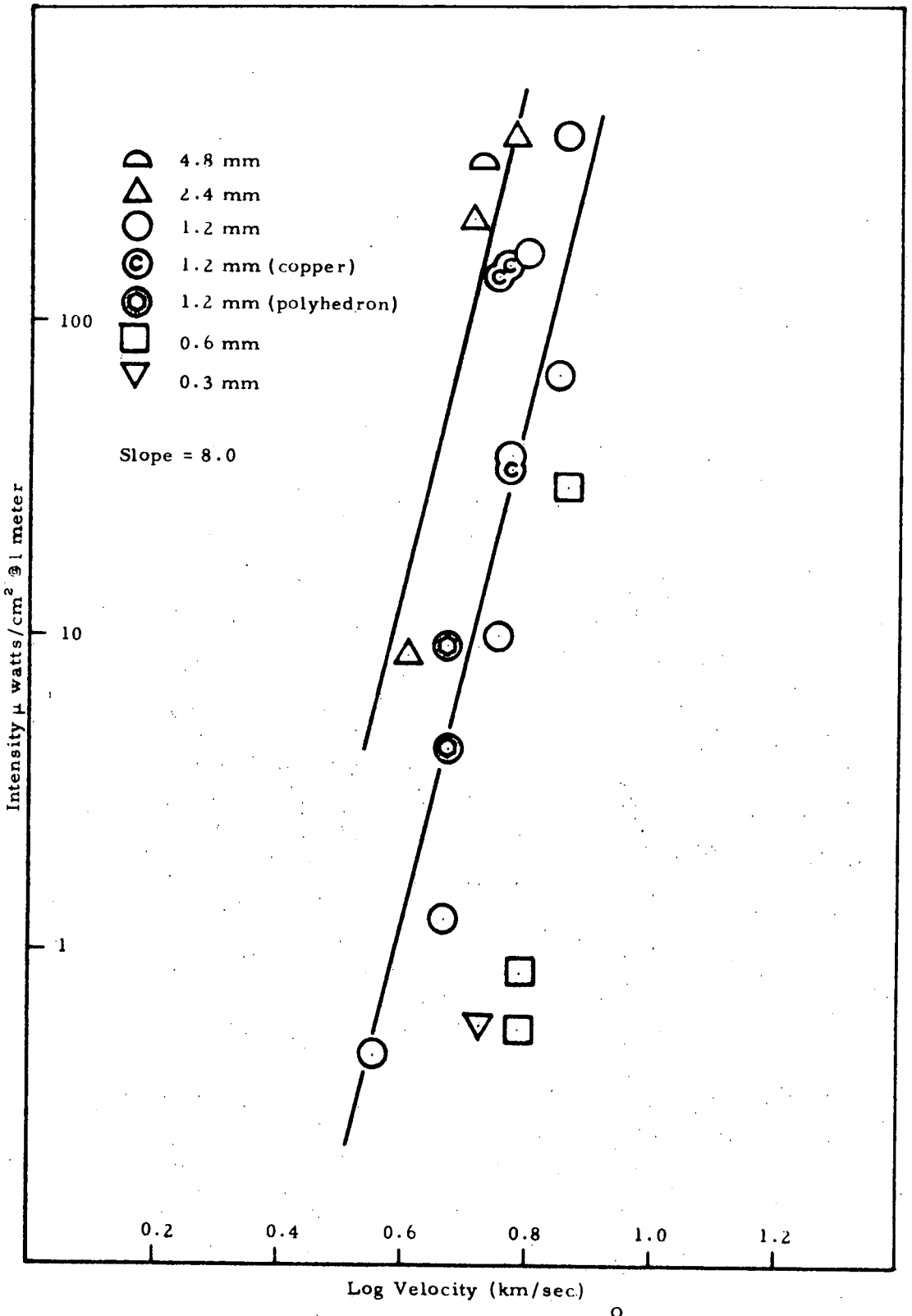


Figure 20. Spike Intensity Variation at 3261Å for CanDi and Copper Projectiles Impacting Cadmium

R134/FR1

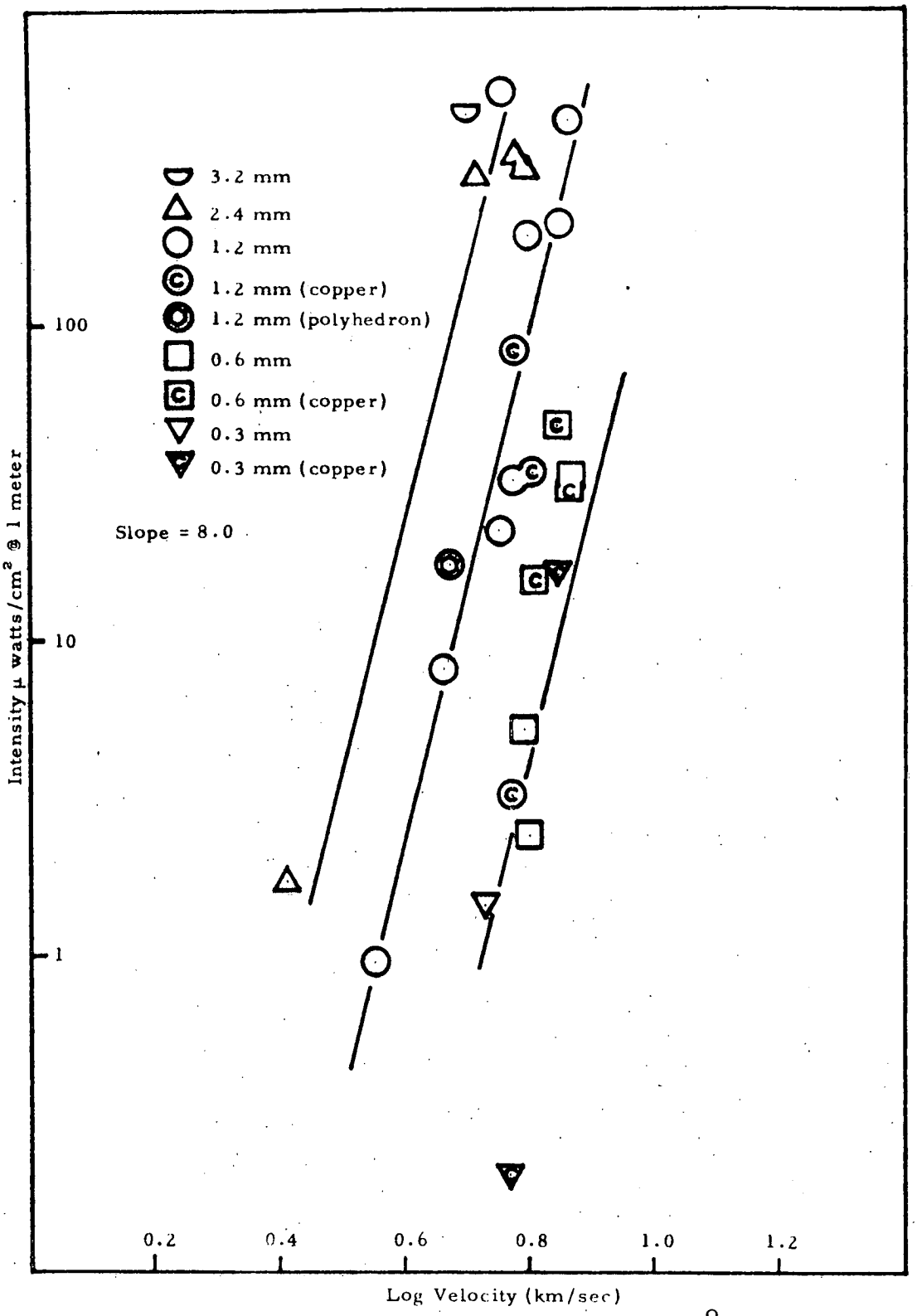


Figure 21. Spike Intensity Variation at 5085Å for CanDi and Copper Projectiles Impacting Cadmium

R134/FR1

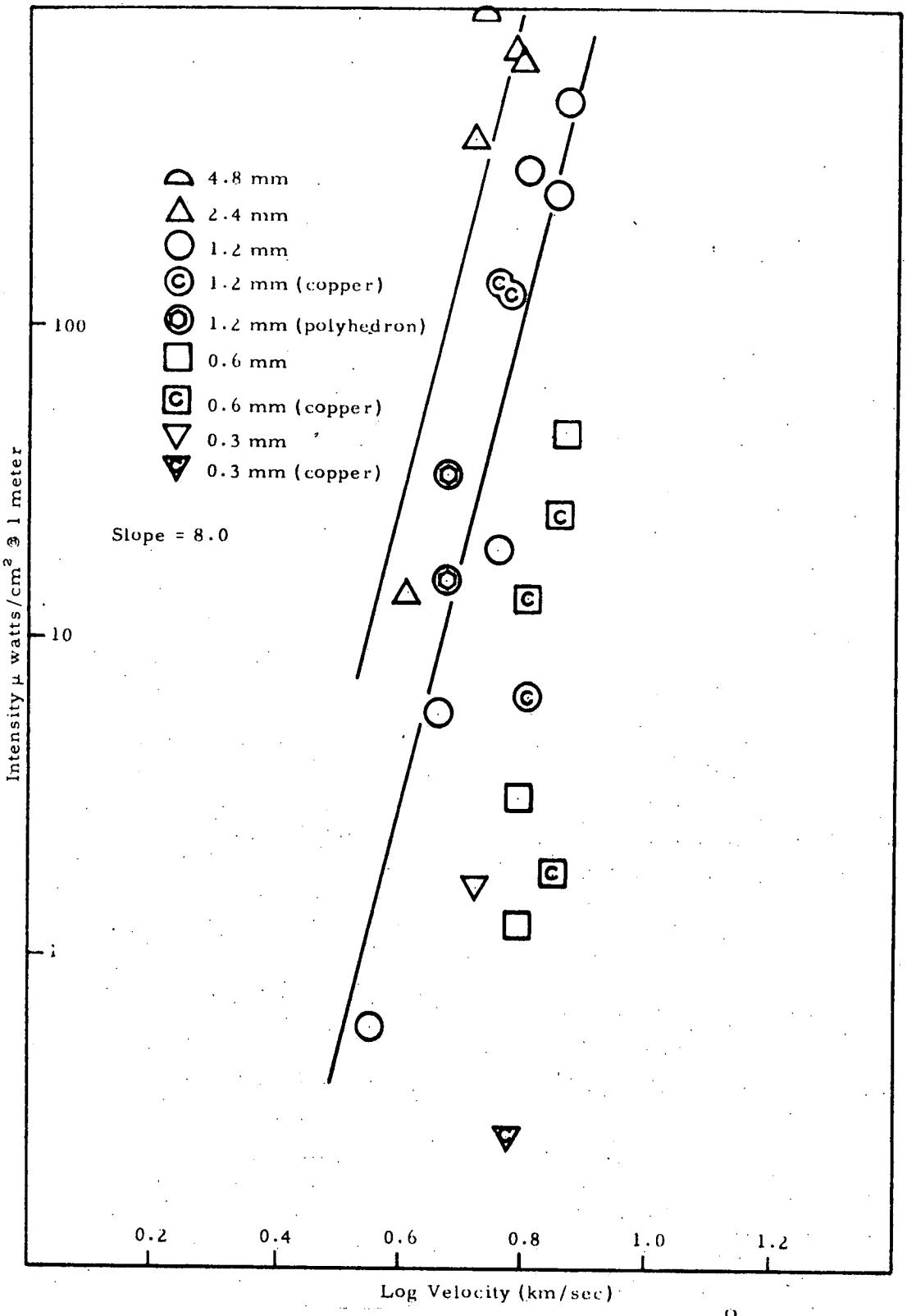


Figure 22. Spike Intensity Variation at 3610Å for CanDi and Copper Projectiles Impacting Cadmium

R134/FR1

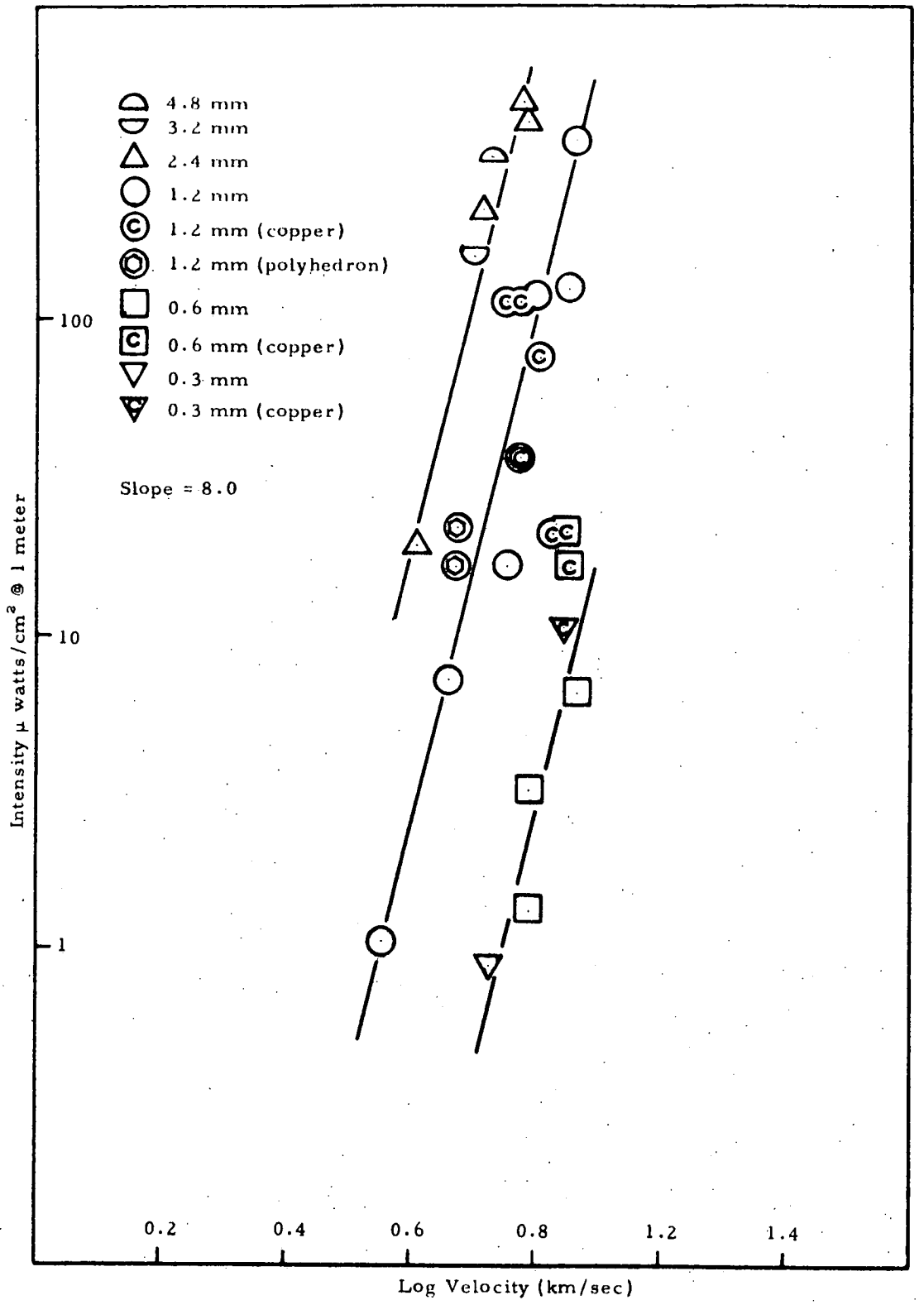


Figure 23. Spike Intensity Variation at 4900Å for CanDi and Copper Projectiles Impacting Cadmium

R134/FR1

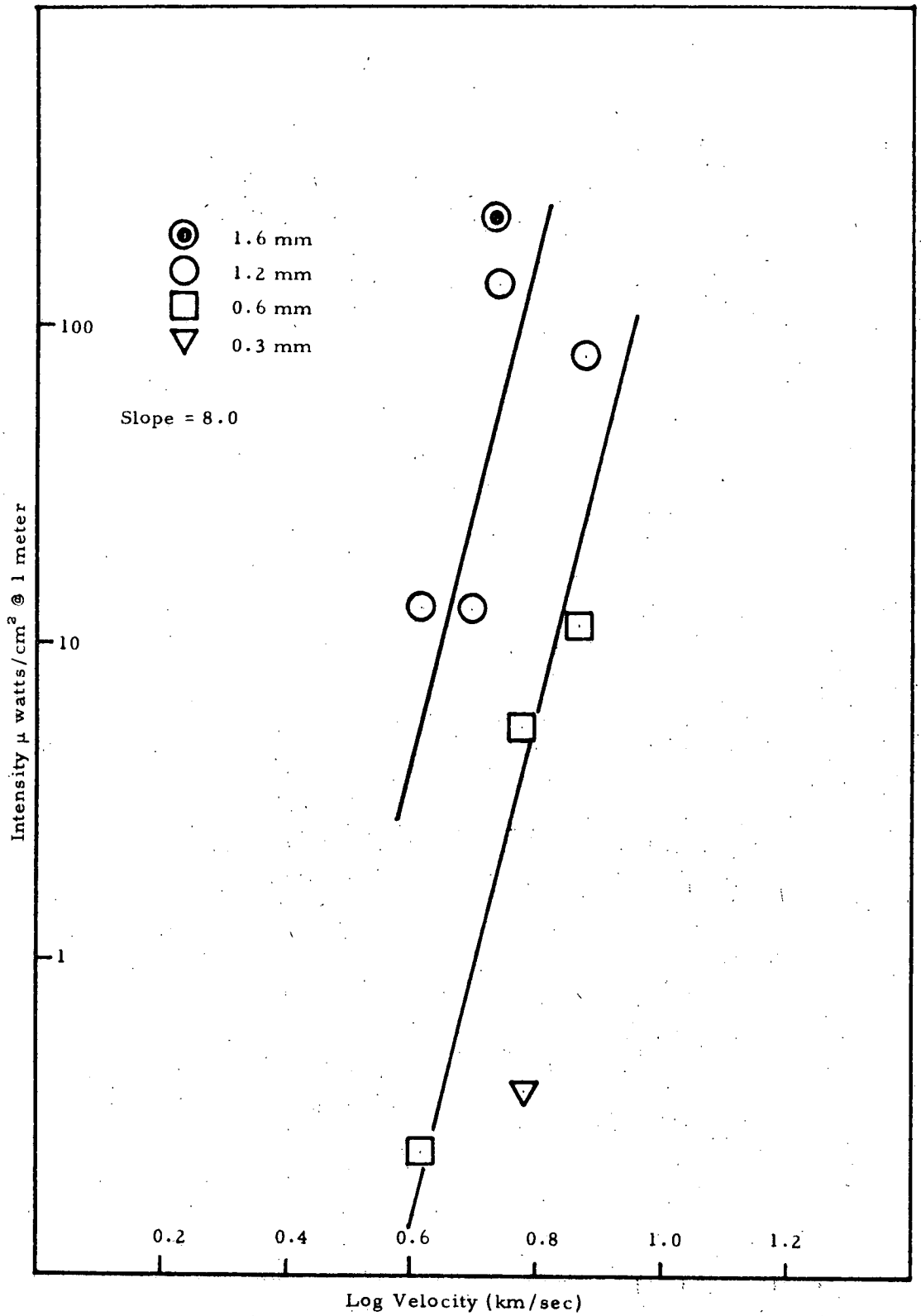


Figure 24. Spike Intensity Variation at 3261Å for Bruderheim Projectiles Impacting Cadmium

R134/FR1

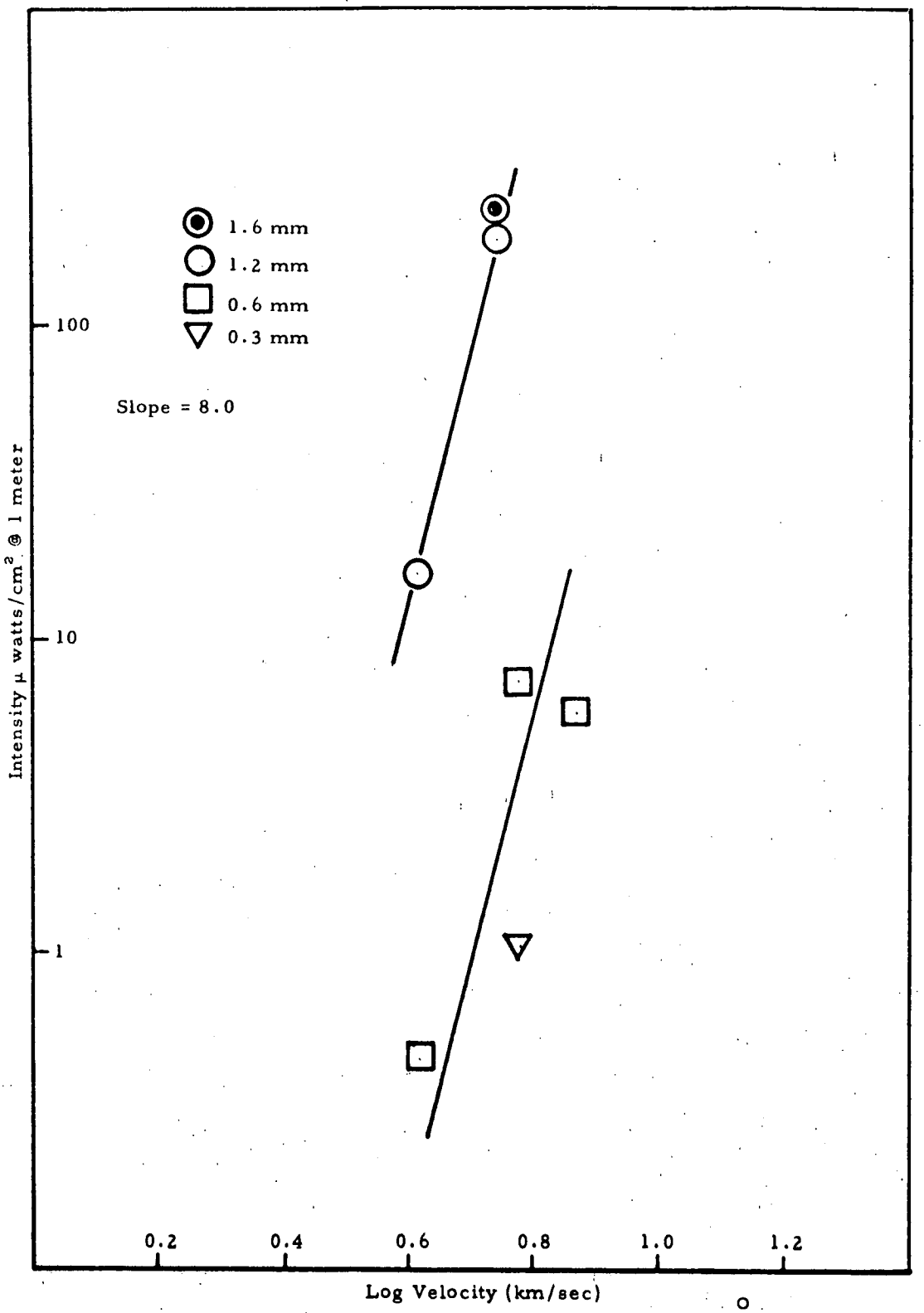


Figure 25. Spike Intensity Variation at 5085Å for Bruderheim Projectiles Impacting Cadmium

R134/FR1

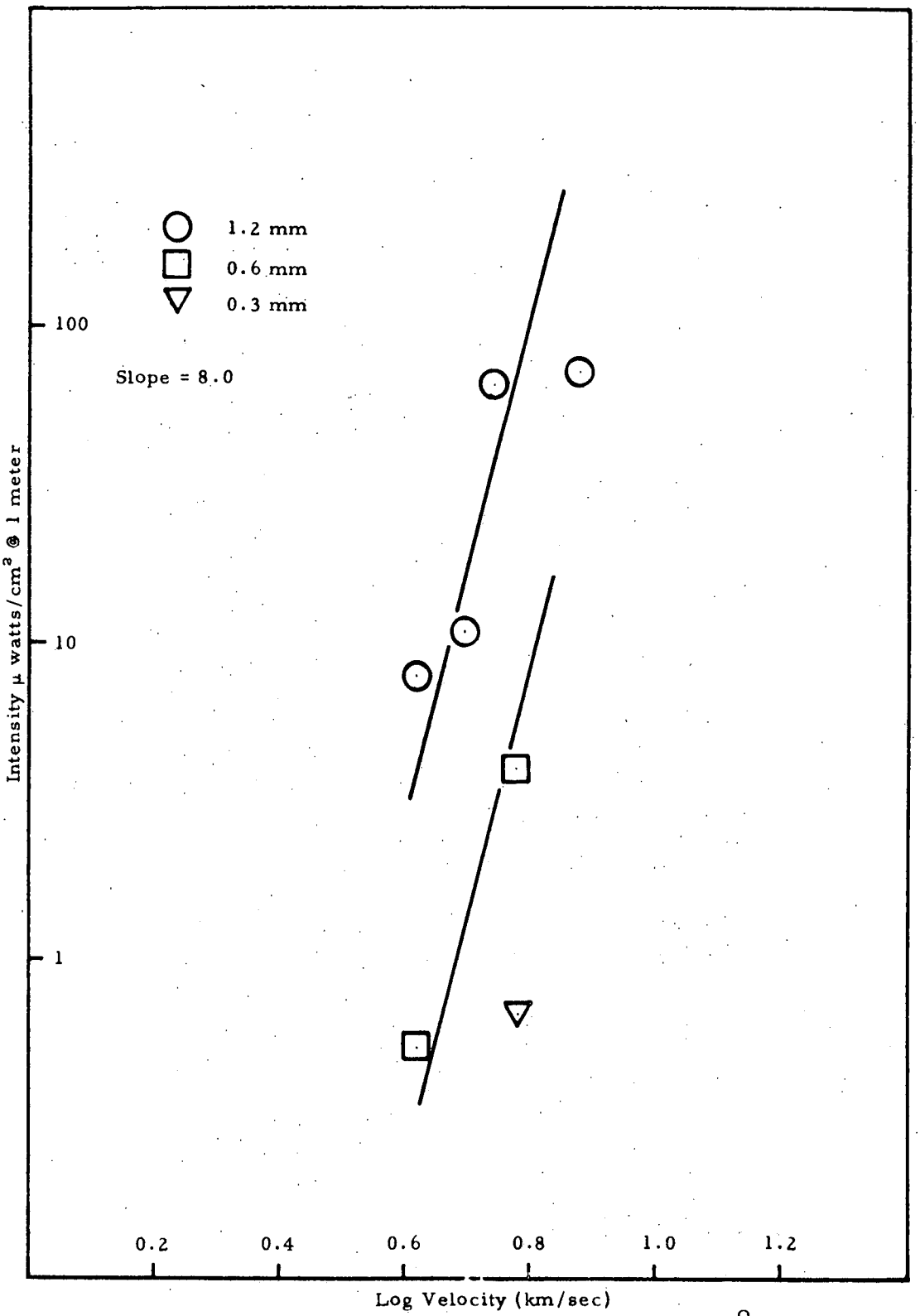


Figure 26. Spike Intensity Variation at 4900Å for Bruderheim Projectiles Impacting Cadmium

R134/FR1

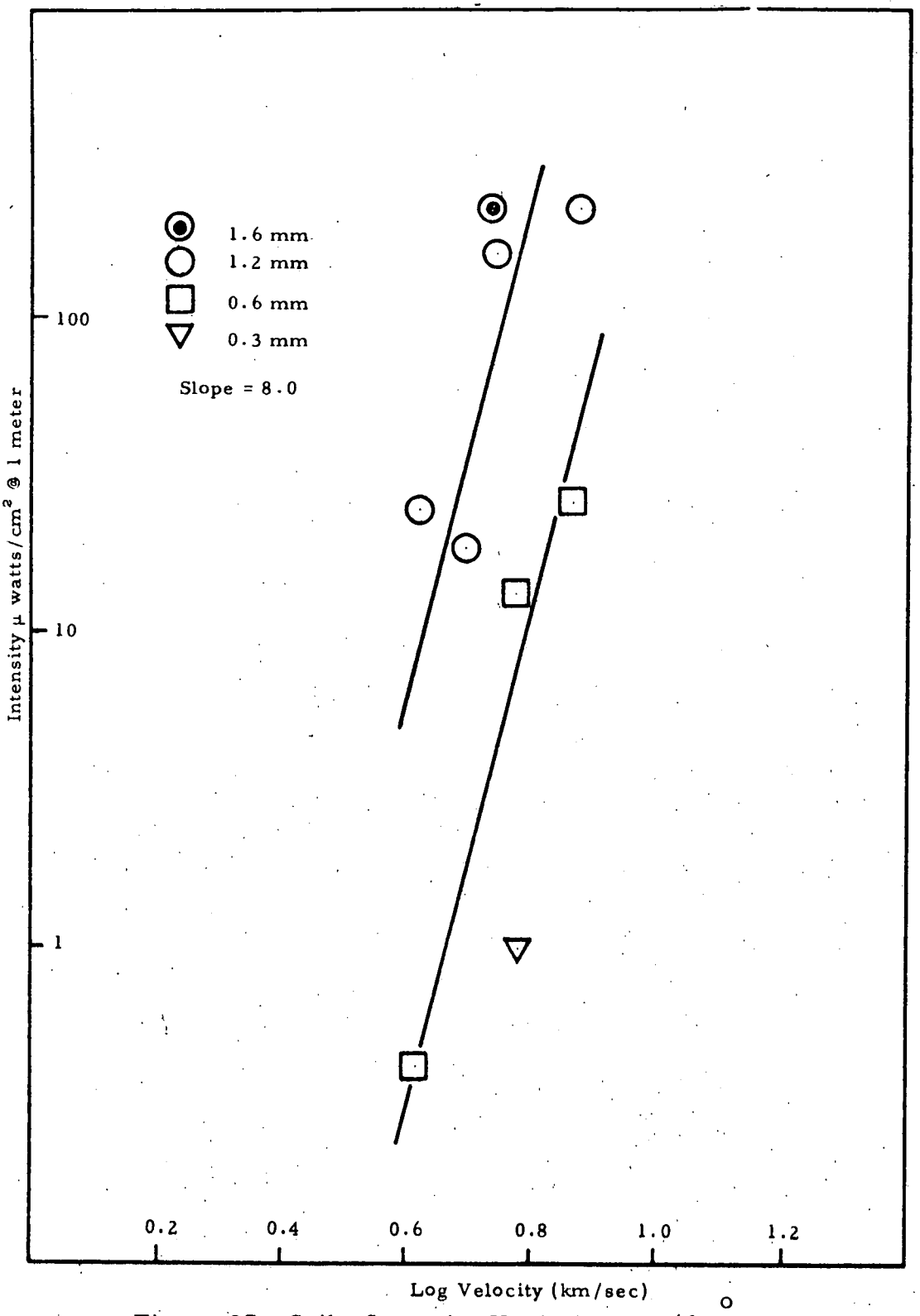


Figure 27. Spike Intensity Variation at 3610Å for Bruderheim Projectiles Impacting Cadmium

R134/FR1

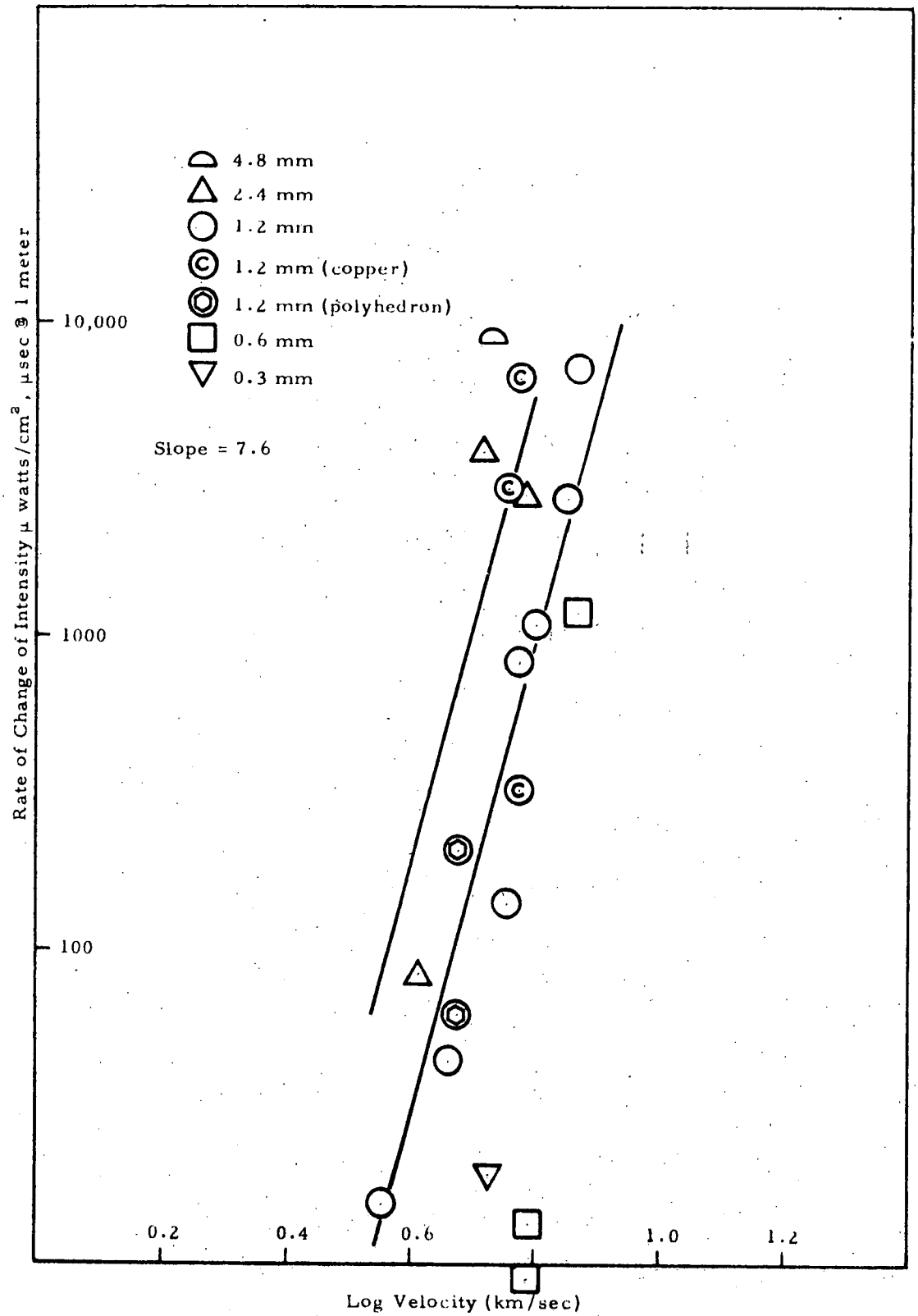


Figure 28. Spike Rate of Change of Intensity at 3261Å for CanDi and Copper Projectiles Impacting Cadmium

R134/FR1

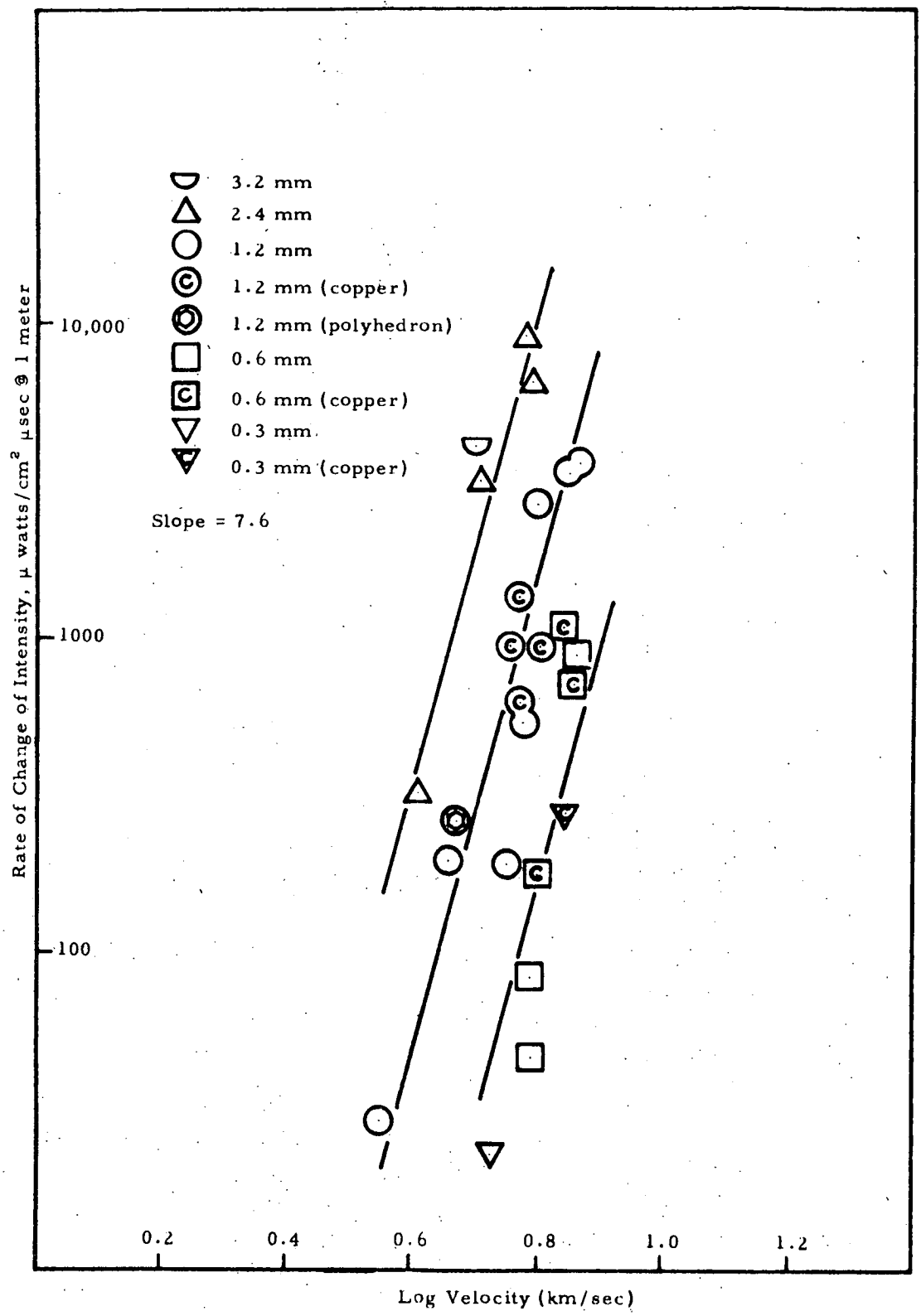


Figure 29. Spike Rate of Change of Intensity at 5085Å for CanDi and Copper Projectiles Impacting Cadmium

R134/FR1

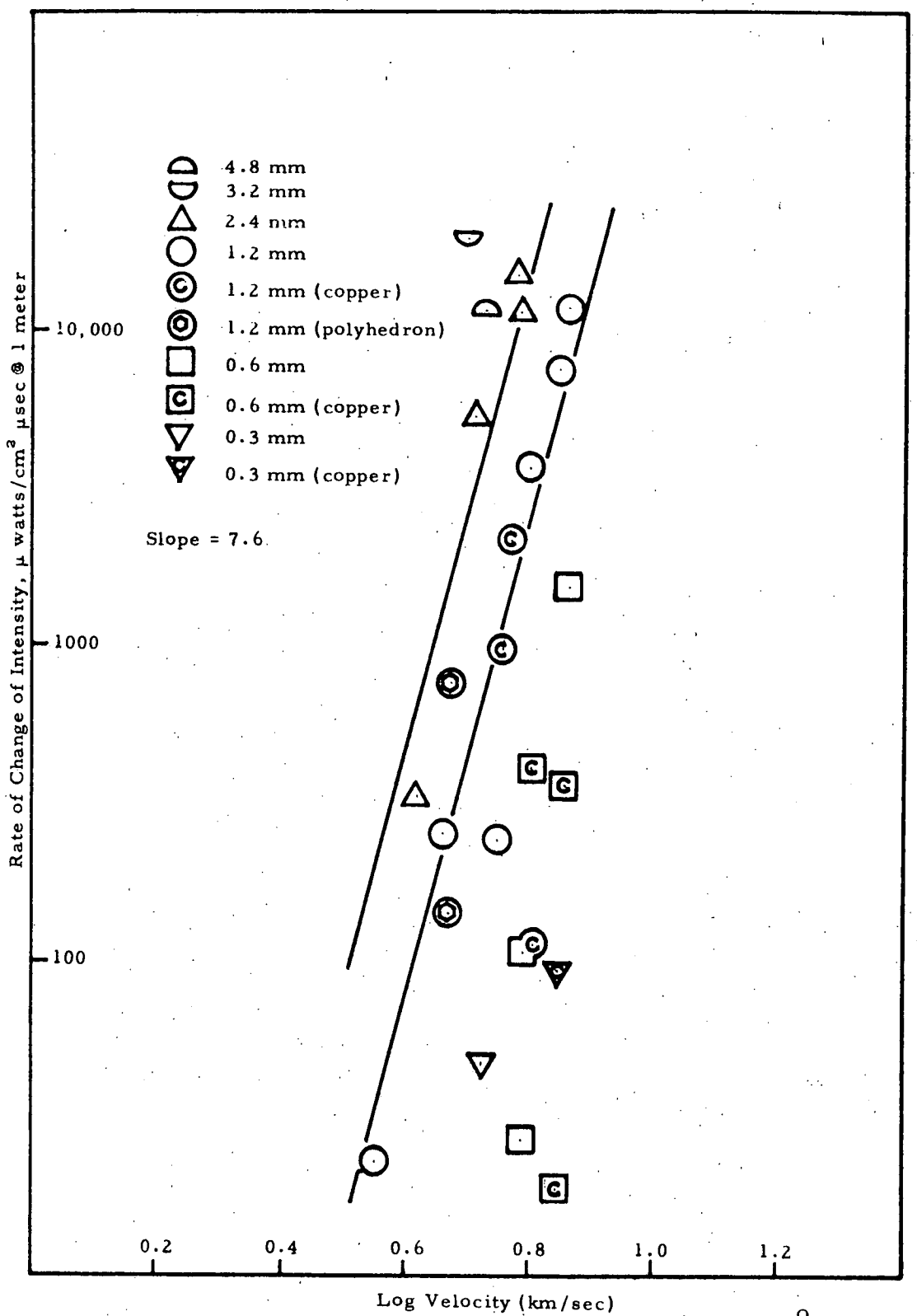


Figure 30. Spike Rate of Change of Intensity at 3610Å for CanDi and Copper Projectiles Impacting Cadmium

R134/FR1

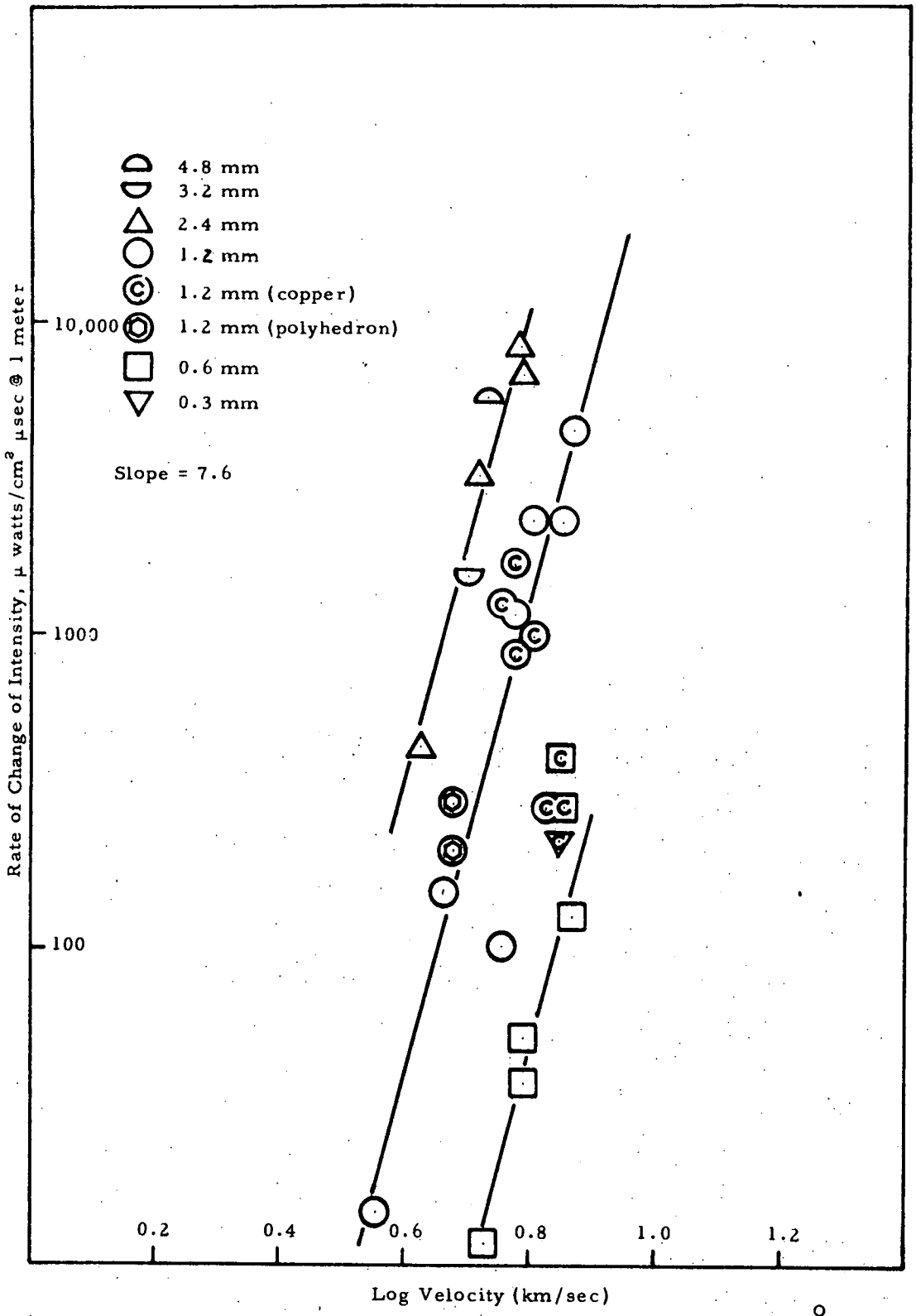


Figure 31. Spike Rate of Change of Intensity at 4900Å for CanDi and Copper Projectiles Impacting Cadmium

R134/FR1

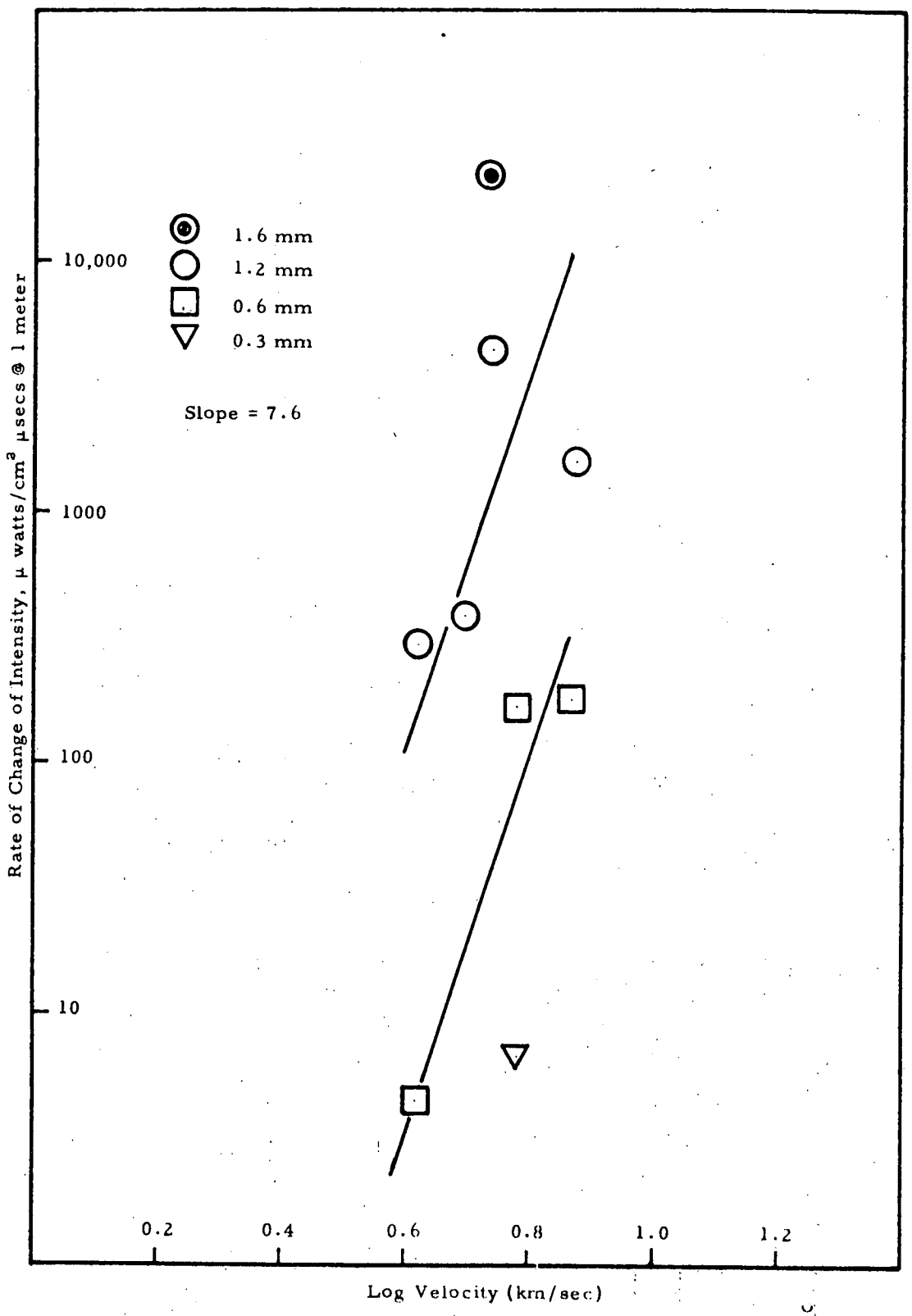


Figure 32. Spike Rate of Change of Intensity at 3261Å for Bruderheim Projectiles Impacting Cadmium

R134/FR1

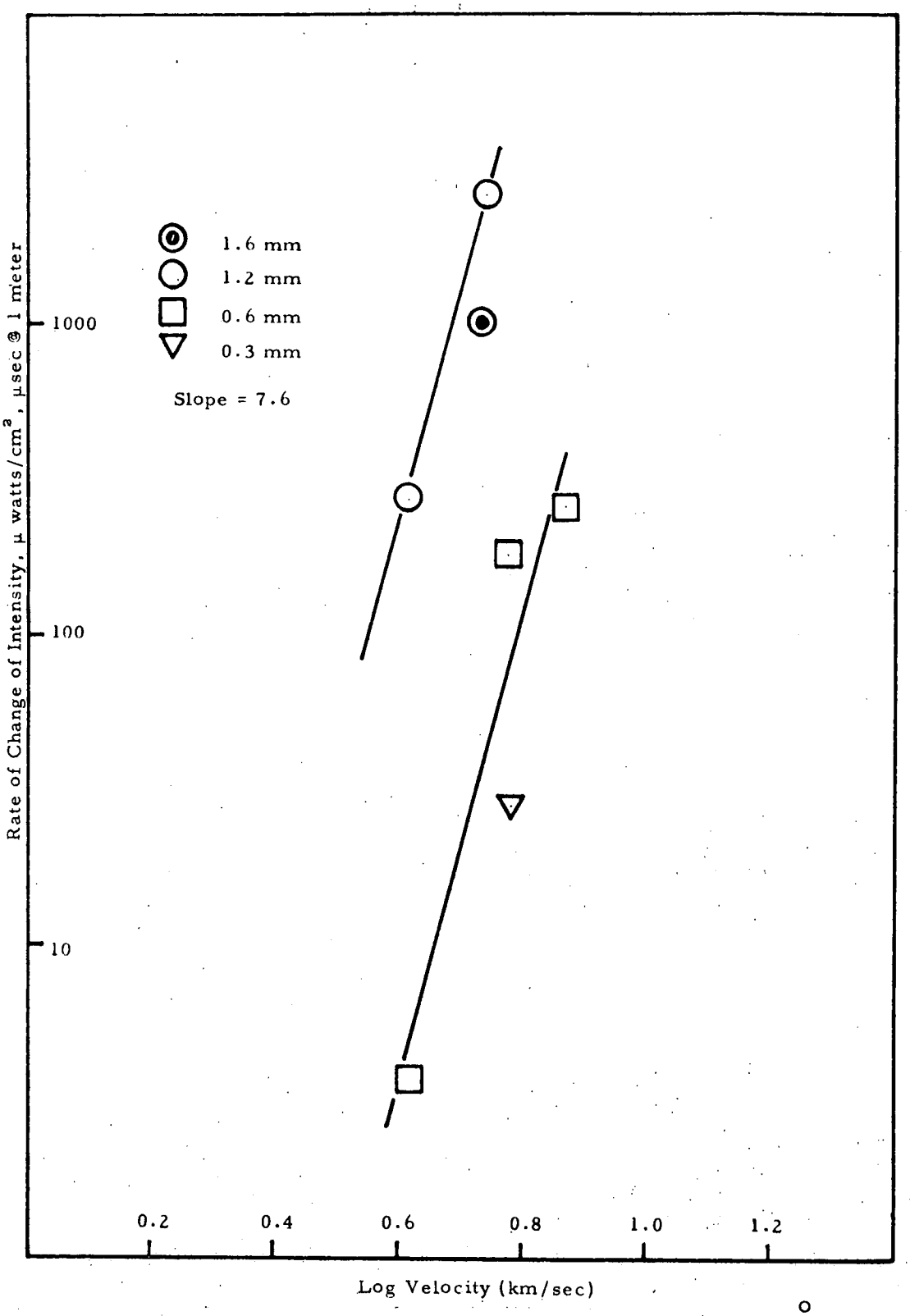


Figure 33. Spike Rate of Change of Intensity at 5085Å for Bruderheim Projectiles Impacting Cadmium

R134/FR1

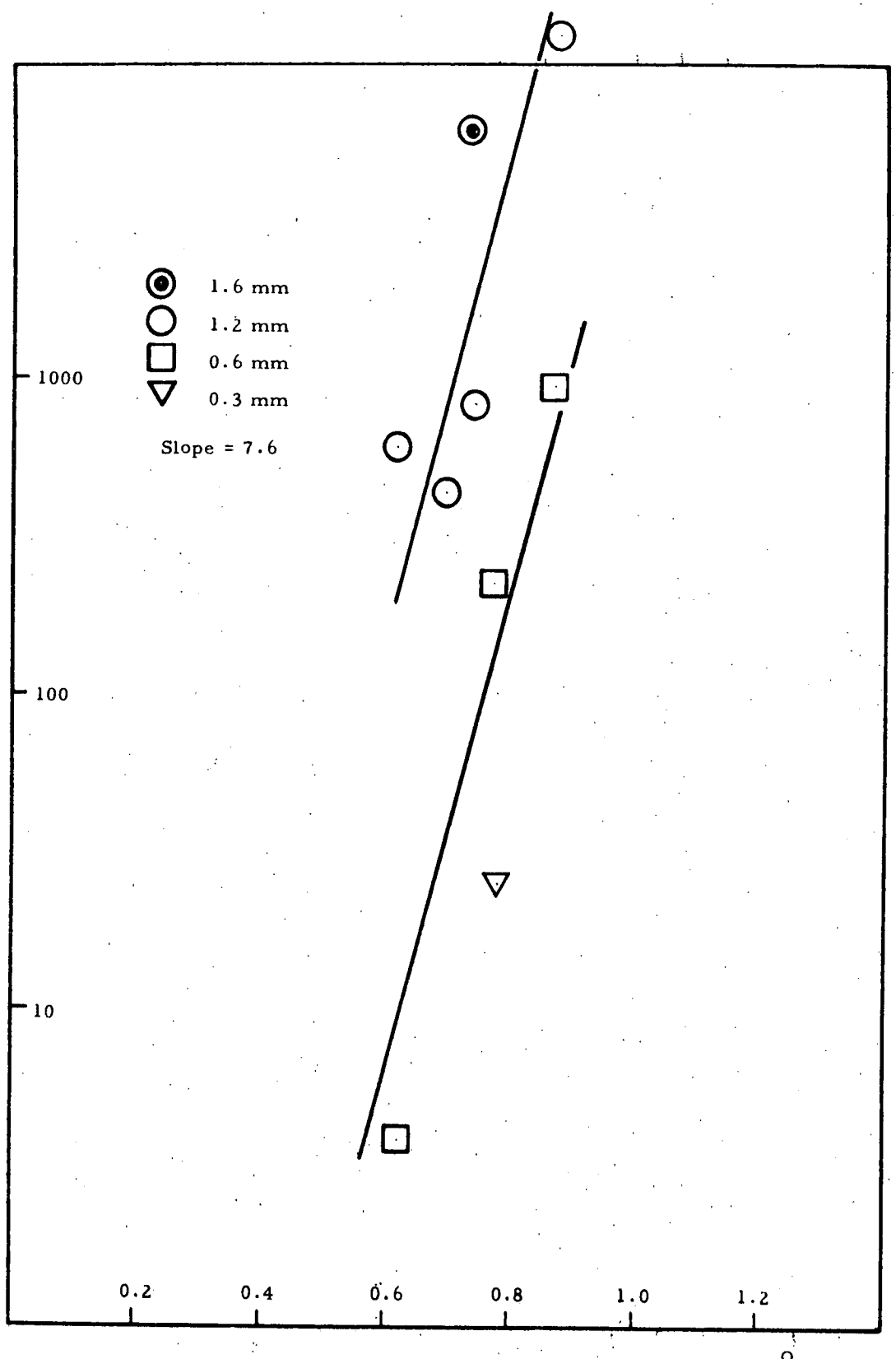


Figure 34. Spike Rate of Change of Intensity at 3610Å for Bruderheim Projectiles Impacting Cadmium

R134/FR1

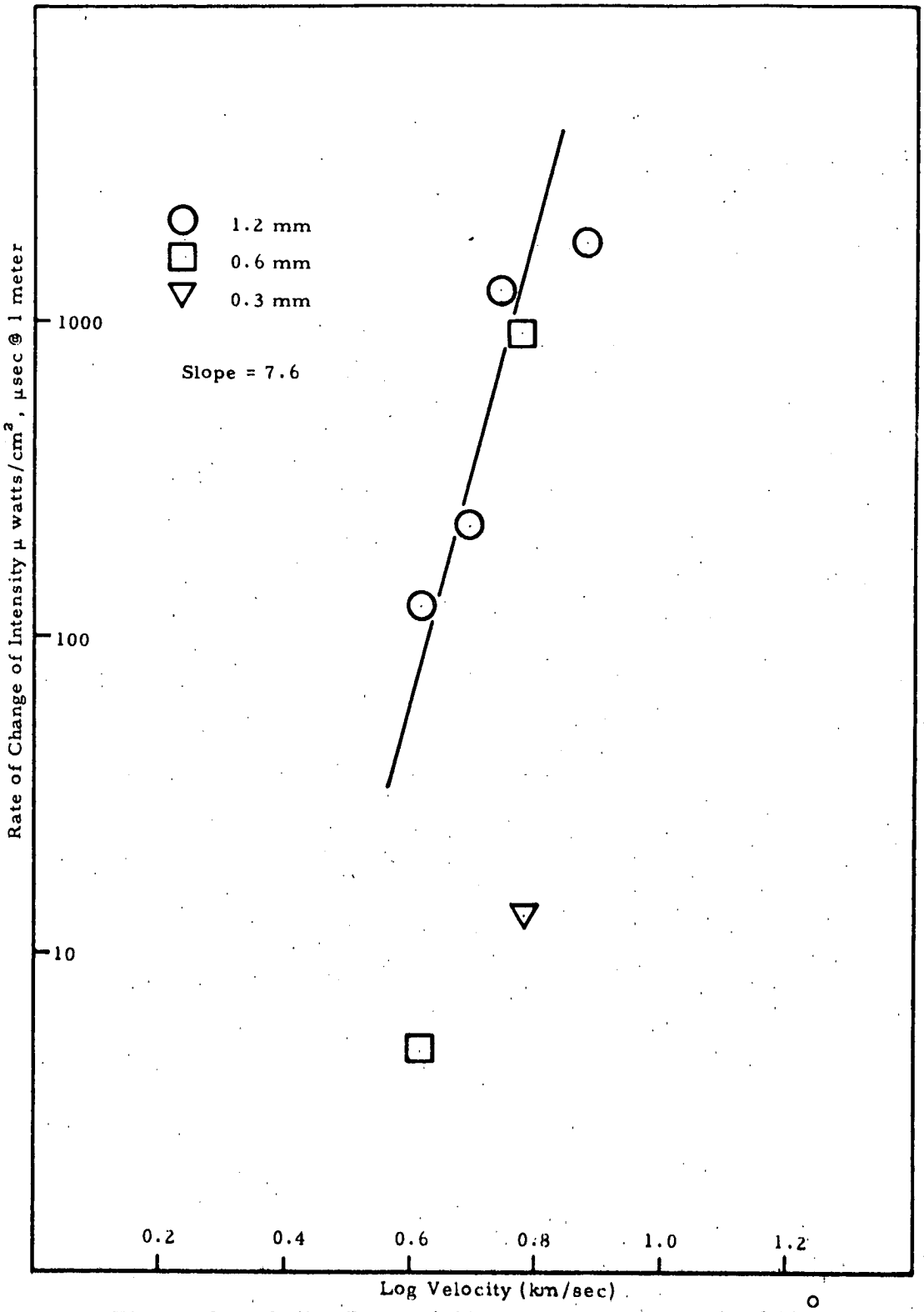


Figure 35. Spike Rate of Change of Intensity at 4900Å for Bruderheim Projectiles Impacting Cadmium

R134/FR1

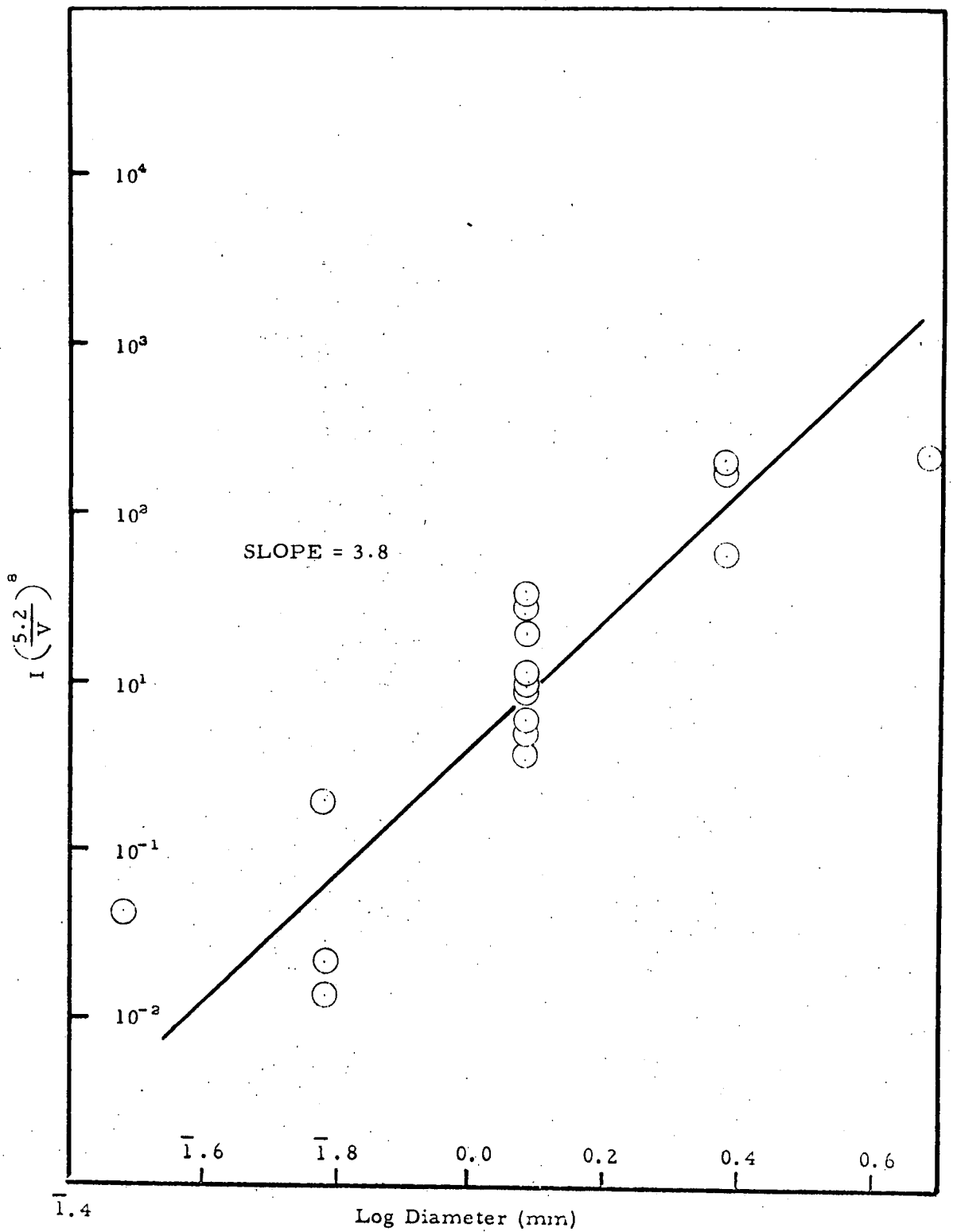


Figure 36. Dependence of Intensity on Projectile Diameter for Canyon Diablo at 3261Å

R134/FR1

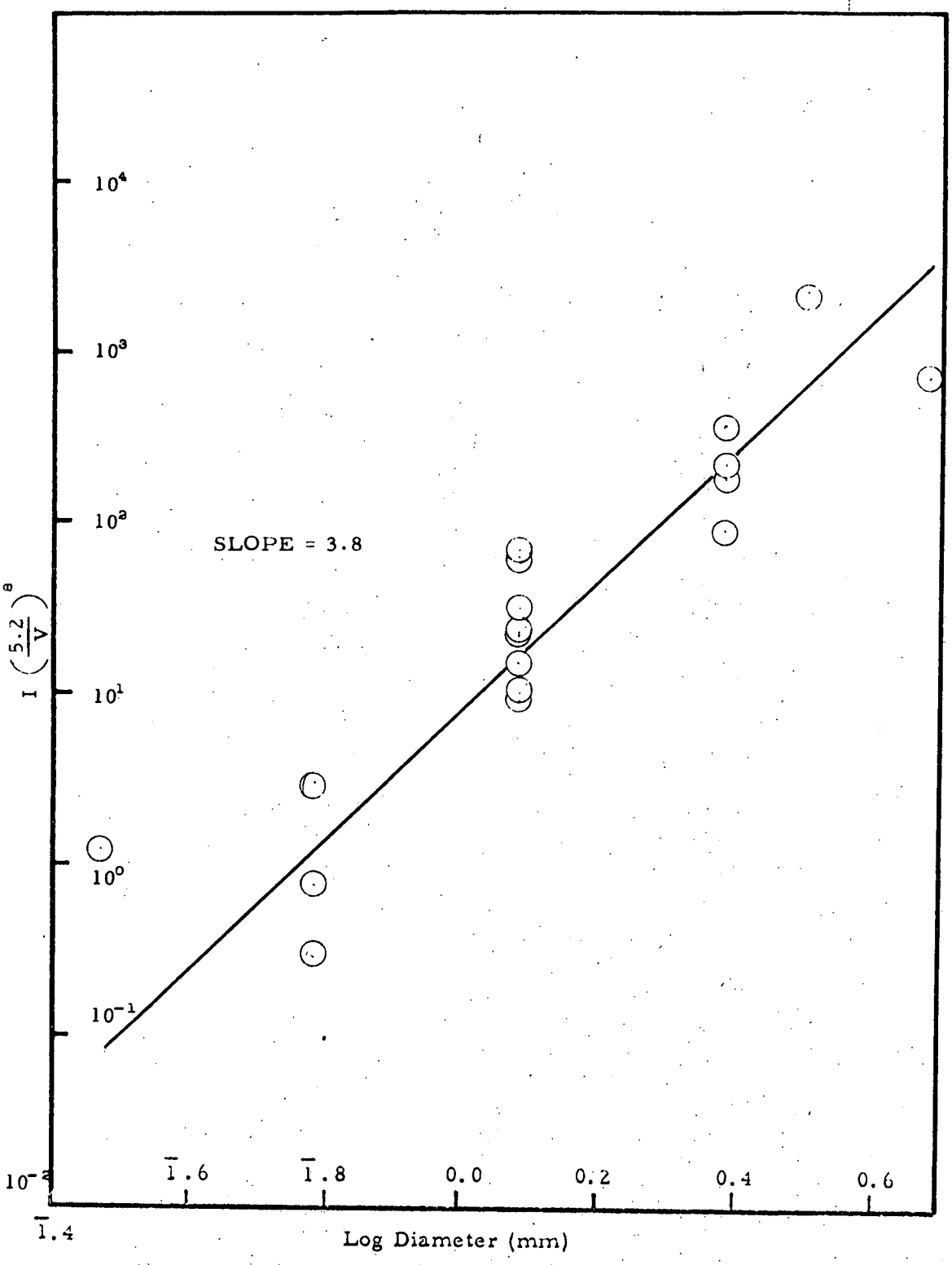


Figure 37. Dependence of Intensity on Projectile Diameter for Canyon Diablo at 3610Å

R134/FR1

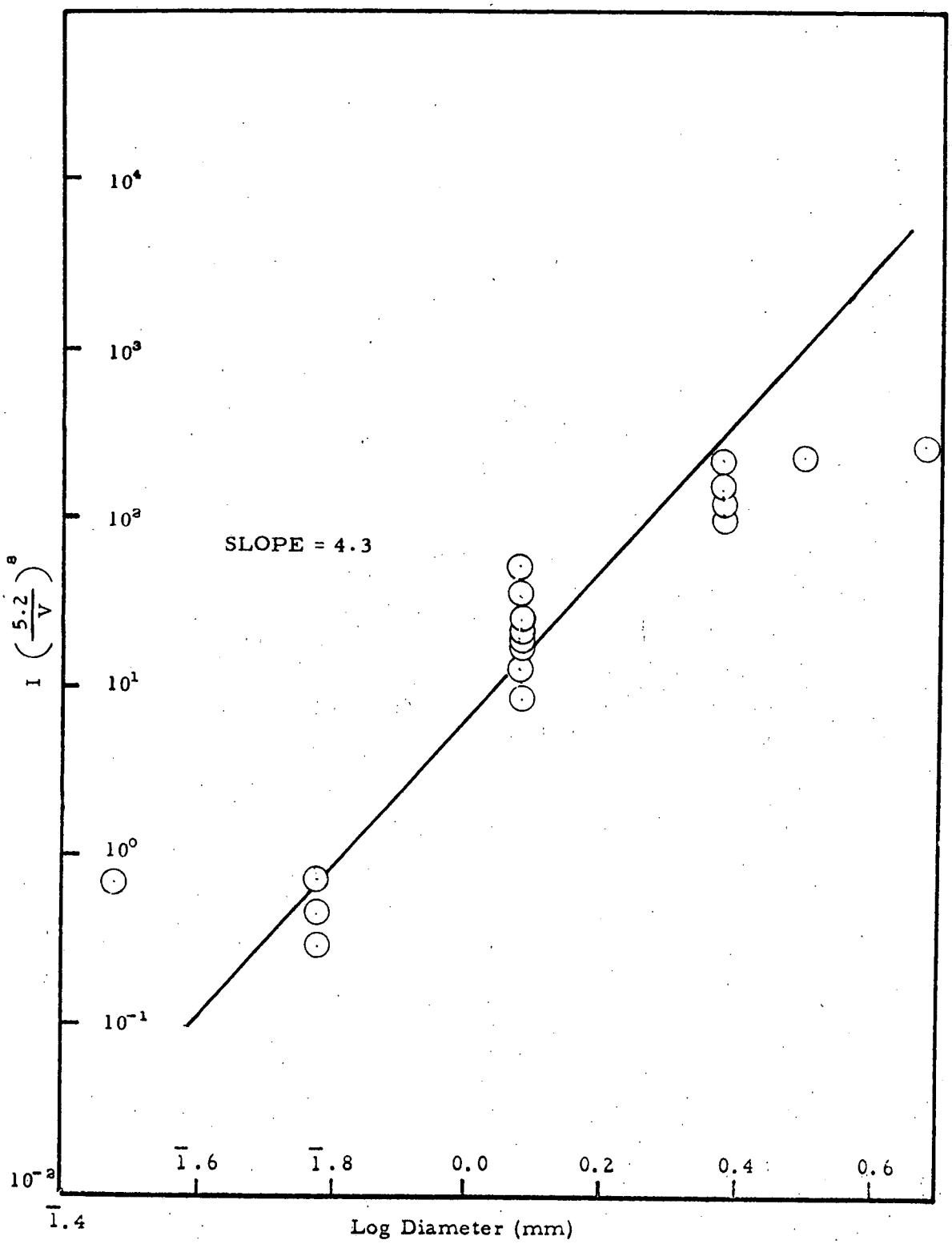


Figure 38. Dependence of Intensity on Projectile Diameter for Canyon Diablo at 4900Å

R134/FR1

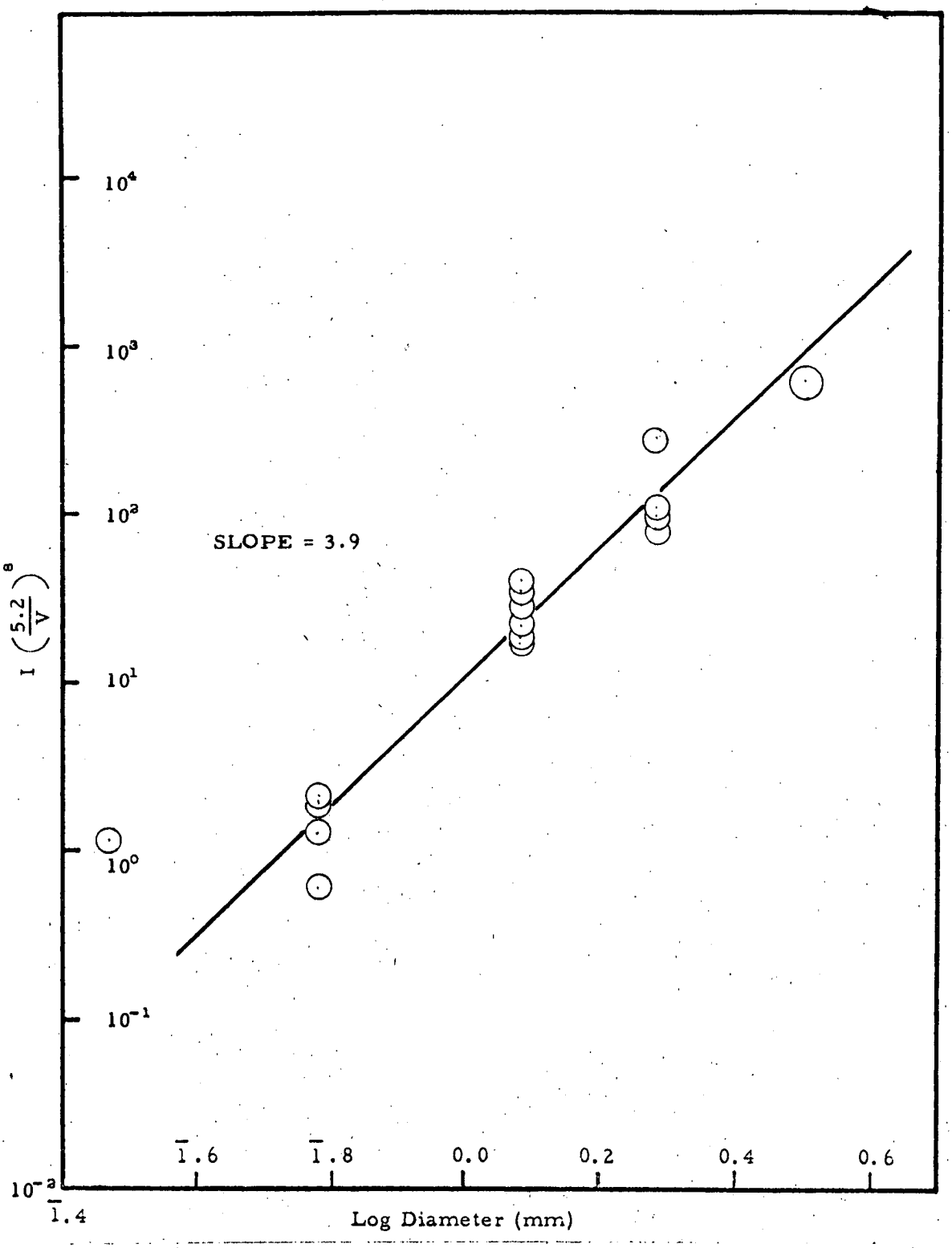


Figure 39. Dependence of Intensity on Projectile Diameter for Canyon Diablo at 5085Å

R134/FR1

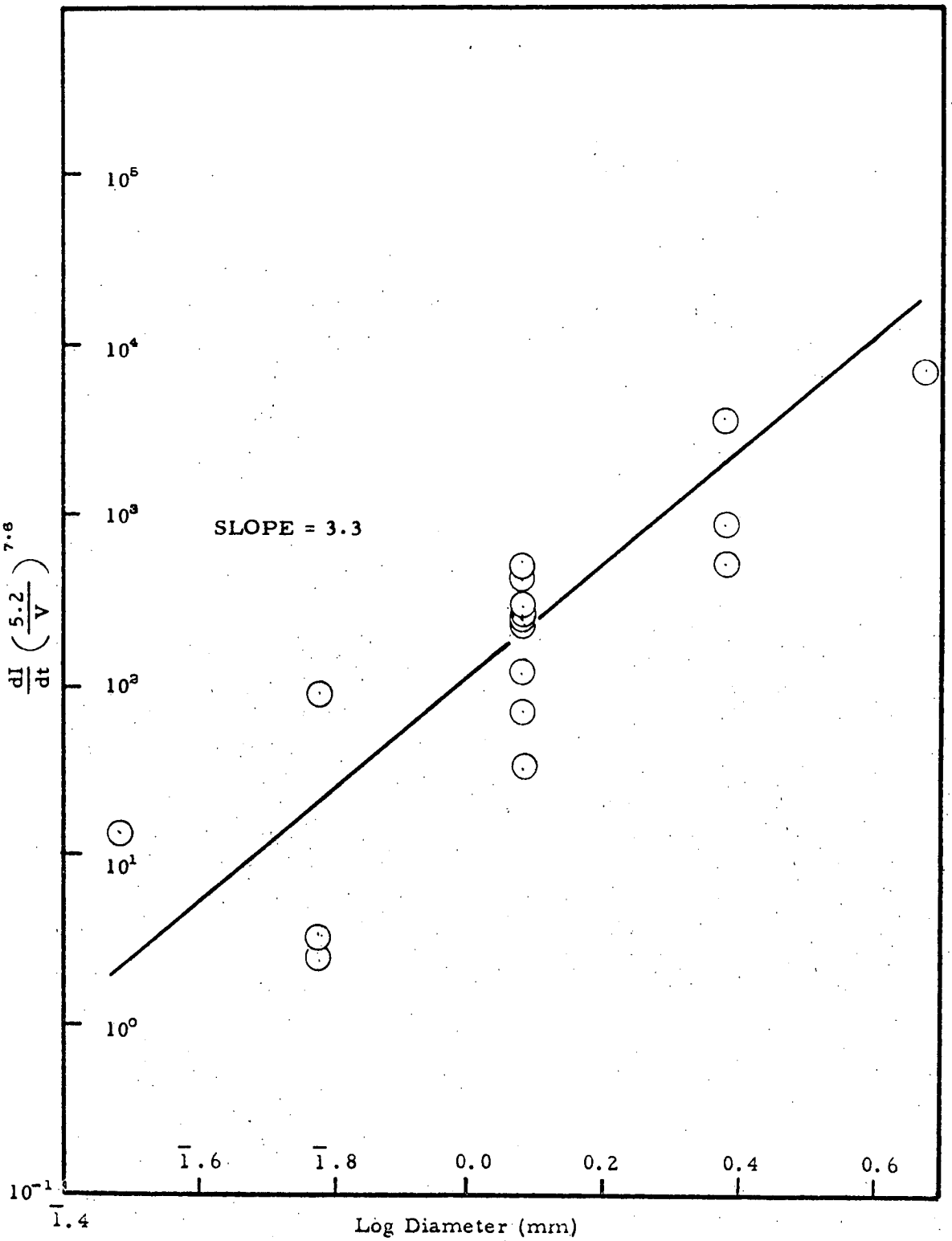


Figure 40. Dependence of dI/dt on Projectile Diameter for Canyon Diablo at 3261Å

R134/FR1

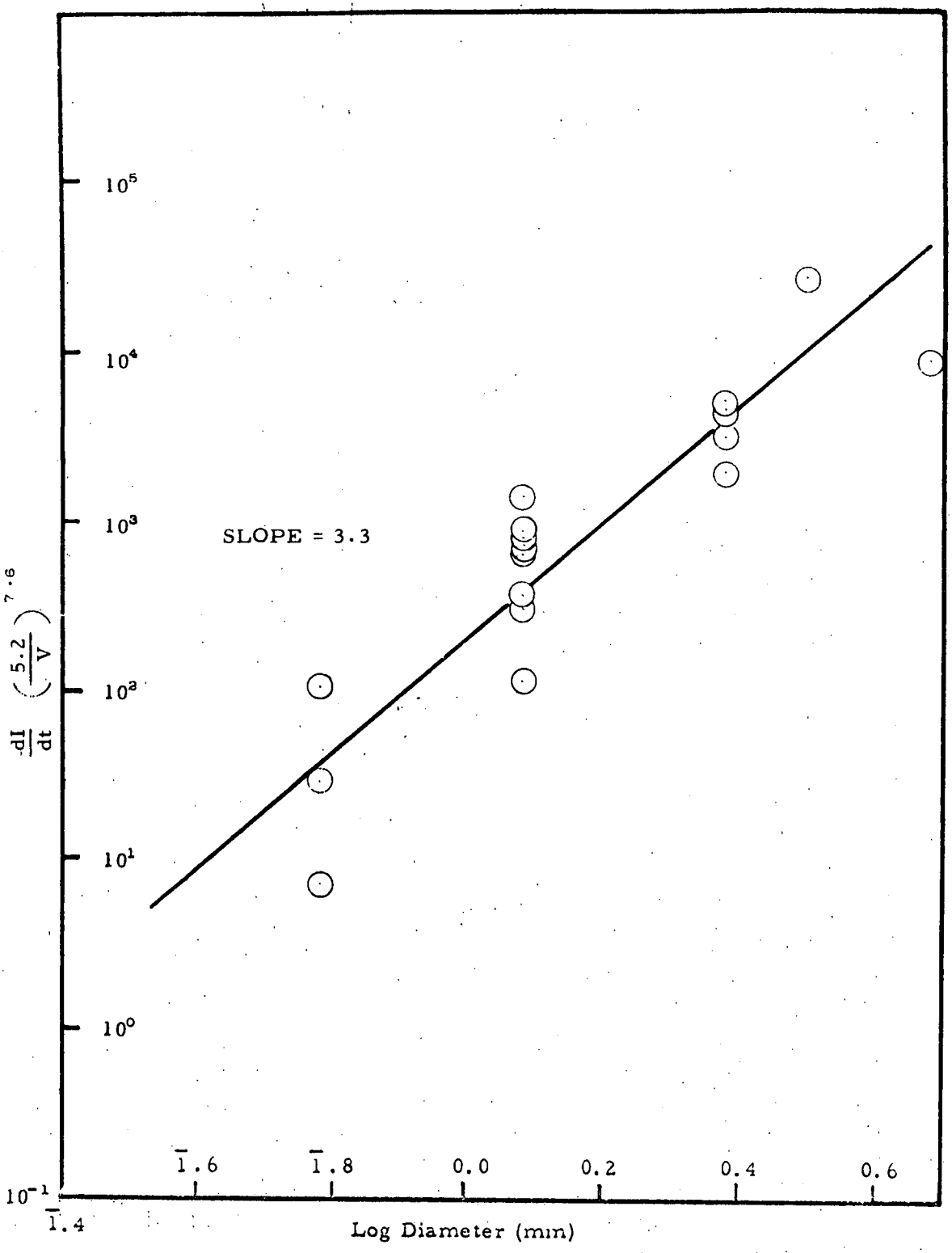


Figure 41. Dependence of dI/dt on Projectile Diameter for Canyon Diablo at 3610Å

R134/FR1

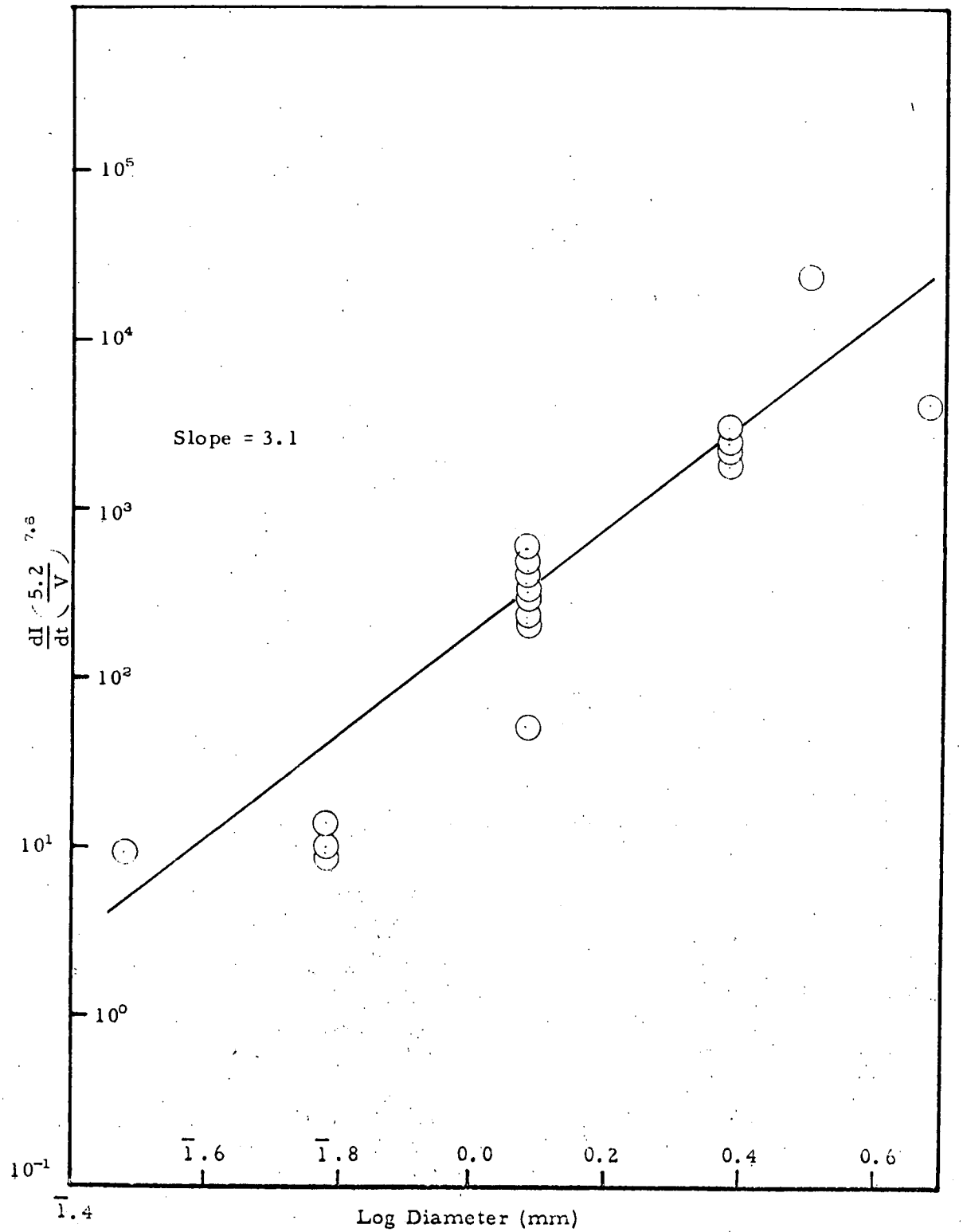


Figure 42. Dependence of dI/dt on Projectile Diameter for Canyon Diablo at 4900Å

R134/FR1

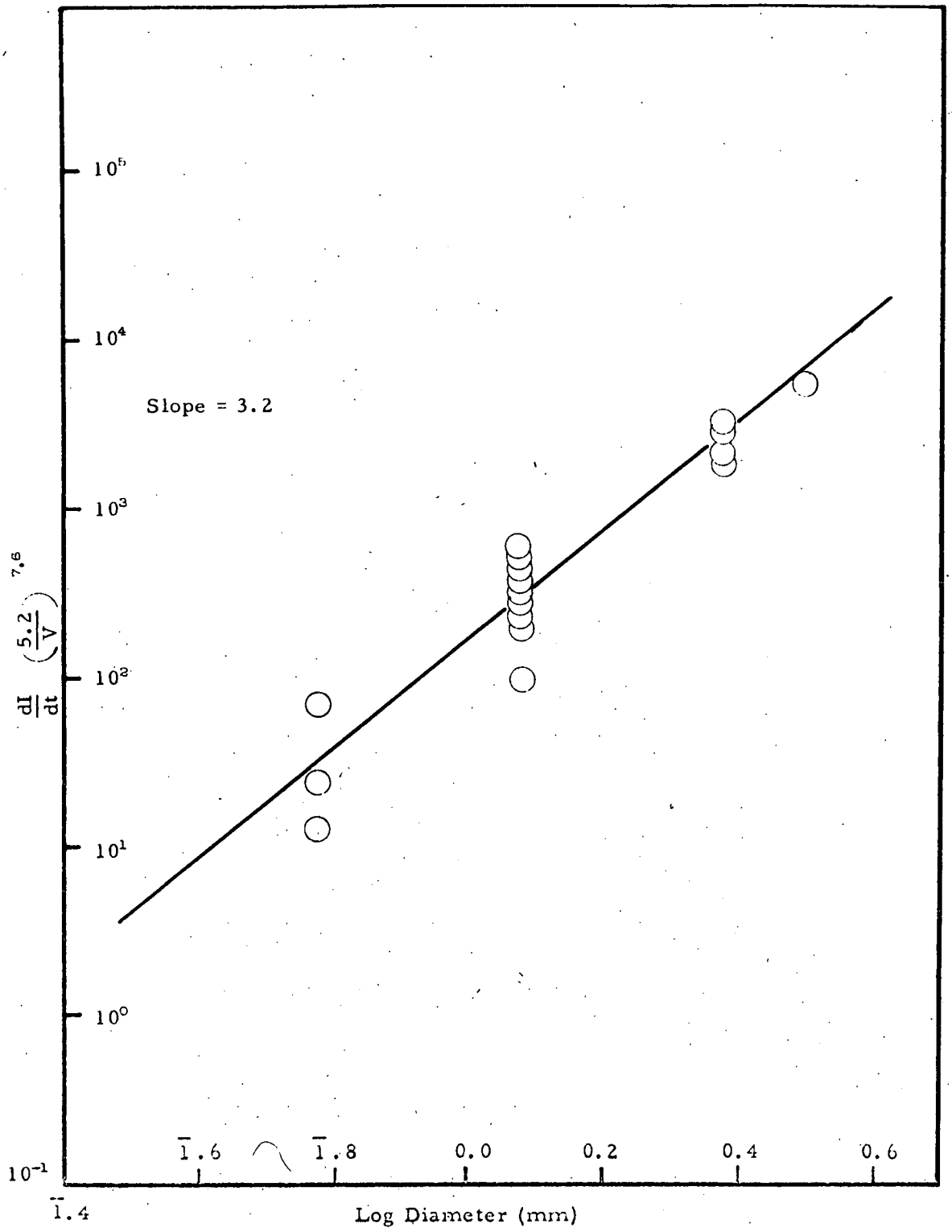


Figure 43. Dependence of dI/dt on Projectile Diameter for Canyon Diablo at 5085Å

R134/FR1

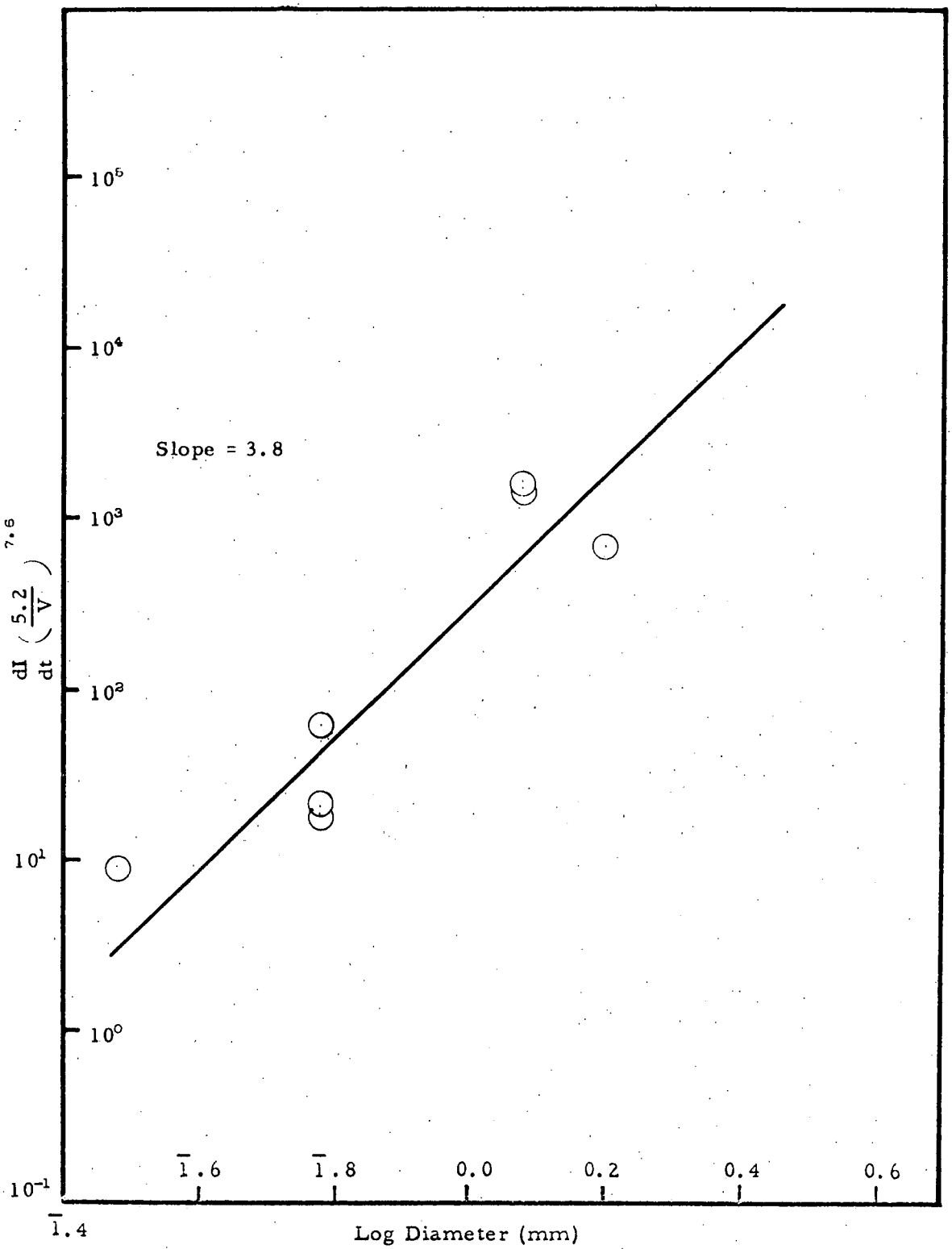


Figure 44. Dependence of $d\bar{I}/dt$ on Projectile Diameter for Bruderheim at 5085Å

R134/FR1

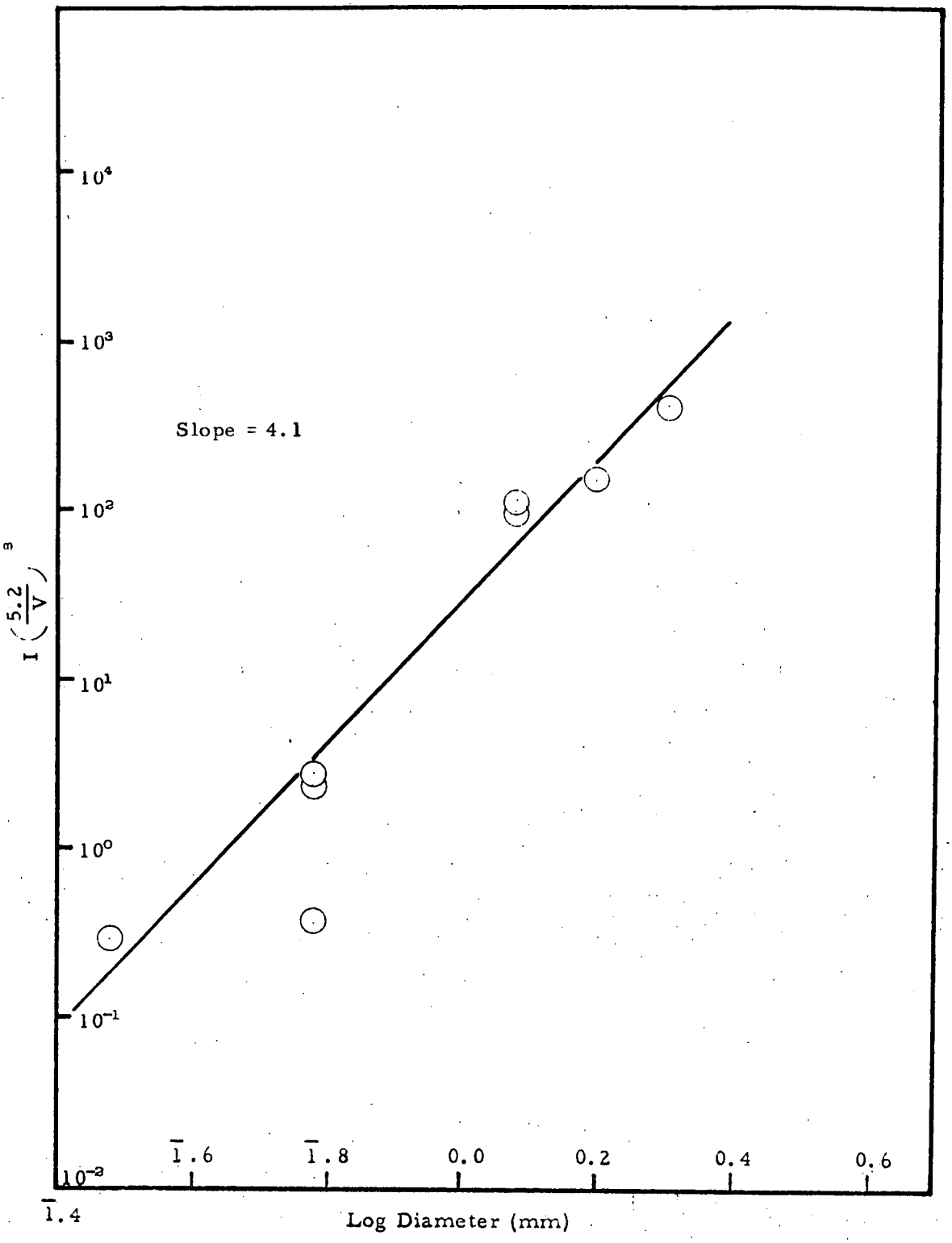


Figure 45. Dependence of Intensity on Projectile Diameter for Bruderheim at 5085Å

R134/FR1

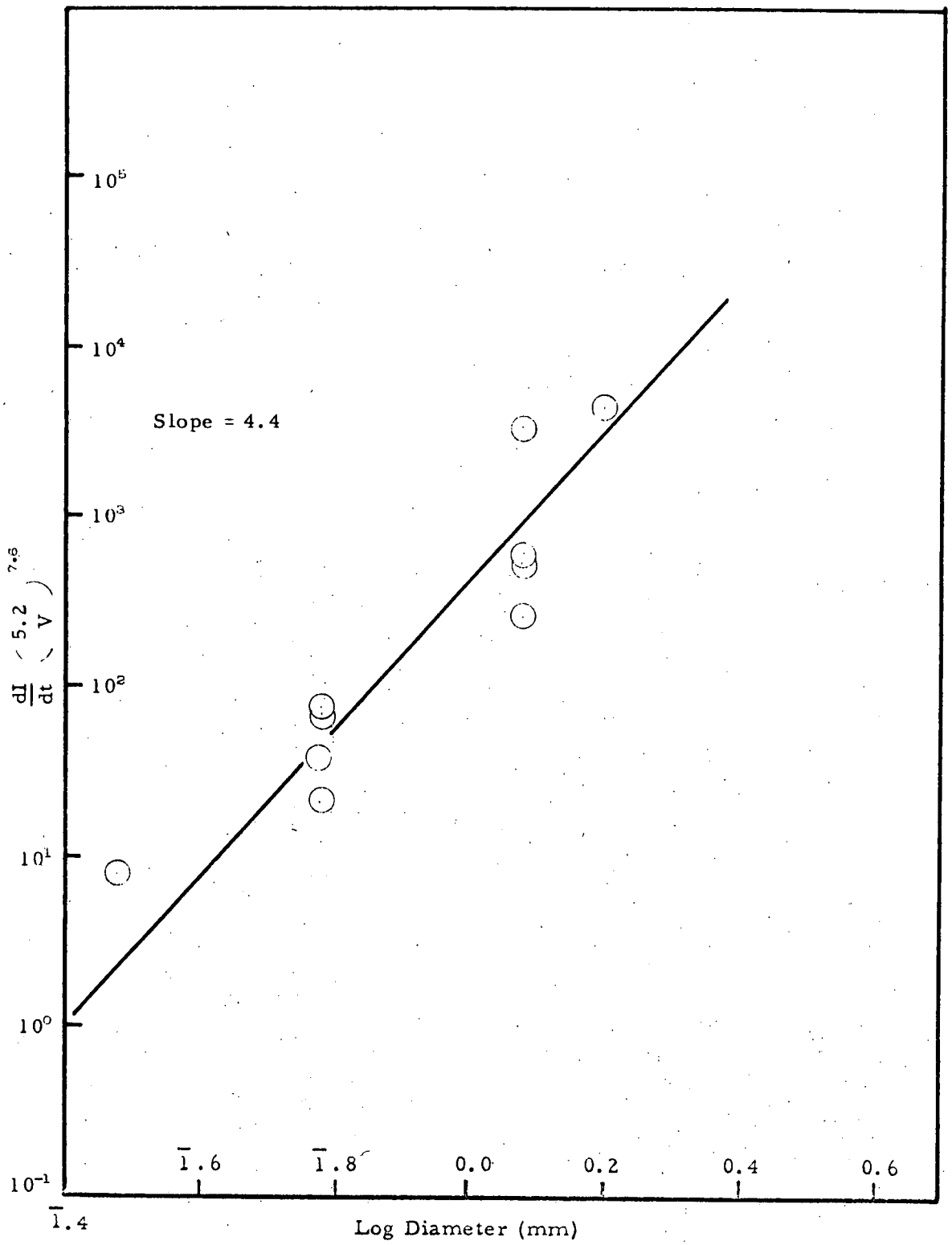


Figure 46. Dependence of dI/dt on Projectile Diameter for Bruderheim at 3610Å

R134/FR1

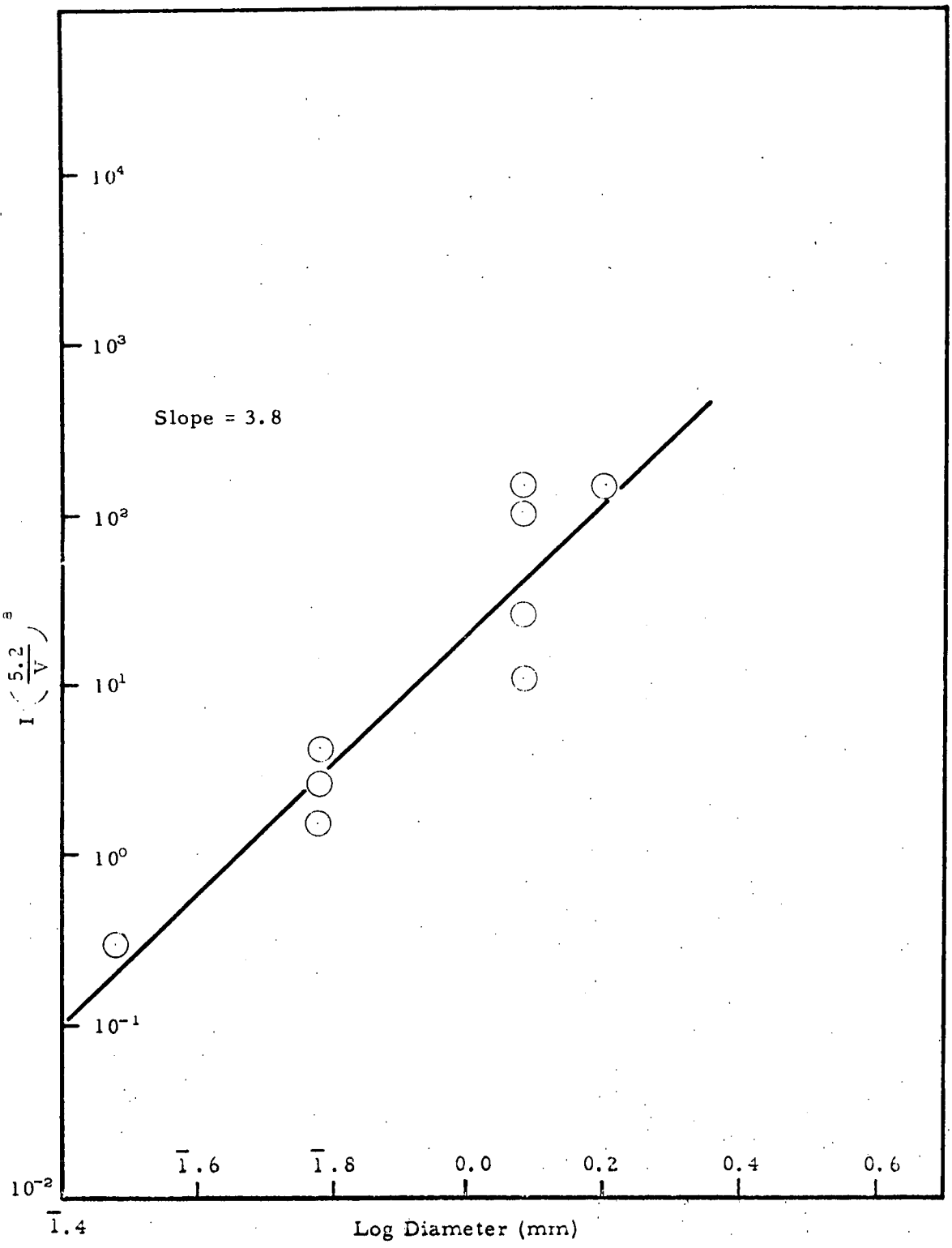


Figure 47. Dependence of Intensity on Projectile Diameter for Bruderheim at 3610Å

R134/FR1

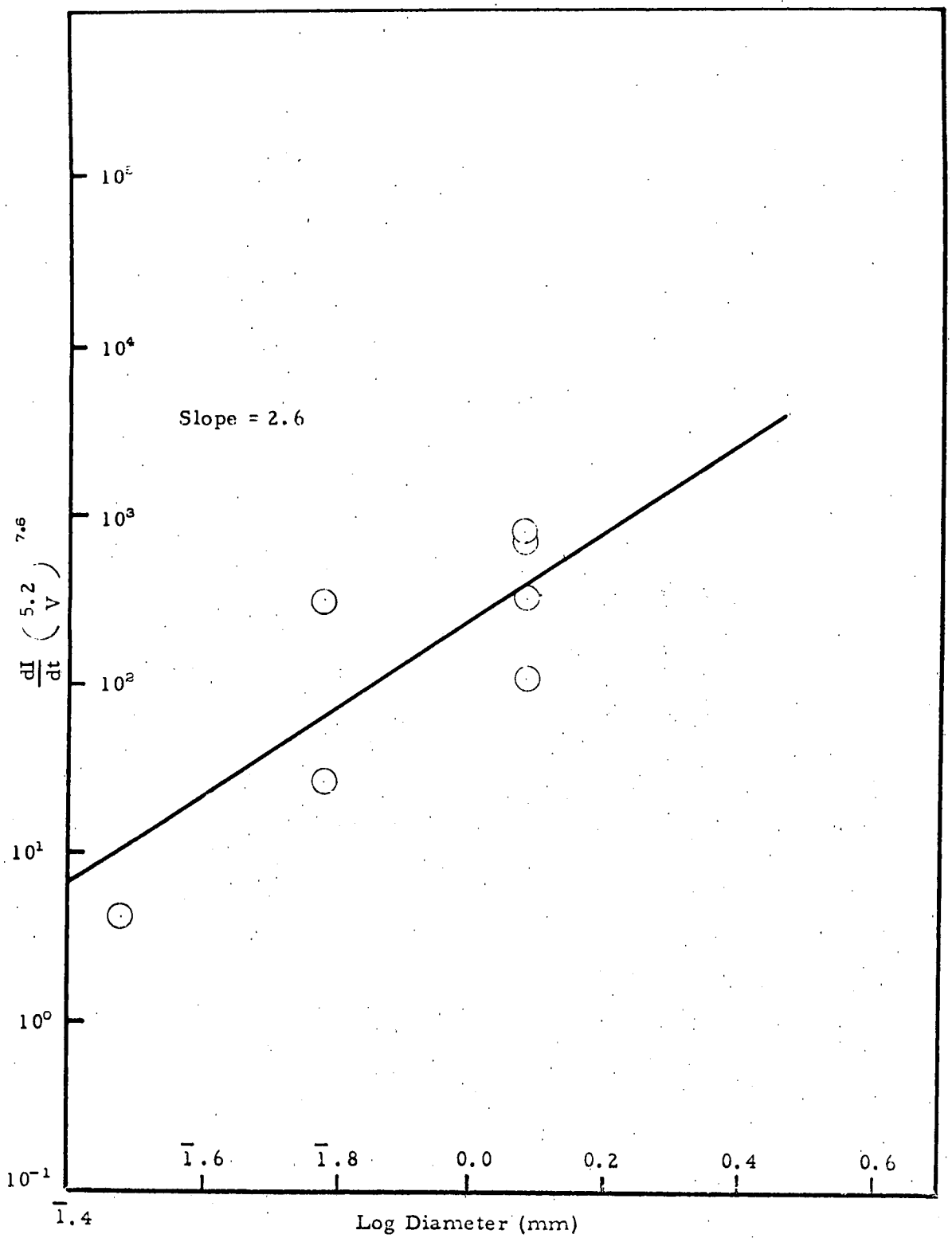


Figure 48. Dependence of dI/dt on Projectile Diameter for Bruderheim at 4900Å

R134/FR1

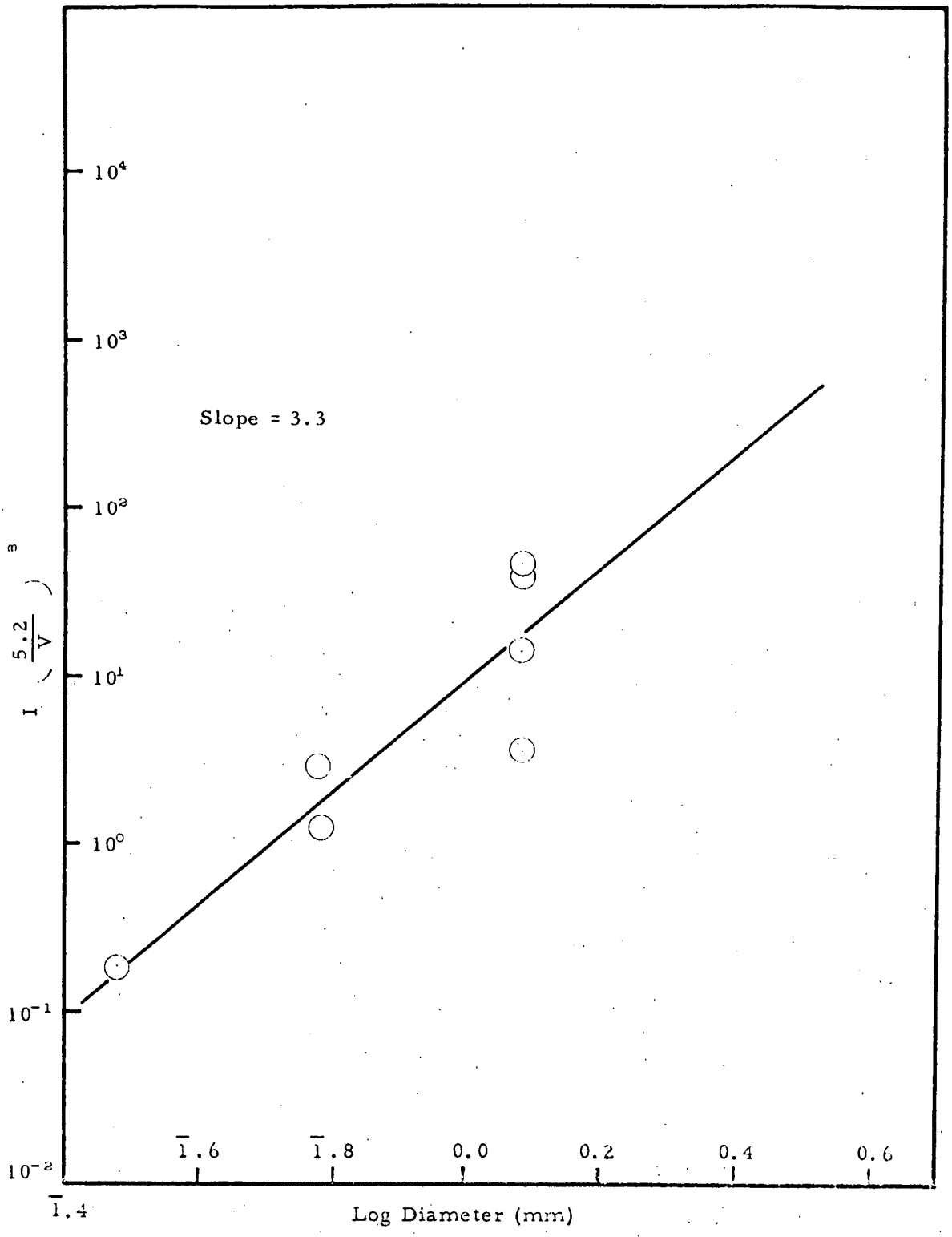


Figure 49. Dependence of Intensity on Projectile Diameter for Bruderheim at 4900Å

R134/FR1

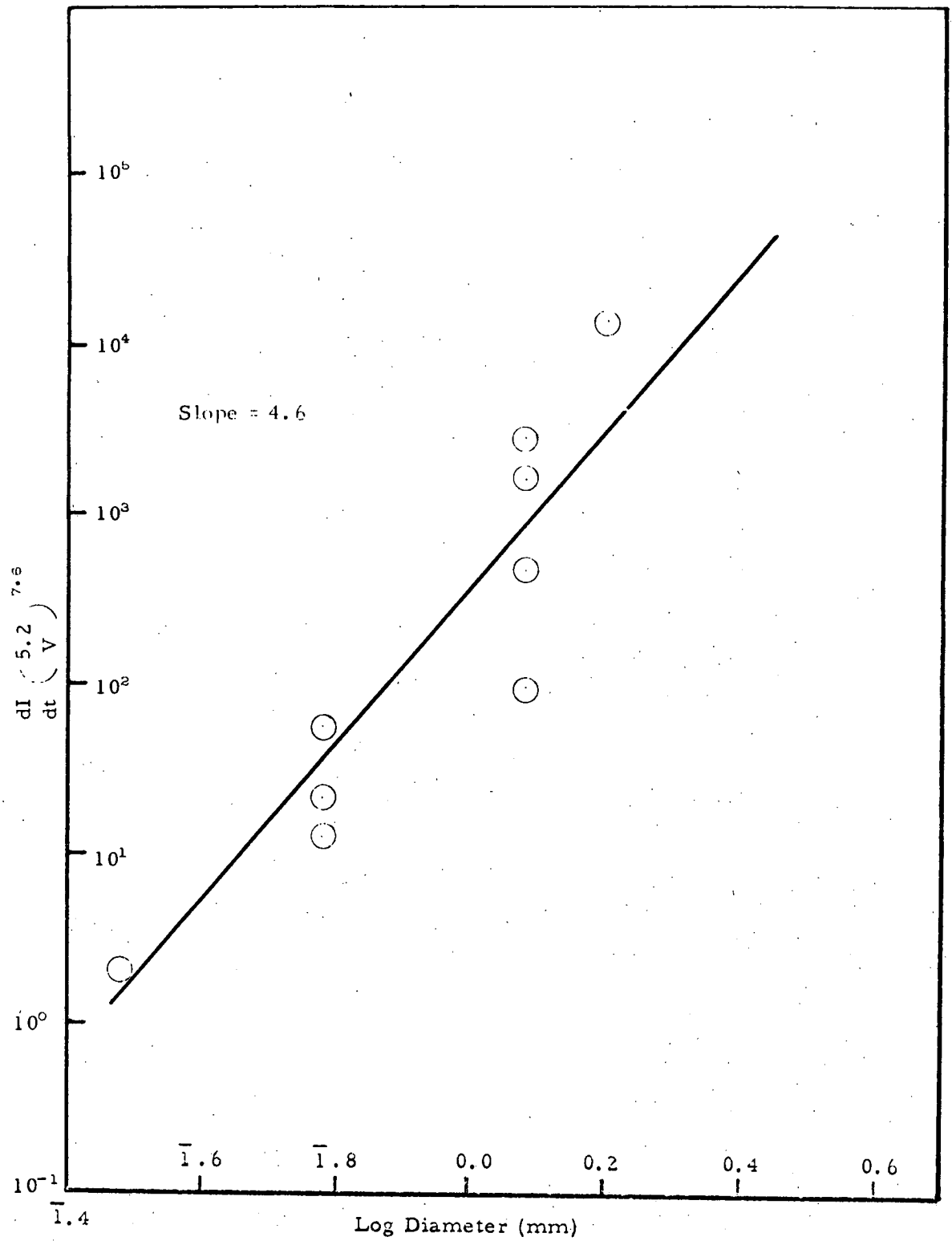


Figure 50. Dependence of dI/dt on Projectile Diameter for Bruderheim at 3261Å

R134/FR1

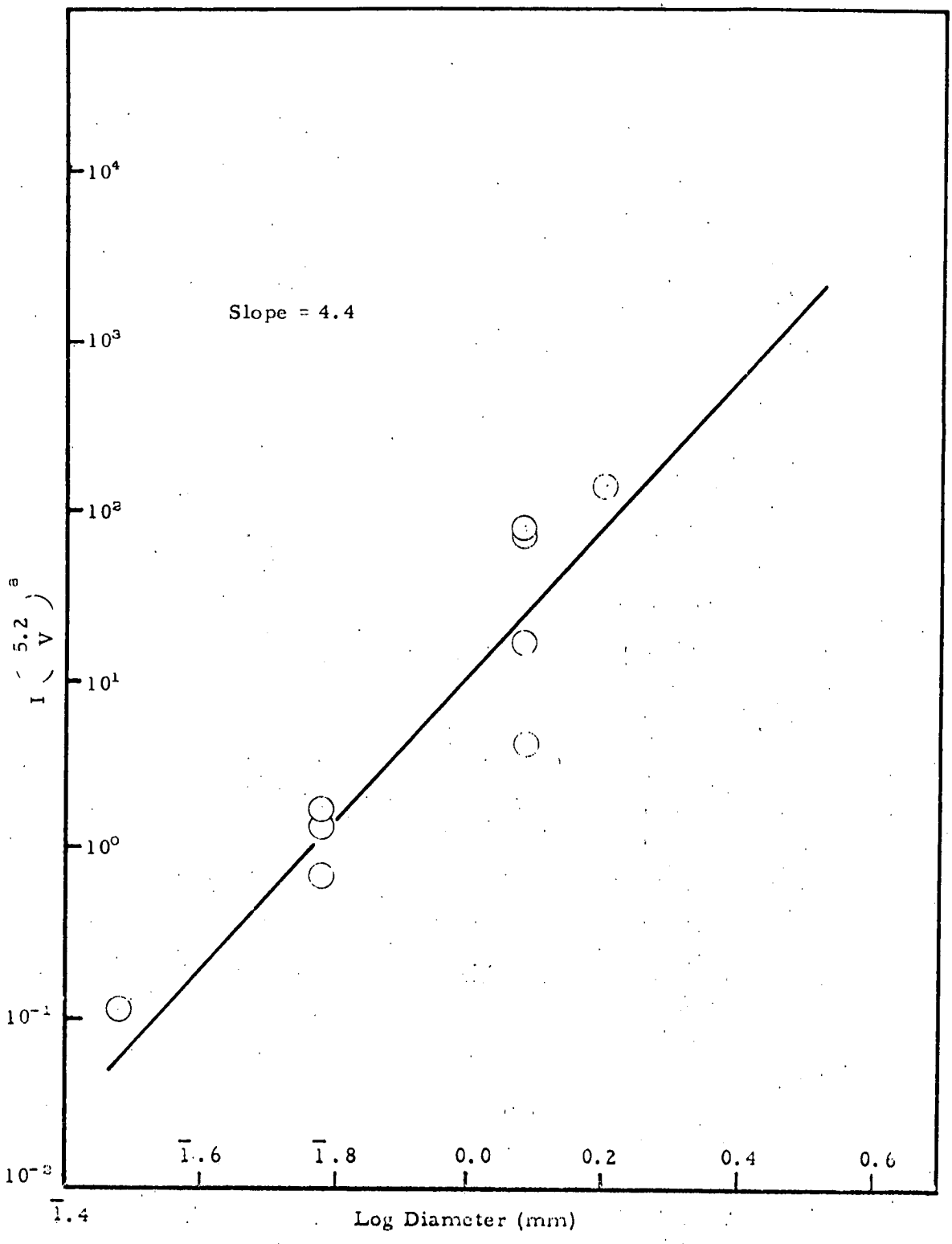


Figure 51. Dependence of Intensity on Projectile Diameter for Bruderheim at 3261Å

R134/FR1

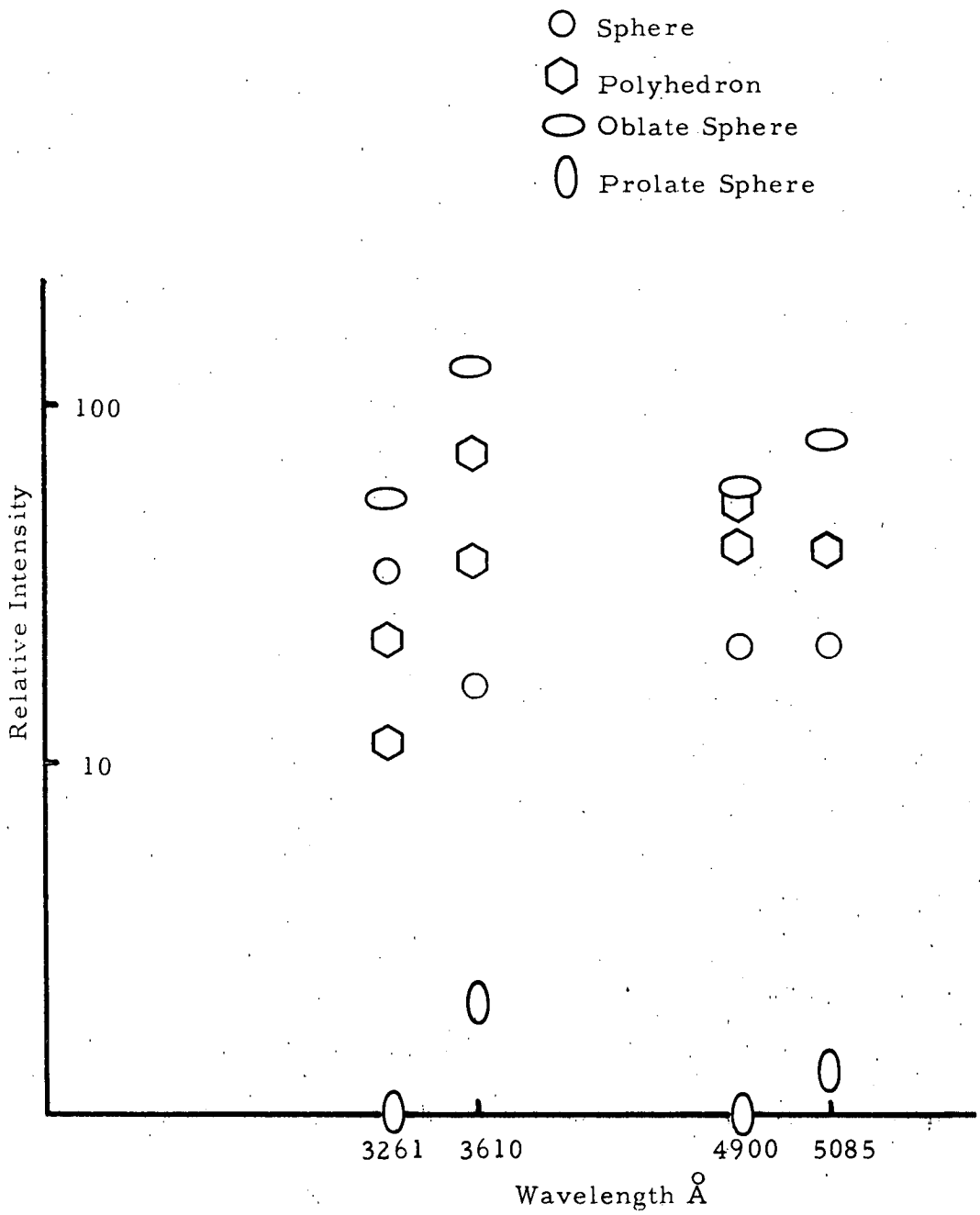


Figure 52. Shape Effect on Intensity at Different Wavelengths for 1.2 mm Canyon Diablo Iron Spheres

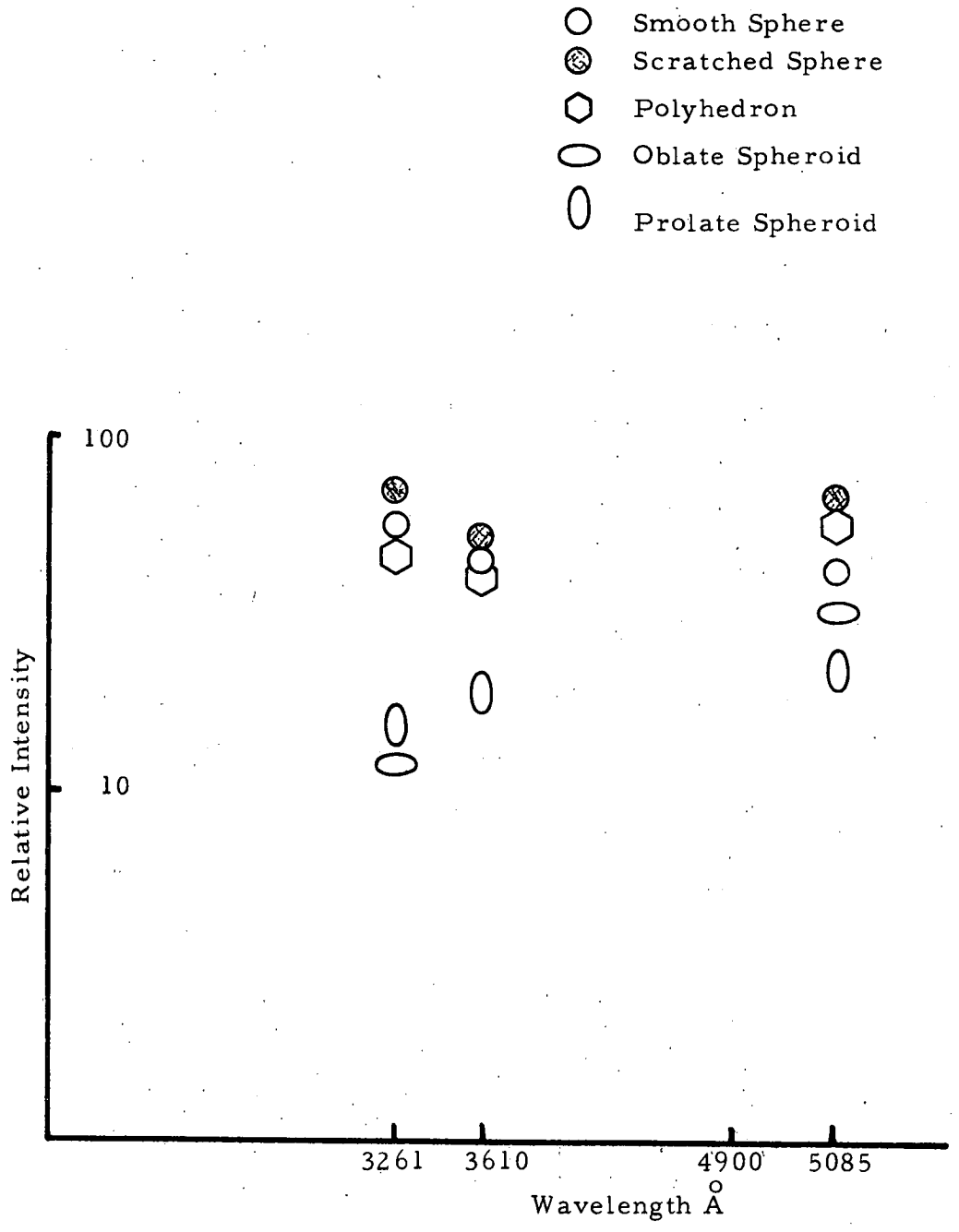


Figure 53. Shape Effect on Intensity at Different Wavelengths for 3.2 mm Copper Spheres

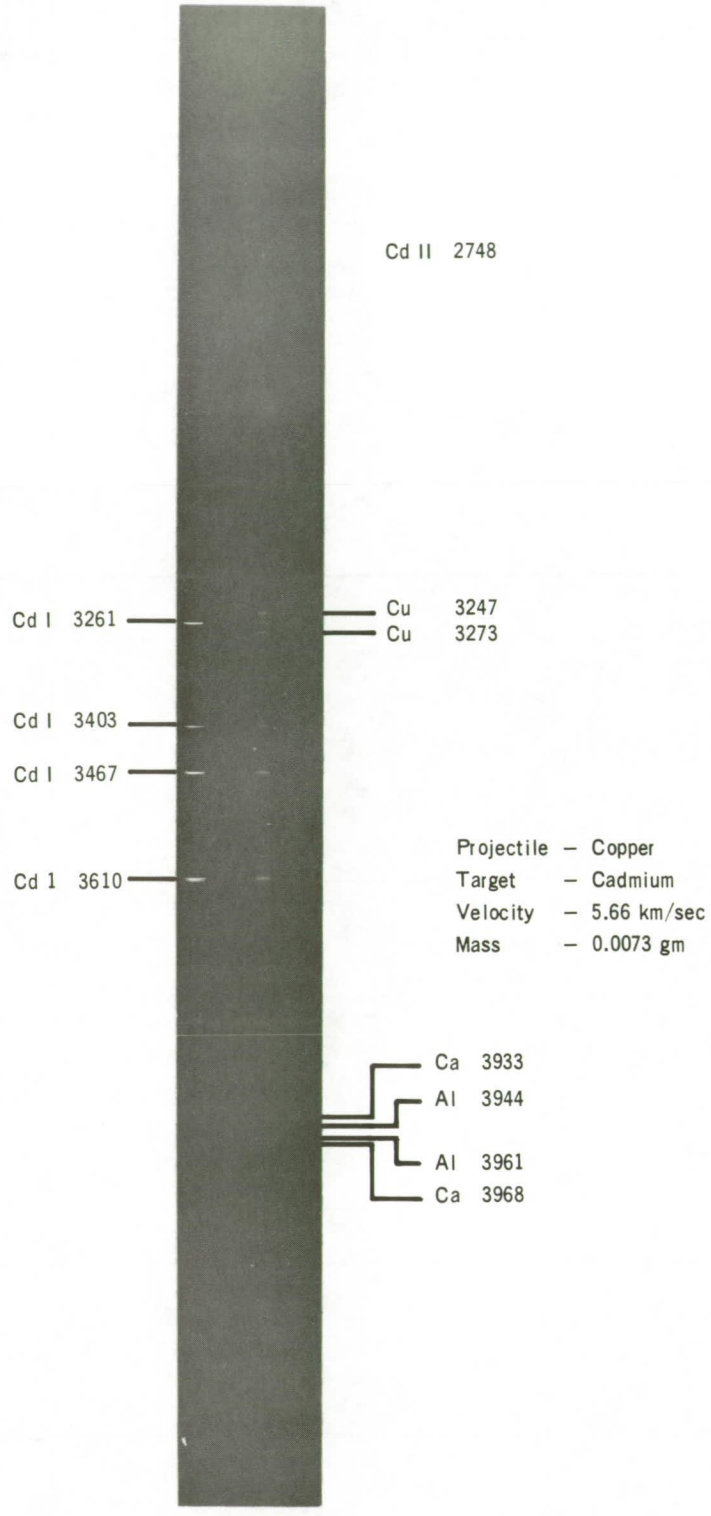


Figure 54. Spectrogram of the Flash Produced by the Impact of a Copper Projectile on a Cadmium Target

R134/FR1

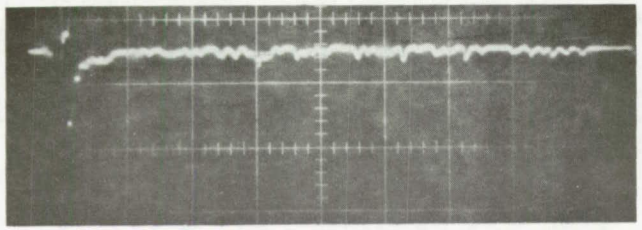

λ band = 2707Å

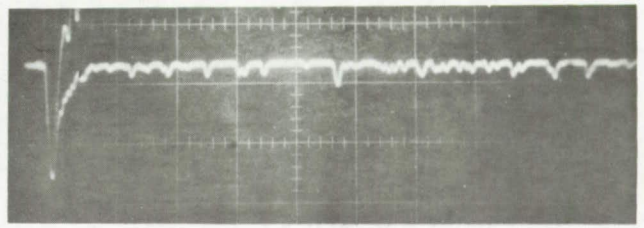

λ band = 2866Å

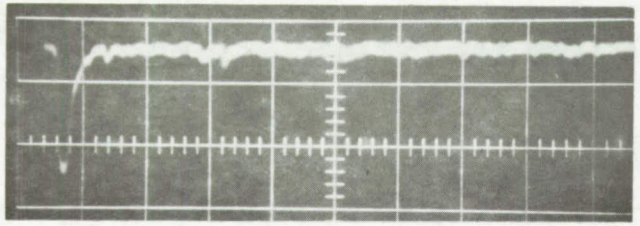

λ band = 3735Å

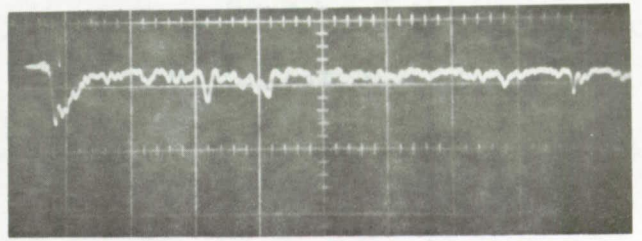

λ band = 3942Å

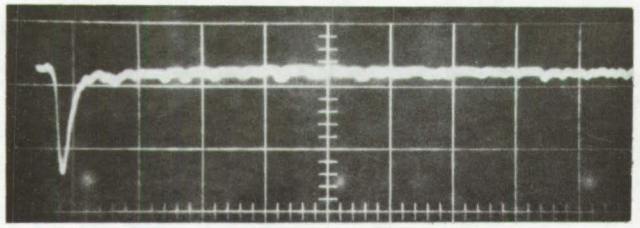

λ band = 2478Å

| | |
|---|---|
| Projectile Material: | Copper |
| Target: | Cadmium |
| Velocity: | 6.09 km/sec |
| Size: | 1.2 mm diameter |
| Sweep: | 0.5 μsec/div. |

Figure 55. Impact Flash Signature for Cu-Cd Impace at 5 Different Wavelength Bands each 80Å wide

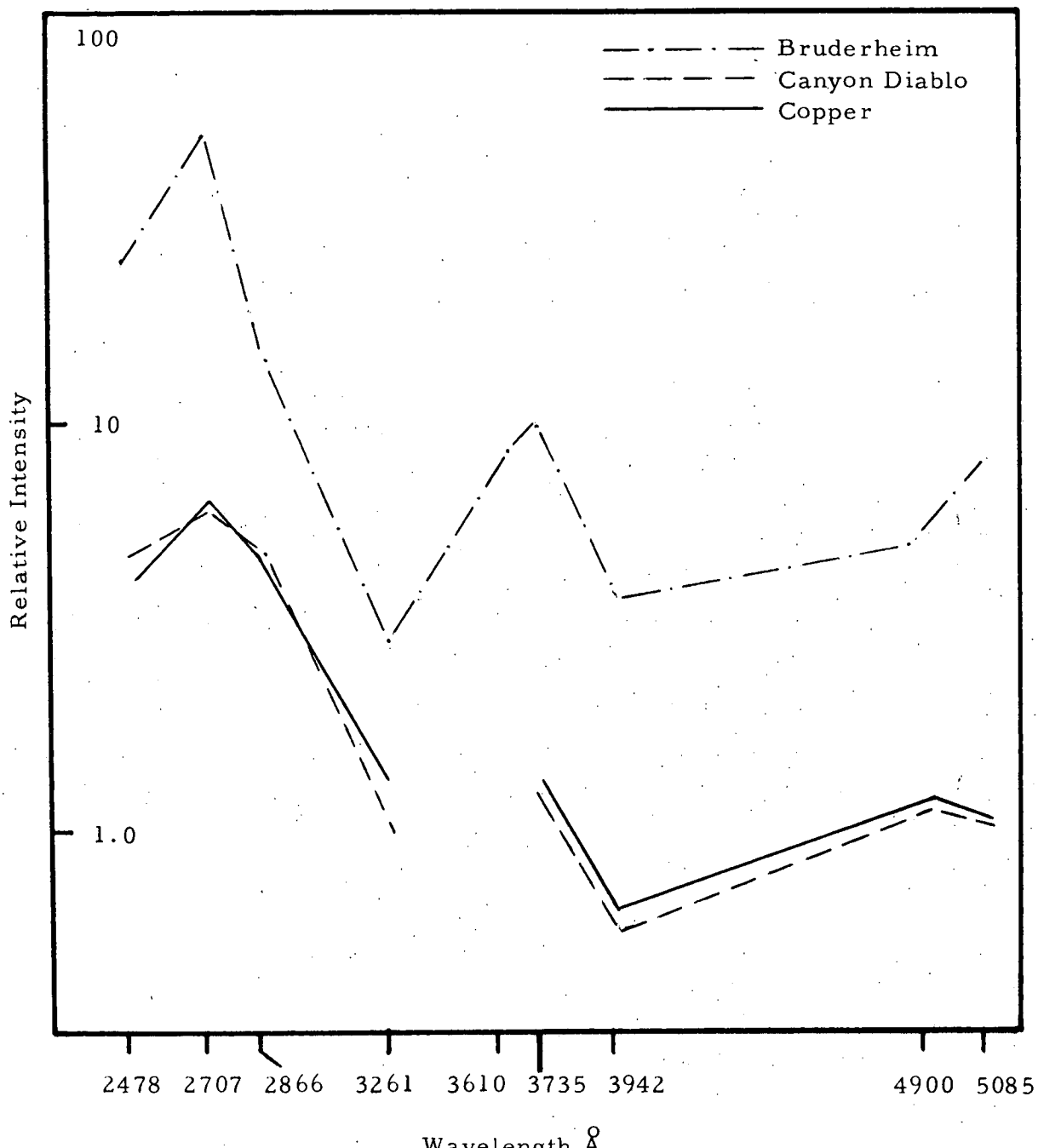


Figure 56. Comparative Intensities at Different Wavelengths for Different Material Impacting Cadmium

R134/FR1

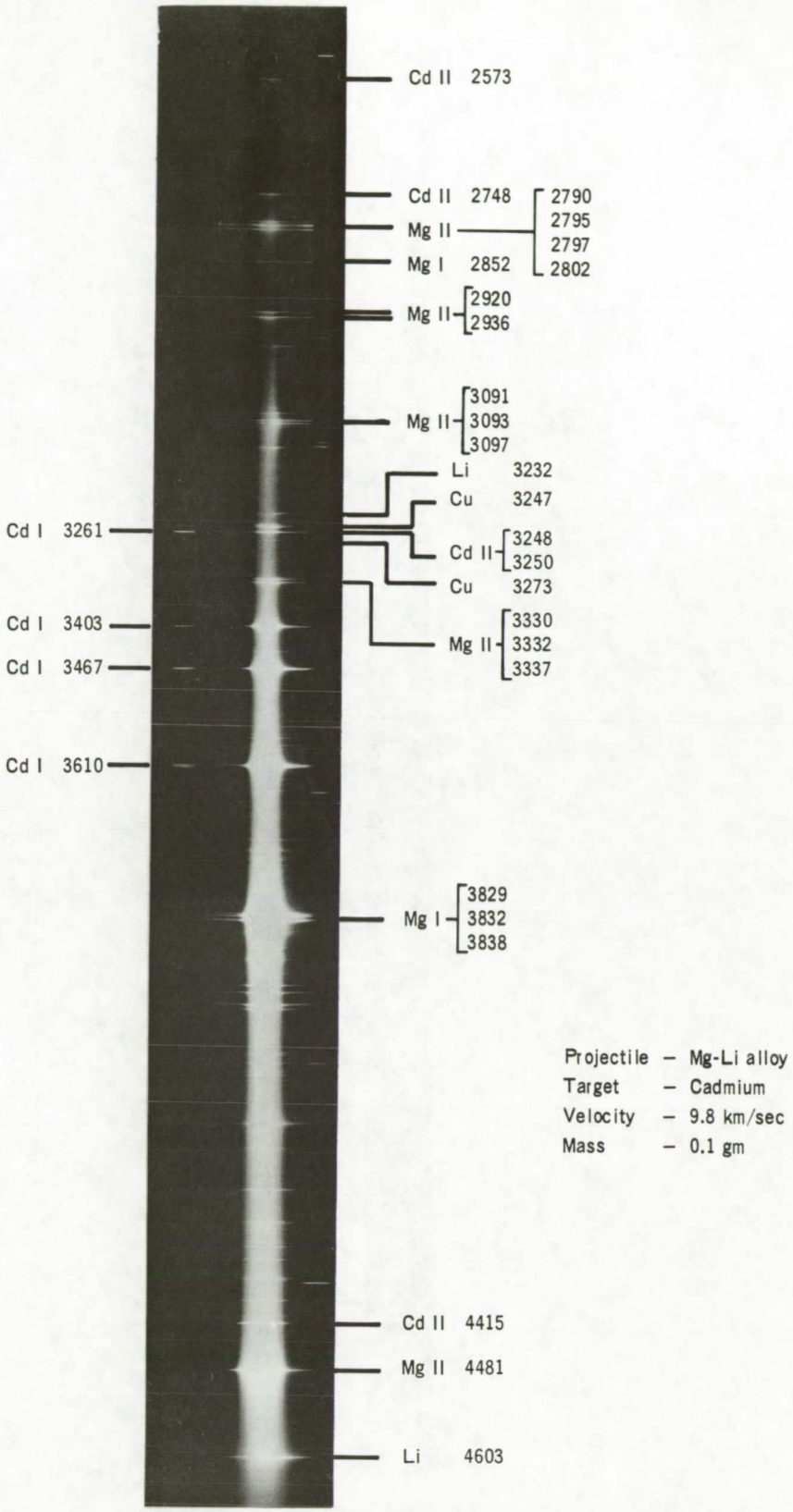


Figure 57. Spectrogram of the Flash Produced by the Impact of a Mg Li Projectile on a Cadmium Target

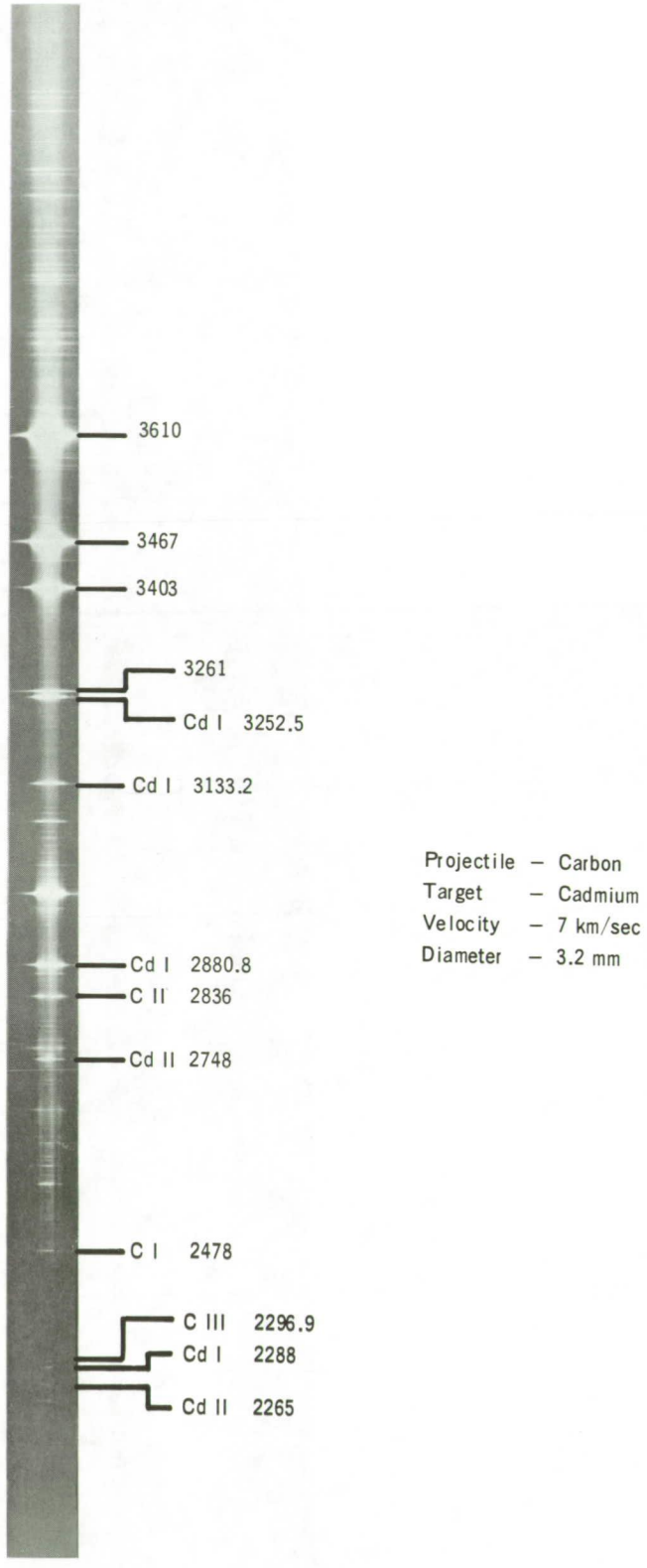


Figure 58. Spectrogram of Radiation Emitted by Carbon Impact on Cadmium

R134/FR1

Printed and published in Canada by
Computing Devices
OF CANADA LIMITED